APPENDIX B. CHARACTERIZATION MEASUREMENTS

This appendix provides a thorough description of the measurement procedures and processing used to characterize the ultrawideband (UWB) signals. It provides an extensive set of temporal, amplitude, and spectral analysis results that support Sections 2.3 and 3.3.

B.1. Measurement Setup

The UWB signals were measured under optimal conditions at the radio frequency (RF) output of the vector signal generator (VSG) as described in Figure B-1. Measurements at RF were made with the vector signal analyzer (VSA) and digital oscilloscope (DO).

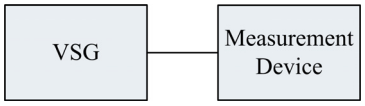

Figure B-1. Setup for RF signal characterization measurements.

Prototype DS and MB devices were made available for these tests; however, we chose to generate simulated signals with a VSG to have more control over modulation parameters and test conditions. Prototype DS and MB signals were characterized to verify corresponding VSG signals. Characteristics of the prototype DS signals matched those of the VSG DS signals. General characteristics of the prototype MB signals resembled those of the VSG MB signals. However, differences attributed to local-oscillator (LO) feed-through in the prototype MB signals were observed. Prototype-generated signal characterization measurements are not included in this report.

The VSG was set up with the procedures described in Appendix B of Part 1 [6]. UWB waveforms were created via software simulation, down-conversion to baseband, and decimation to the sampling frequency of the VSG. In order to ensure optimal use of the analog-to-digital converters in the VSG, DP and DS signals were normalized according to their maximum values shown in Table B-1. In contrast, MB-02 – MB-09 were normalized by the maximum value of MB-01 from which they were derived. In the composite plots of Section 2.3, discrepancies due to different normalization factors were removed so the relative average powers are proportional to T_{pulse}. Plots in this appendix, however, were not adjusted according to the individual normalization factors.

VSA instrument settings are summarized in Table B-2. As discussed in Appendix E of Part 1, VSG amplitudes were adjusted to ensure that the dynamic range of the VSA was optimally utilized. Table B-1 provides the VSG amplitudes used for RF signal characterization of DP and DS signals. The VSG amplitude for MB signals was -28.62 dBm.

Table B-1. Maximum Waveform Values and VSG Amplitudes for RF VSA Measurements

Type	Index	Maximum	VSG Amplitude (dBm)
DP	01	0.014	-31.61
	02	0.014	
	03	0.018	
	04	0.053	
DS	01	0.048	-29.86
	02	0.025	-30.71
	03	0.016	-31.62
	04	0.032	-33.31
	05	0.009	-33.61
	06	0.029	-33.23

Table B-2. RF VSA Measurement Settings

Post-Processing Bandwidths (MHz)	Span (MHz)	Number of Samples	Center Frequency (MHz)	Input Range (dBm)
36, 19.51, 10	36	> 360,000	3820	-30
1	4.5	> 450,000		
0.1	0.5625	> 562,500		

DO measurements at the maximum sample rate, i.e., 20 GSps, provided real, time-domain representations of RF signals. DO measurements were made with the VSG output level set to a higher value, i.e., 0 dBm, to compensate for low DO sensitivity at the maximum sample rate.

UWB interference signals were also measured at the IF output of the low-noise block downconverter (LNB) with the setup described in Figure 20 of Part 1 with the VSG output level corresponding to INR_{TOV}. The simplified block diagram of the hardware components that affect the IF signal characterization measurements is shown in Figure B-2. Bandpass filter BPF1 has a 1-dB bandwidth equal to 40 MHz.

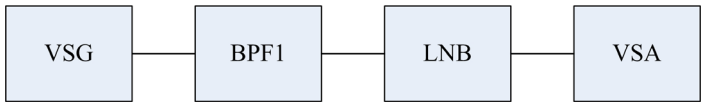

Figure B-2. Simplified setup for IF signal characterization measurements.

Measurements at IF were made with the VSA only. VSA settings for IF measurements were the same as those used for RF measurements described in Table B-2, except the center frequency was set to 1330 MHz.

B.2. Temporal Analysis

Time or crossing statistics are provided via the pulse duration distribution (*PDD*) and the pulse interval distribution (*PID*). *PDD* is presented in terms of the percentage of pulses that exceed various time durations in seconds. It provides statistics on how long a signal crosses and stays above a specified threshold. *PID* gives the probability distribution for the times a signal falls and stays below a threshold. *PDD* and *PID* are plotted on Rayleigh graph where the ordinate is plotted on a log scale. Poisson-distributed crossings with exponentially-distributed *PD* and *PI* values would plot as a straight line on this graph.

Figure B-3 is an illustration of *PD* statistics from VSA measurements of the gated-noise signal, GN-10, i.e., τ_{on} = 1 µs and 50% duty cycle, when the crossing threshold is set to -70 dBm. There are three *PD* categories: non-interrupted on-times in black, interrupted on-times in green, and anomalous spikes in red. Non-interrupted pulse durations are identified by the horizontal portion at low percentiles. Nearly 40% of *PD*s are approximately 1.13 µs corresponding to a τ_{on} slightly broadened by band-limiting.

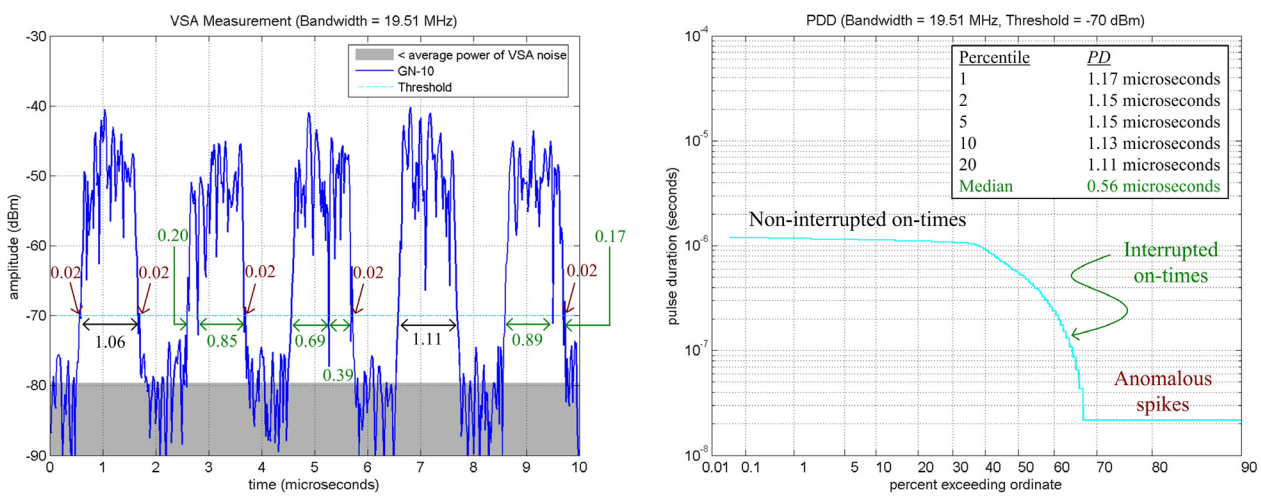

Figure B-3. Pulse duration statistics of gated noise with 50% duty cycle and 1-µs on-time.

Figure B-4 is an illustration of *PI* estimates from VSA measurements of GN-10 when the crossing threshold is set to -70 dBm. Interestingly, the interrupted off-time category is absent because there are negligible disruptions from higher amplitudes. The resulting *PID* is nearly a step function. Similar to the *PD* analysis, non-interrupted *PI* estimates are identified by the horizontal portion at low percentiles.

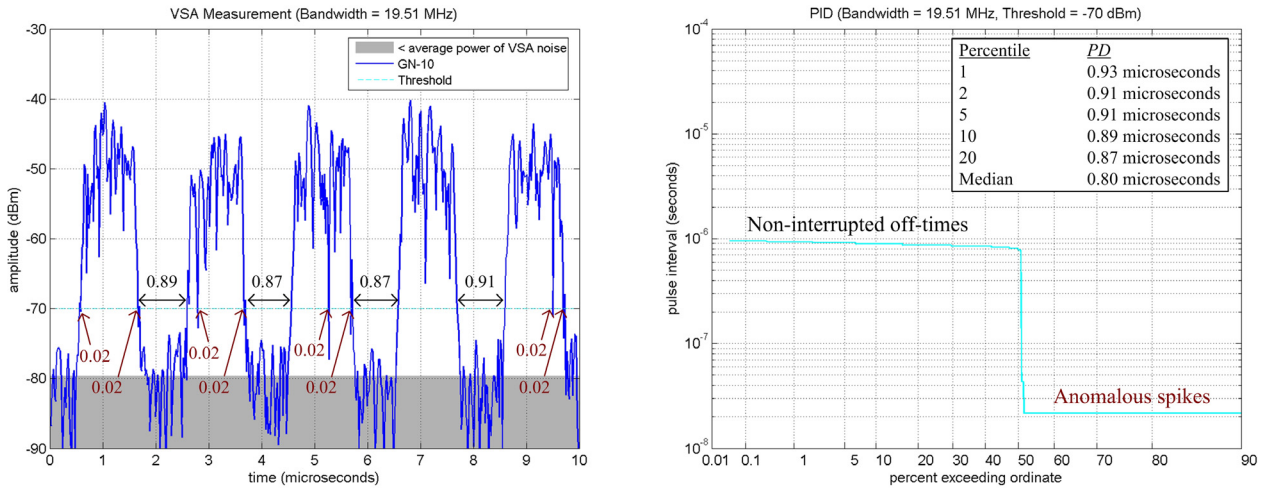

Figure B-4. Pulse interval statistics of gated noise with 50% duty cycle and 1-µs on-time.

Figure B-5 is an illustration of *PI* estimates from VSA measurements of complex Gaussian noise, GN-01, when the crossing threshold is set to -70 dBm. For the given measurement procedure, this choice for the crossing threshold is too low to quantify meaningful time statistics of continuous signals. As illustrated, GN-01 only triggered time statistic estimates at anomalous noise spikes. Therefore, it is useful to provide curves for a range of crossing thresholds.

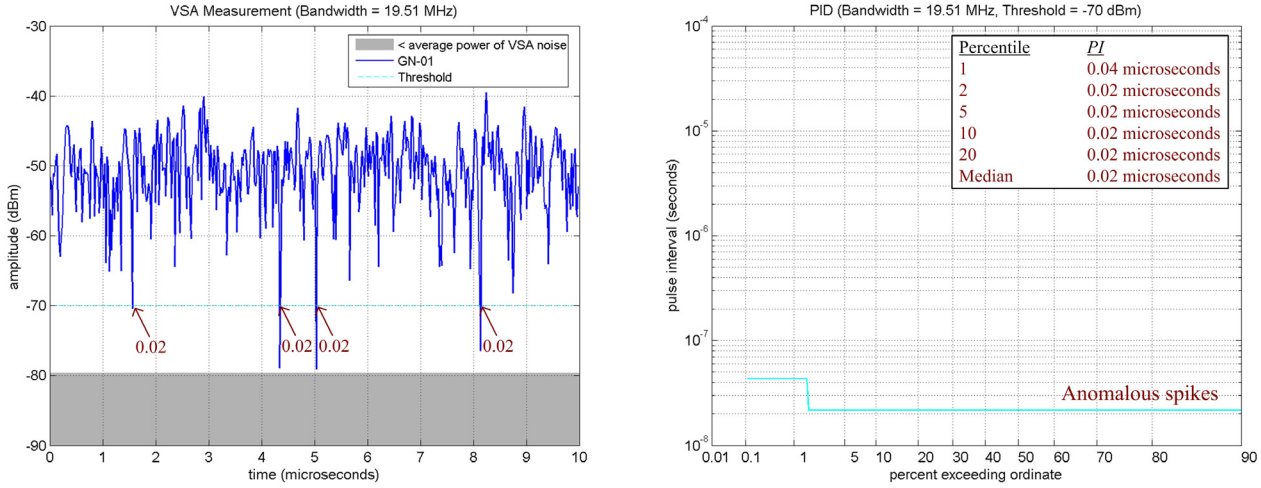

Figure B-5. Pulse interval statistics of complex Gaussian noise.

Figures B-6 – B-24 provide *PDD* and *PID* for the UWB signals when the crossing threshold was set to mean amplitude, -50 dBm, -60 dBm, and -70 dBm. Tenth percentile *PD* and *PI* estimates when the crossing threshold was set to -70 dBm were chosen as meaningful metrics to quantify the on- and off-times of band-limited signals and were specified in the main text as burst duration (*BD*) and burst interval (*BI*), respectively.

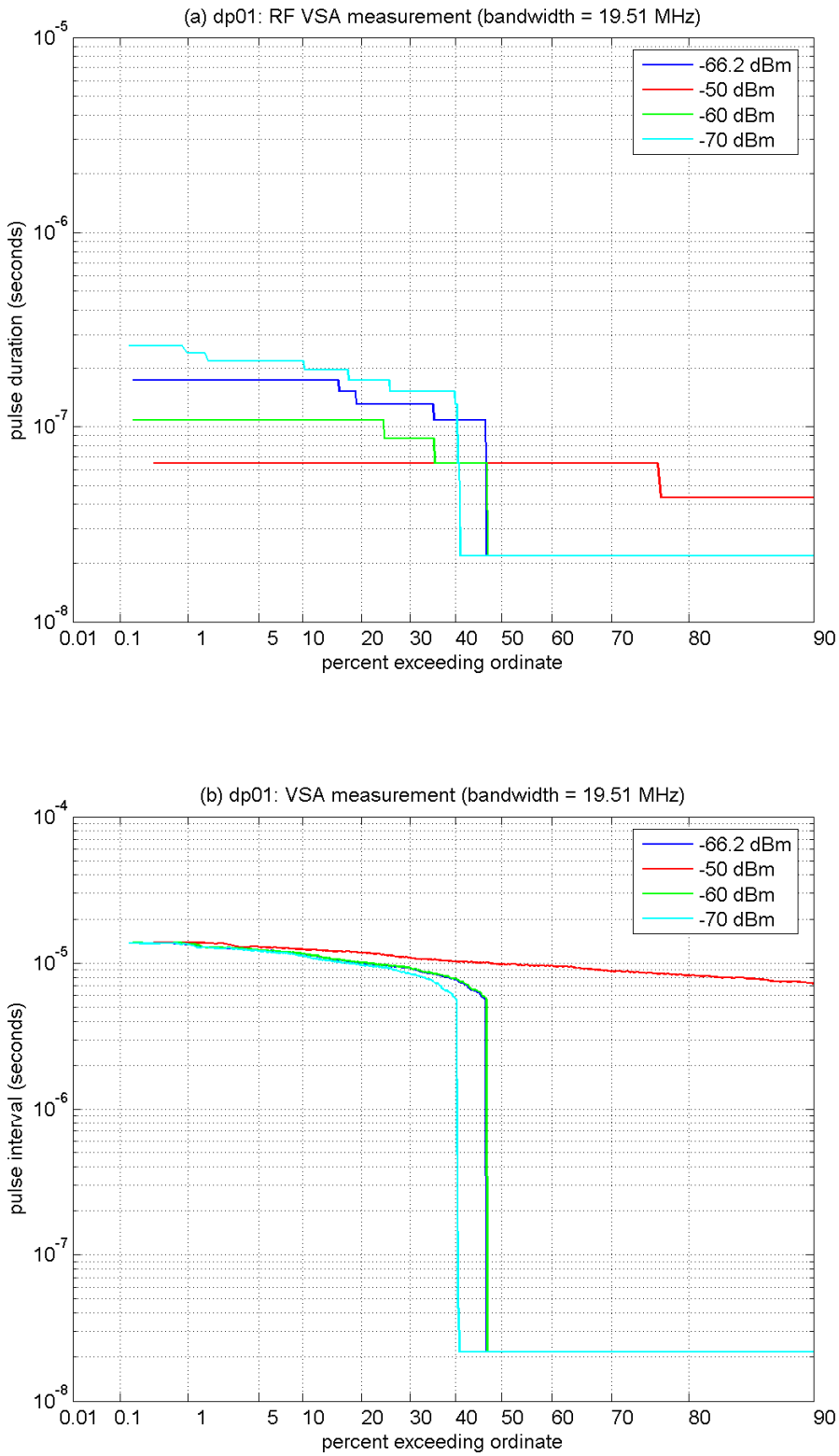

Figure B-6. RF temporal analyses of DP-01 (T_{pulse} = 10,000 ns, w = 0.094 ns, f_D = 0.5).

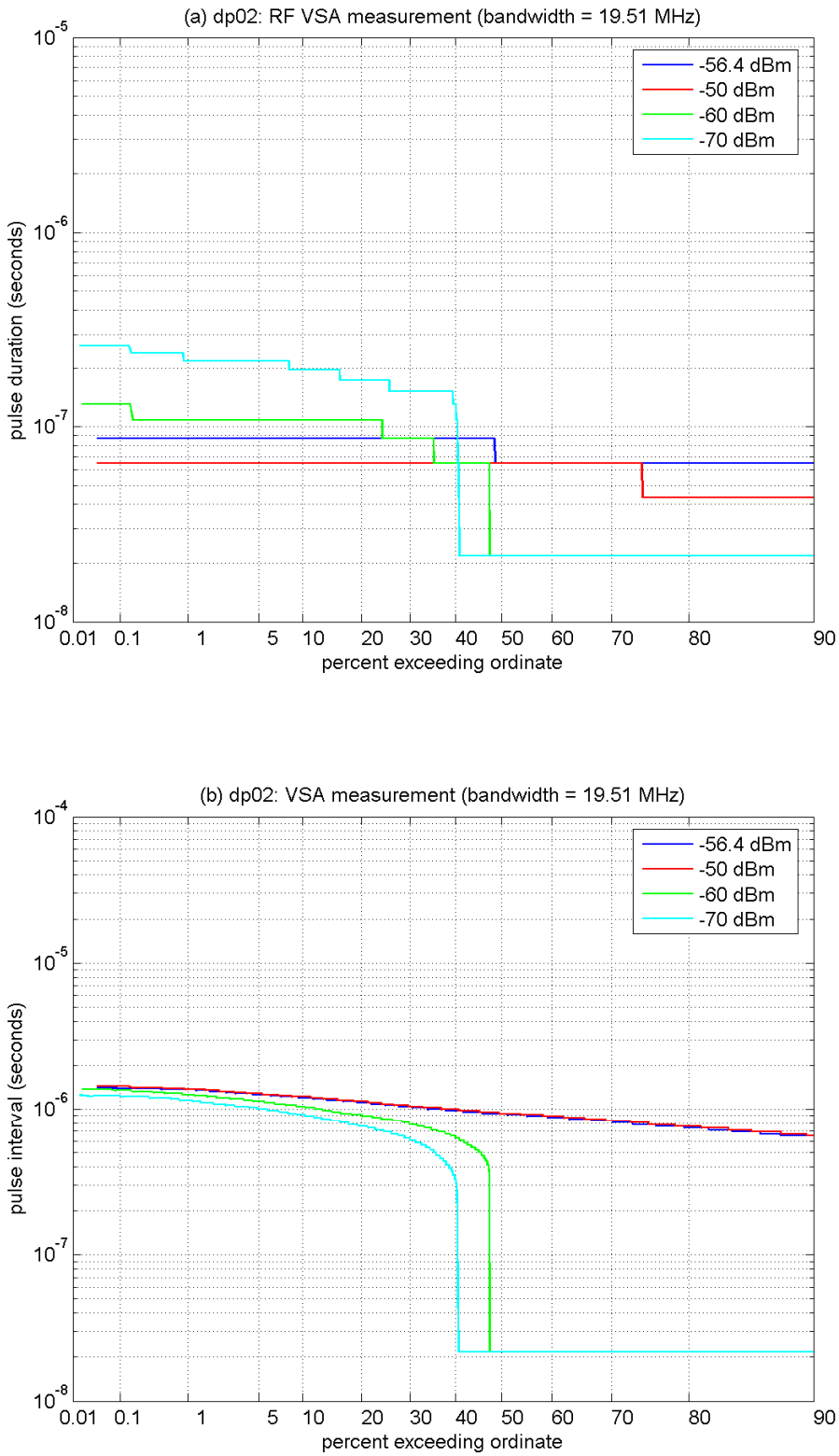

Figure B-7. RF temporal analyses of DP-02 (T_{pulse} = 1000 ns, w = 0.094 ns, f_D = 0.5).

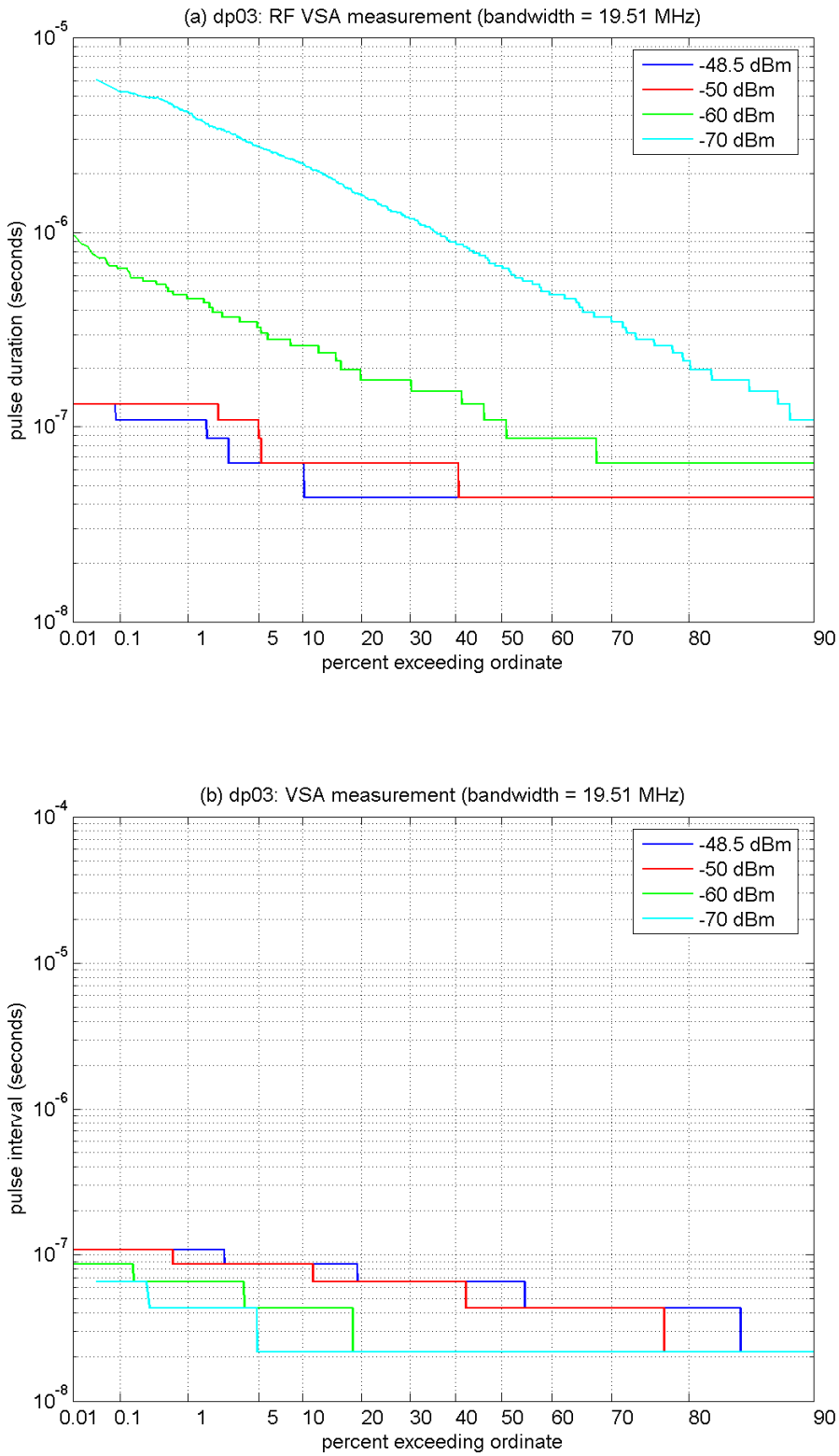

Figure B-8. RF temporal analyses of DP-03 (T_{pulse} = 100 ns, w = 0.094 ns, f_D = 0.5).

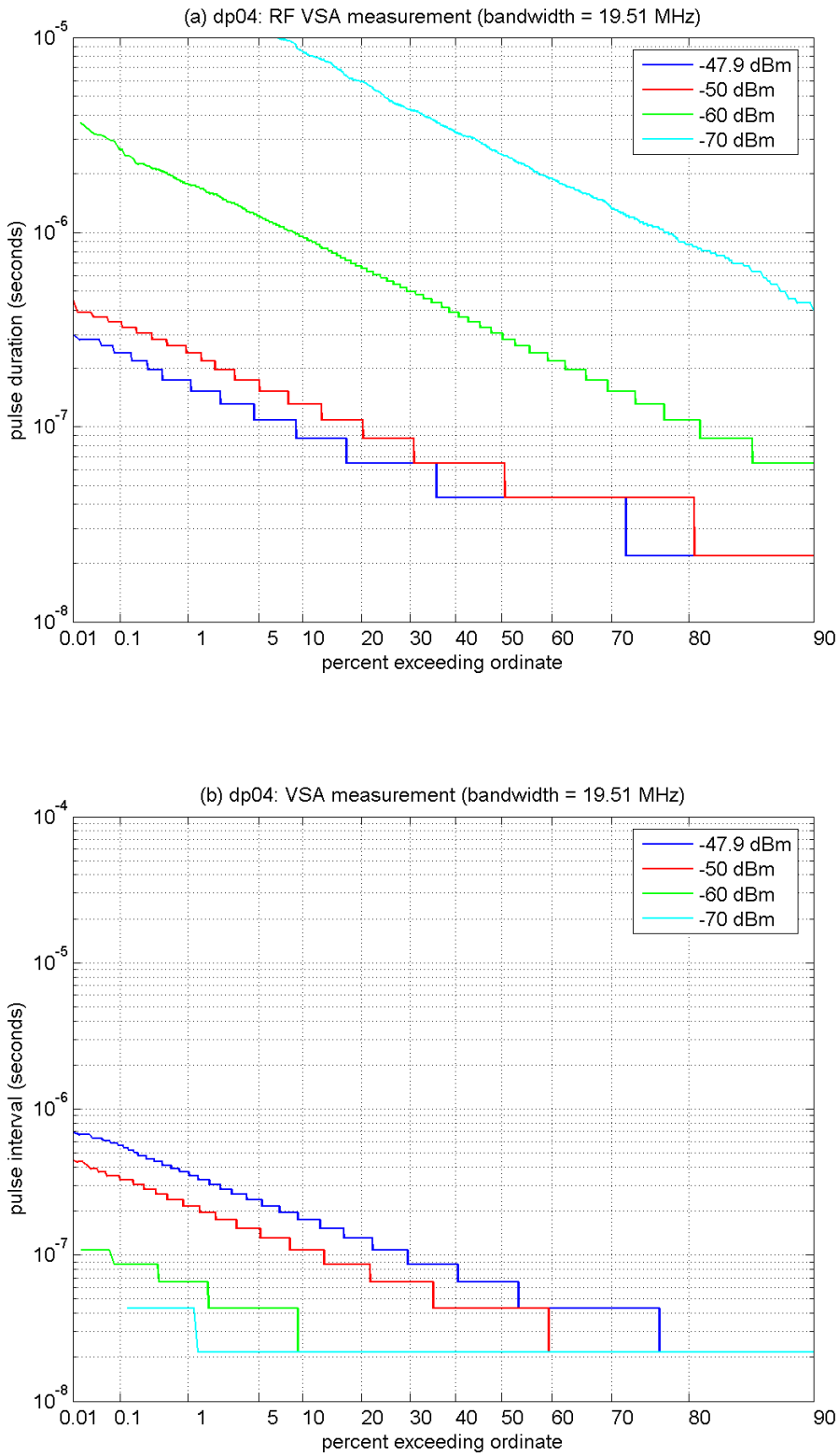

Figure B-9. RF temporal analyses of DP-04 (T_{pulse} = 10 ns, w = 0.094 ns, f_D = 0.5).

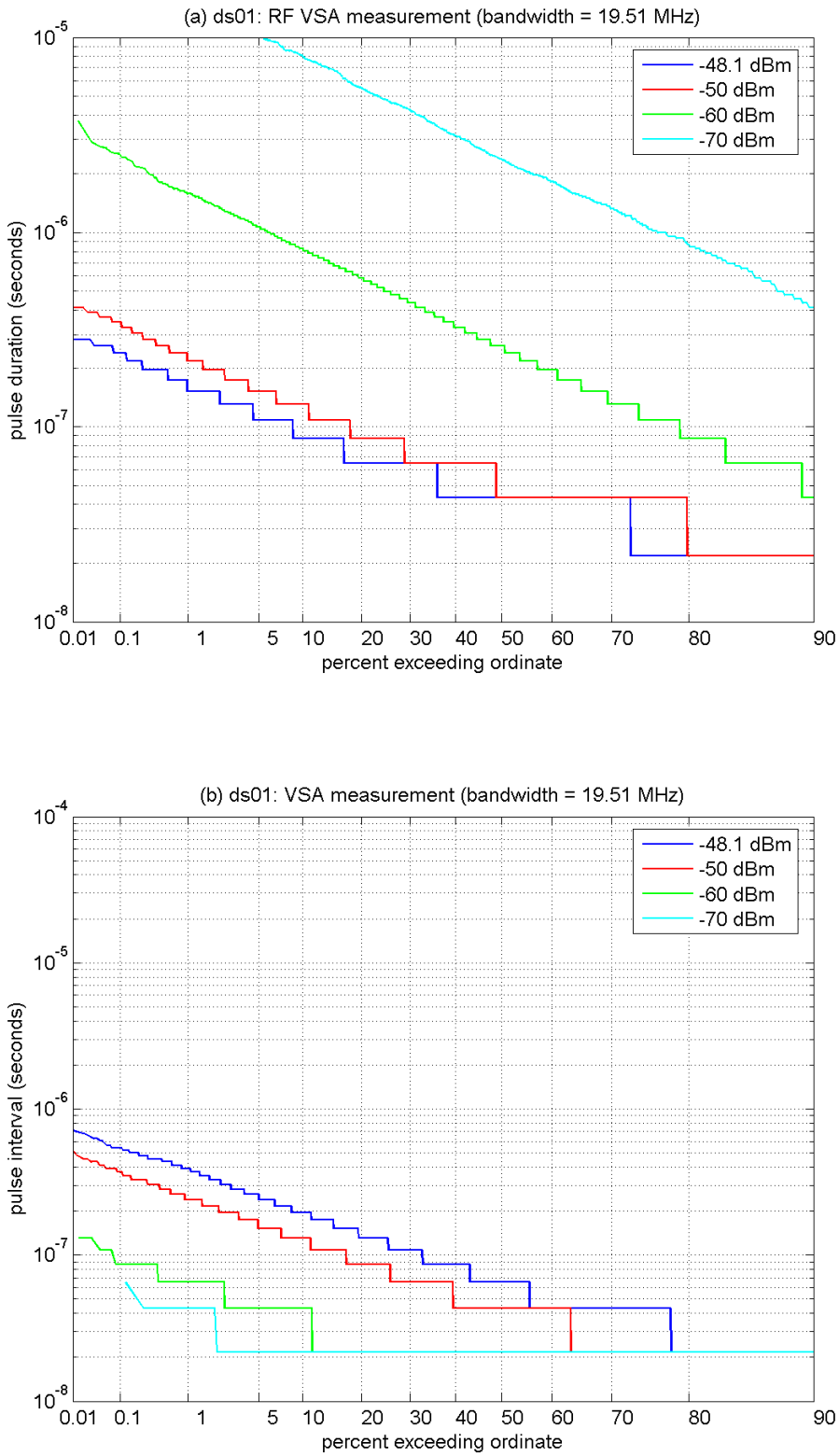

Figure B-10. RF temporal analyses of DS-01 (L = 1).

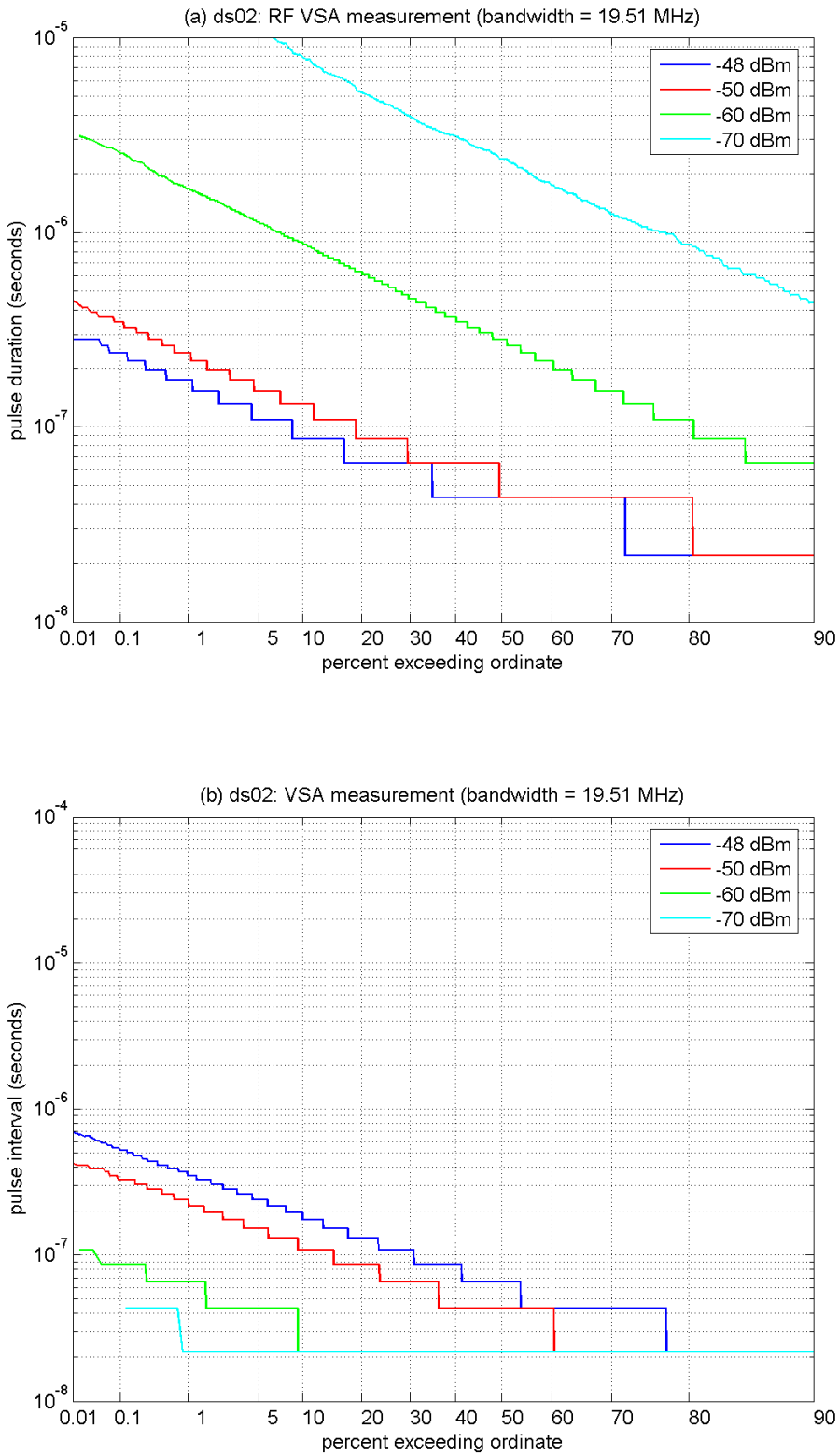

Figure B-11. RF temporal analyses of DS-02 (L = 3, sparse code).

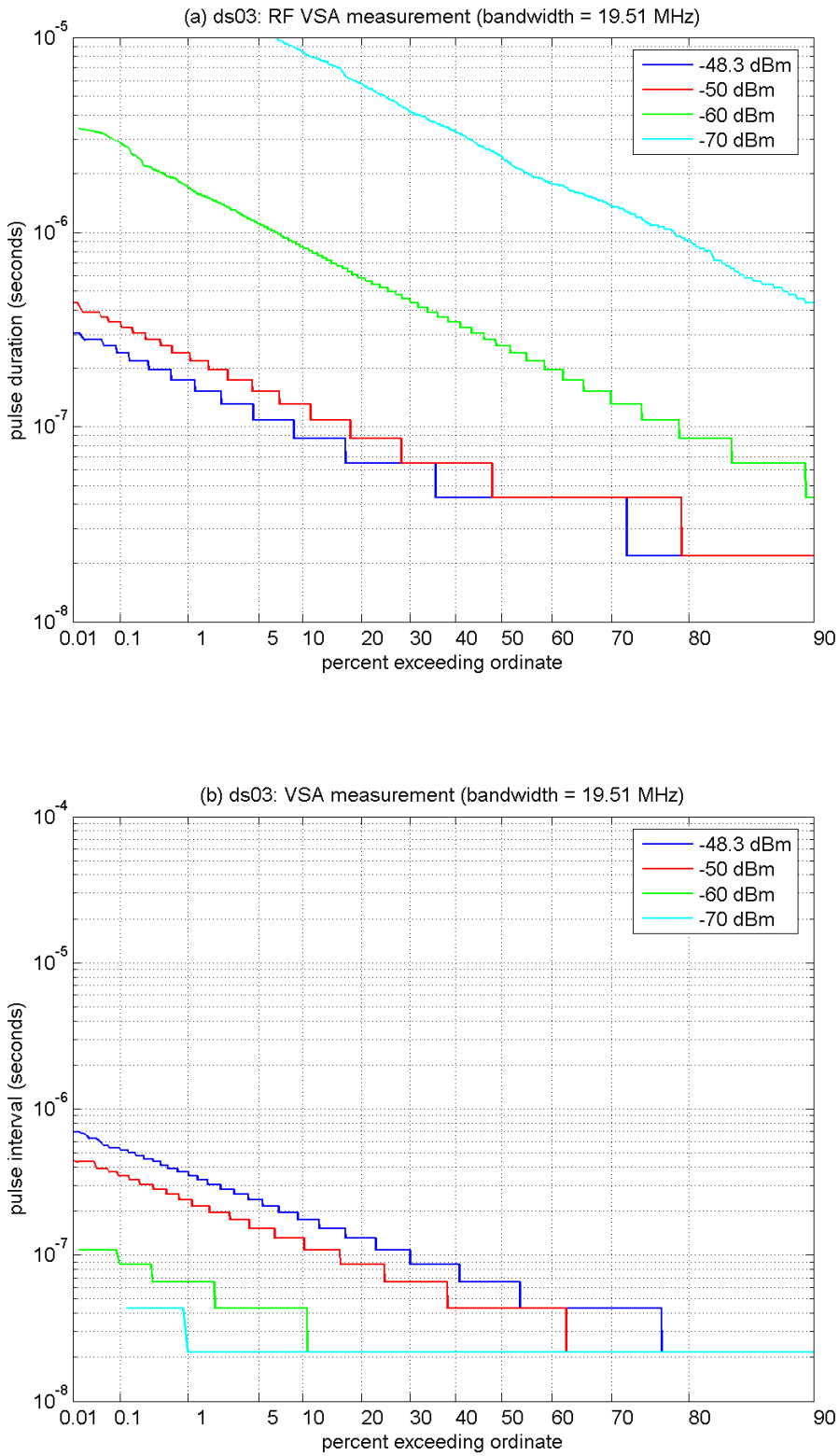

Figure B-12. RF temporal analyses of DS-03 (L = 6, sparse code).

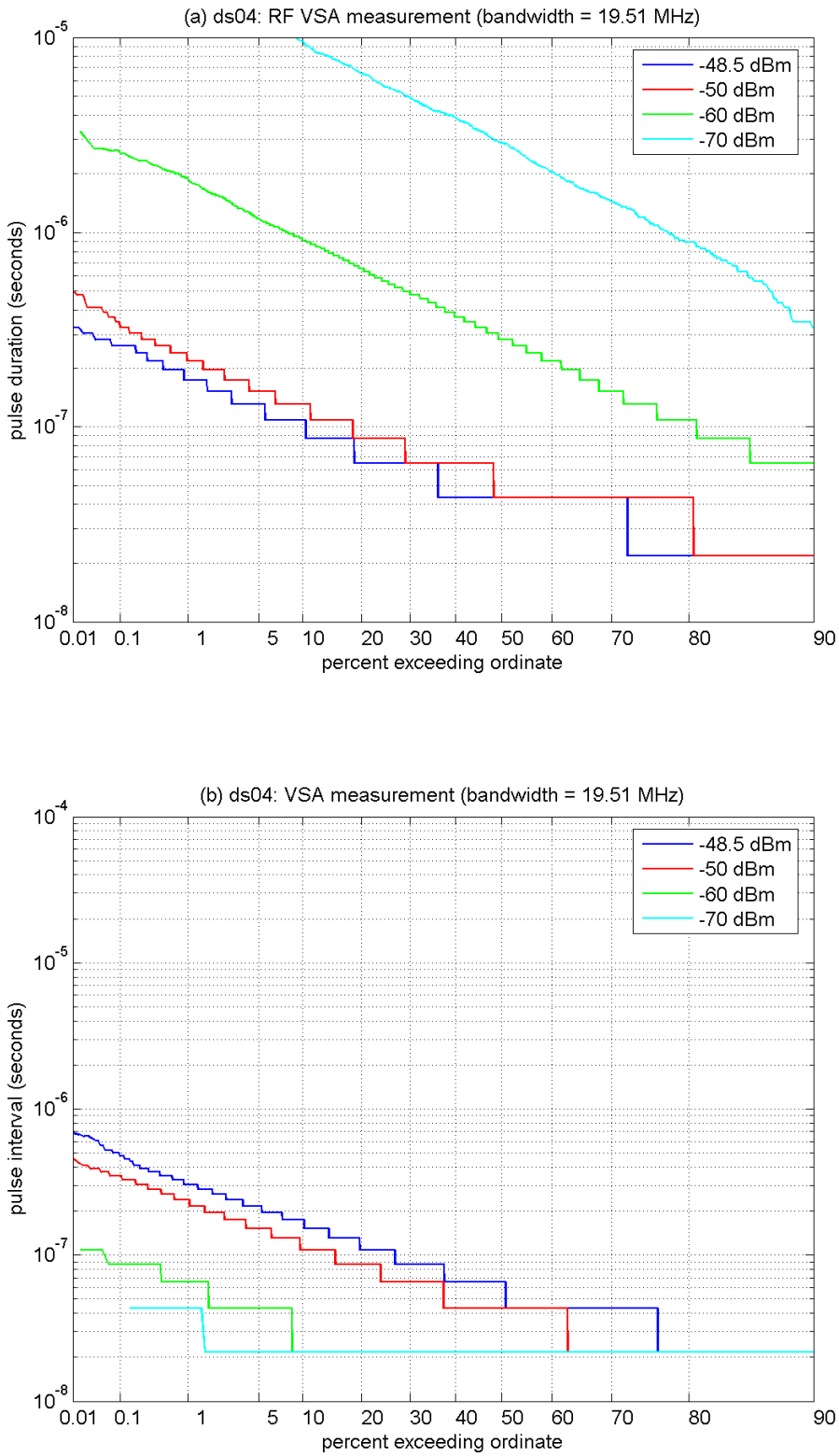

Figure B-13. RF temporal analyses of DS-04 (L = 12, DS code).

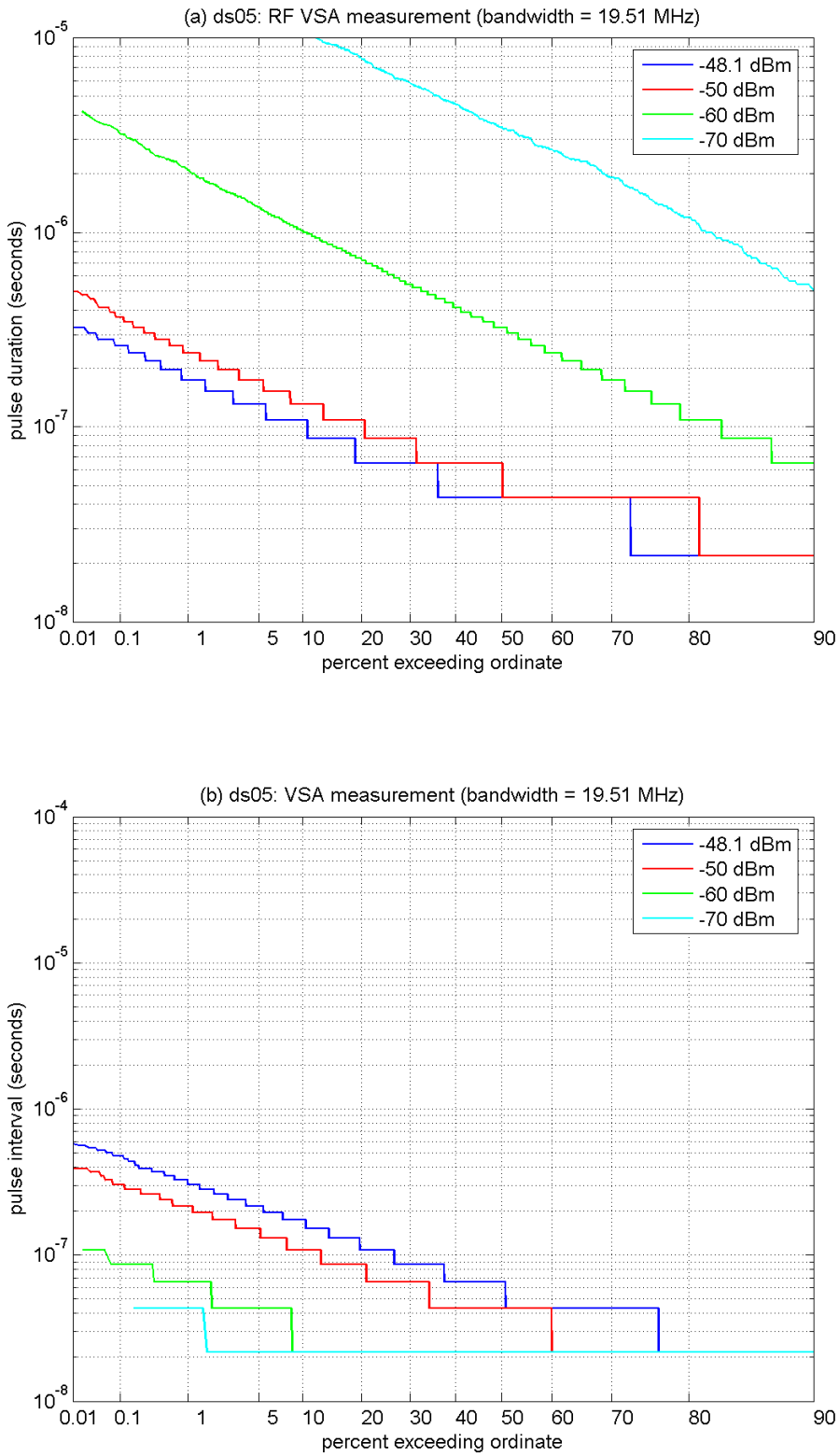

Figure B-14. RF temporal analyses of DS-05 (L = 12, sparse code).

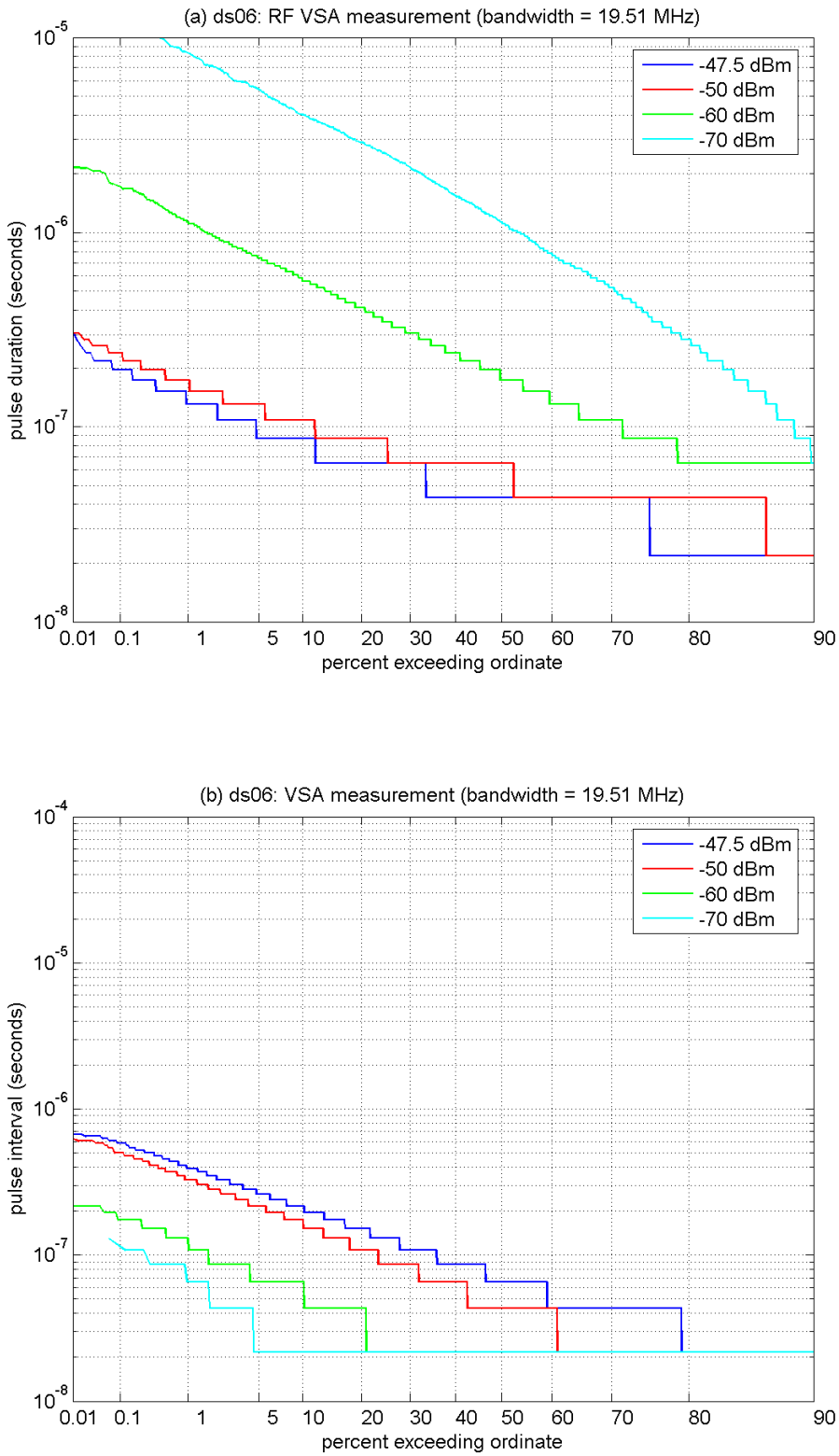

Figure B-15. RF temporal analyses of DS-06 (L = 24, DS code).

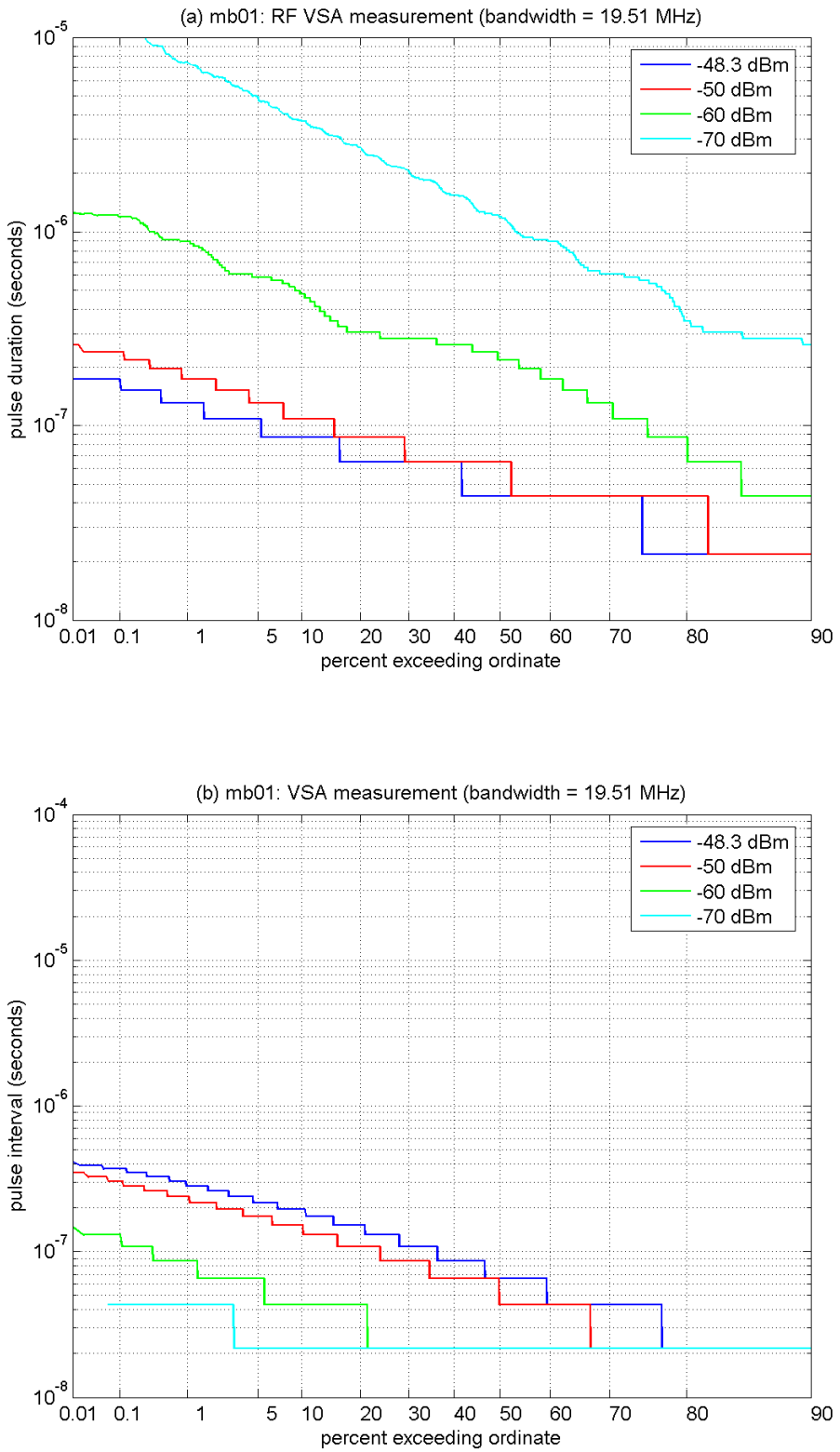

Figure B-16. RF temporal analyses of MB-01 (b = 1).

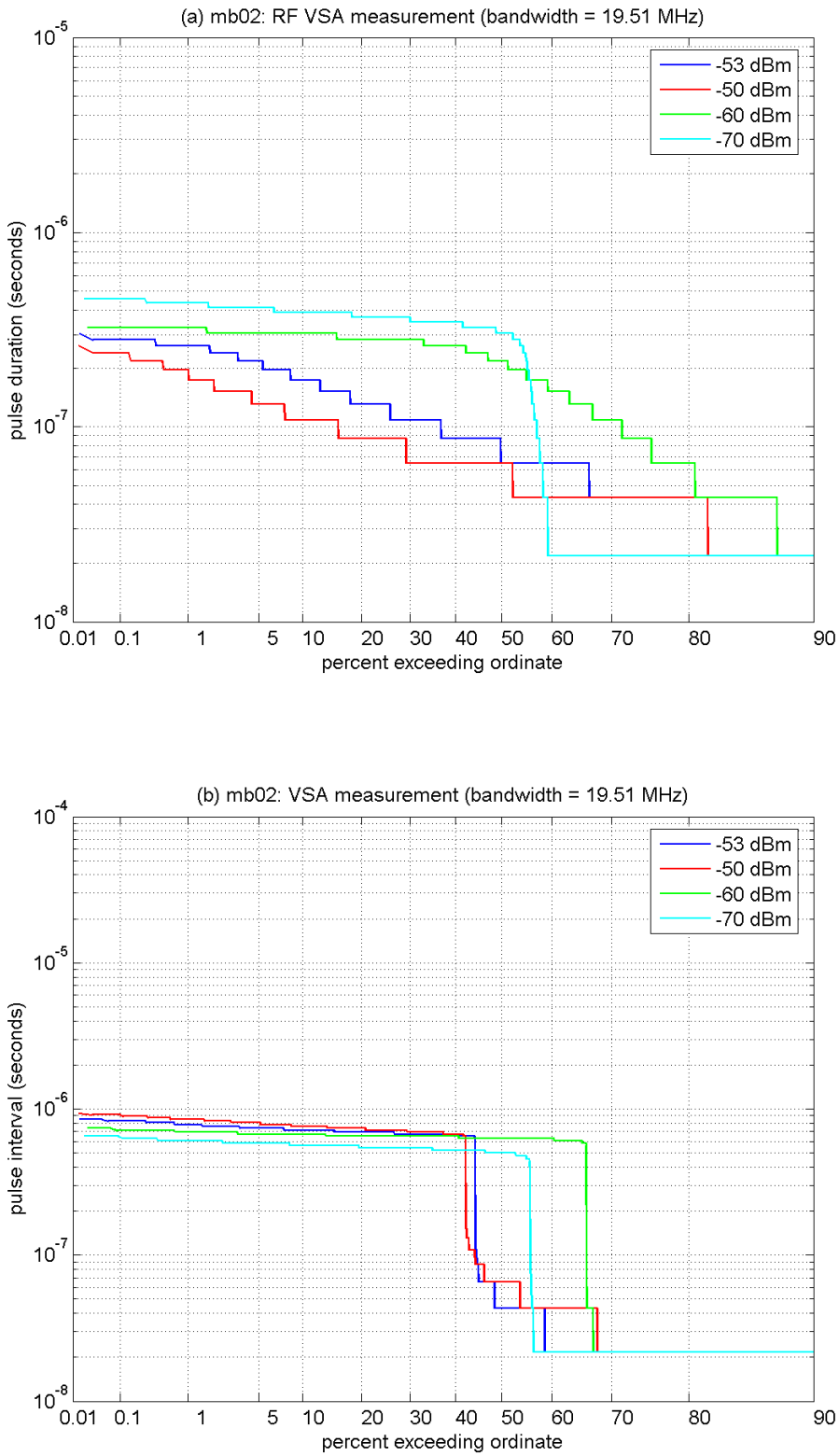

Figure B-17. RF temporal analyses of MB-02 ($b = 3$, $d = 1$).

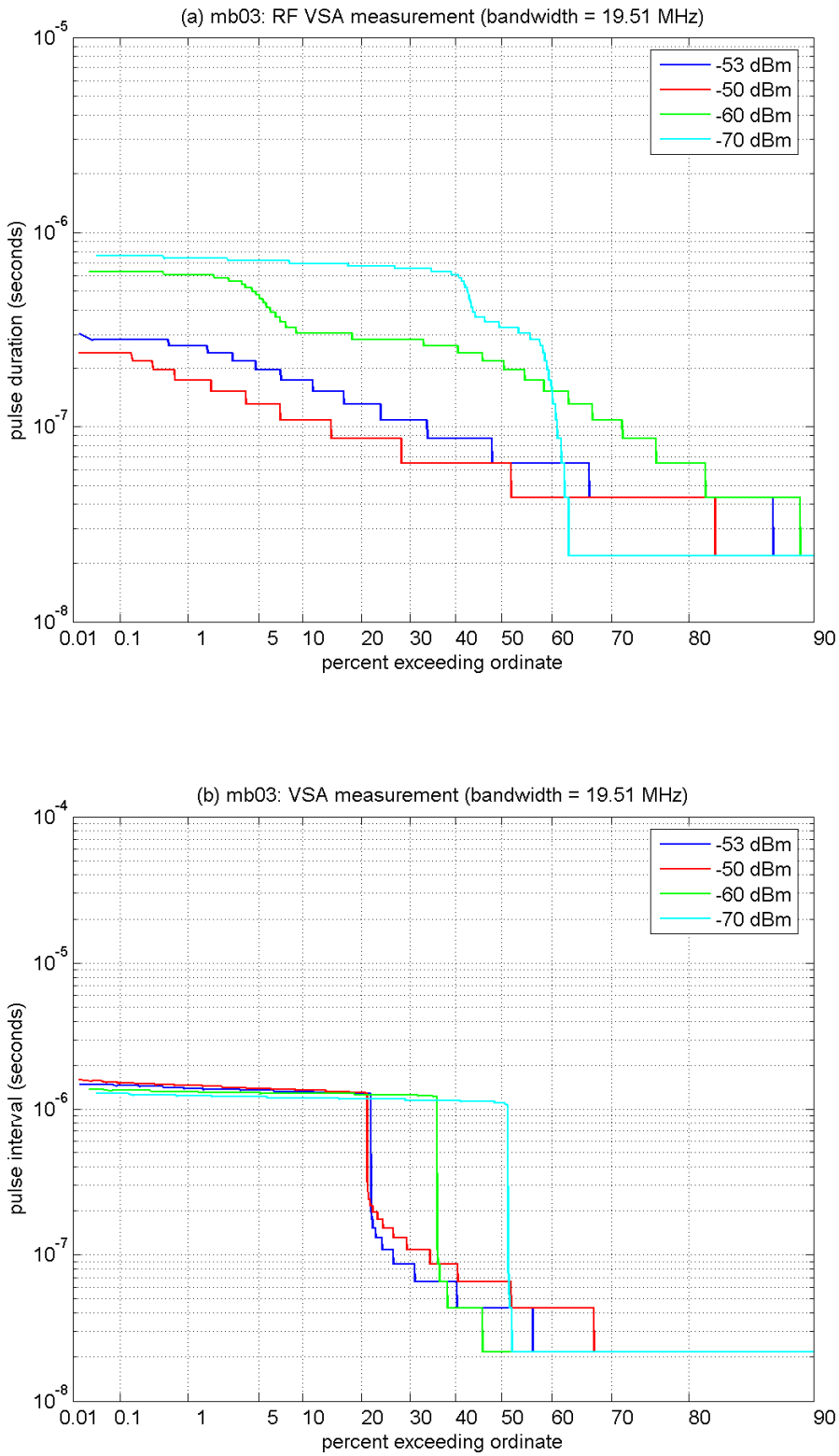

Figure B-18. RF temporal analyses of MB-03 ($b = 3$, $d = 2$).

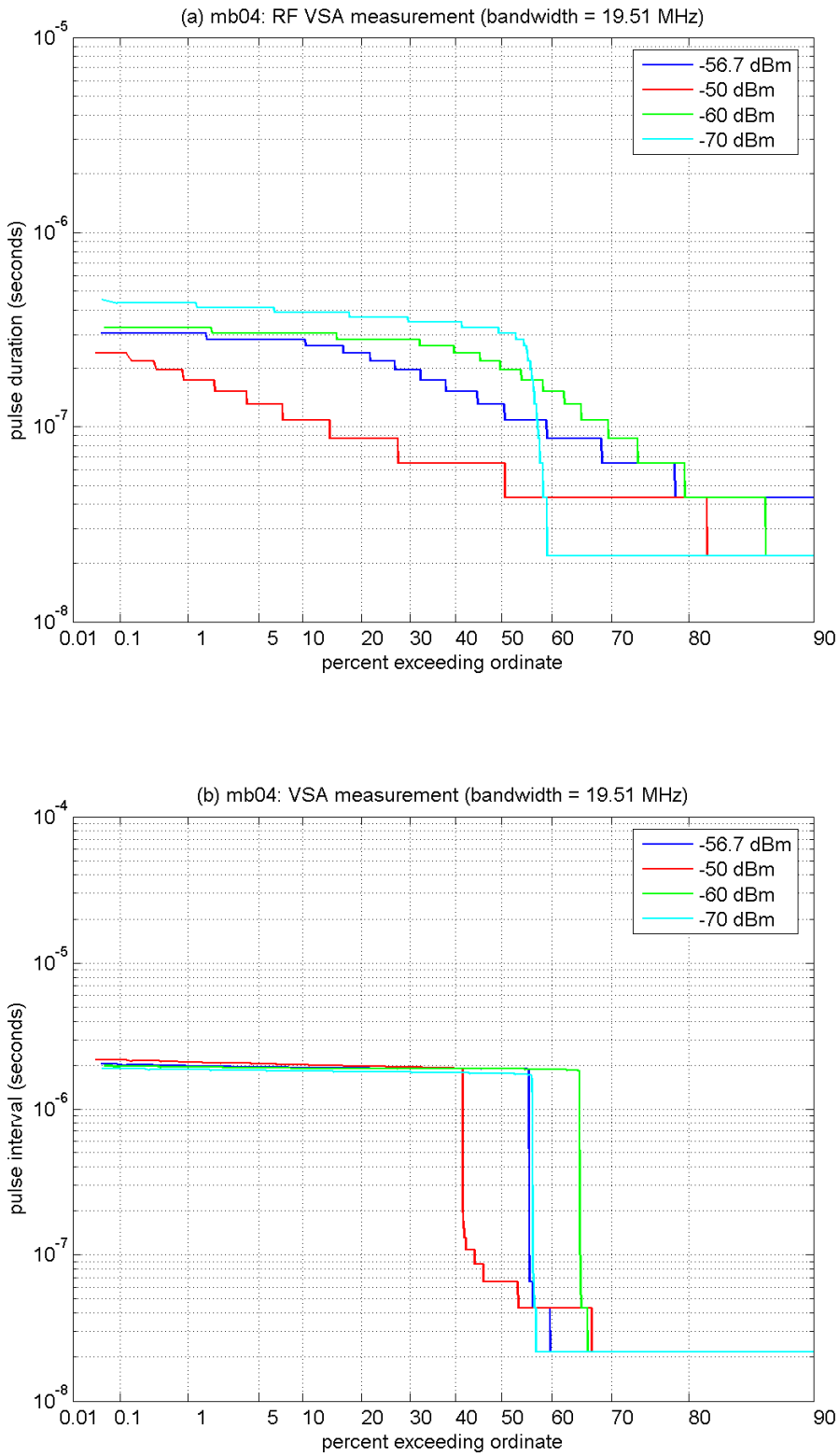

Figure B-19. RF temporal analyses of MB-04 (b = 7, d = 1).

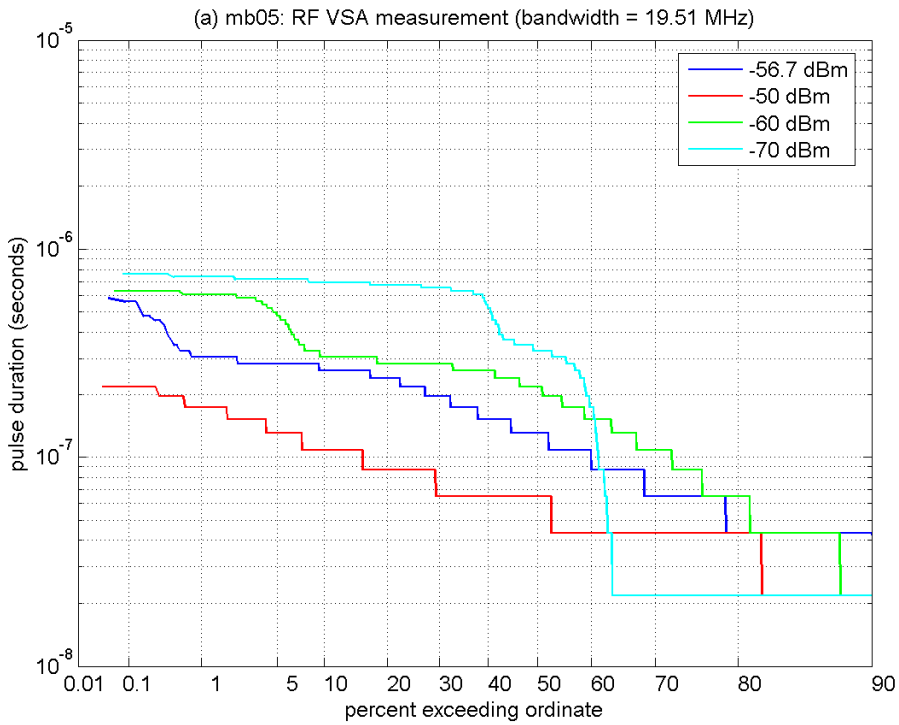

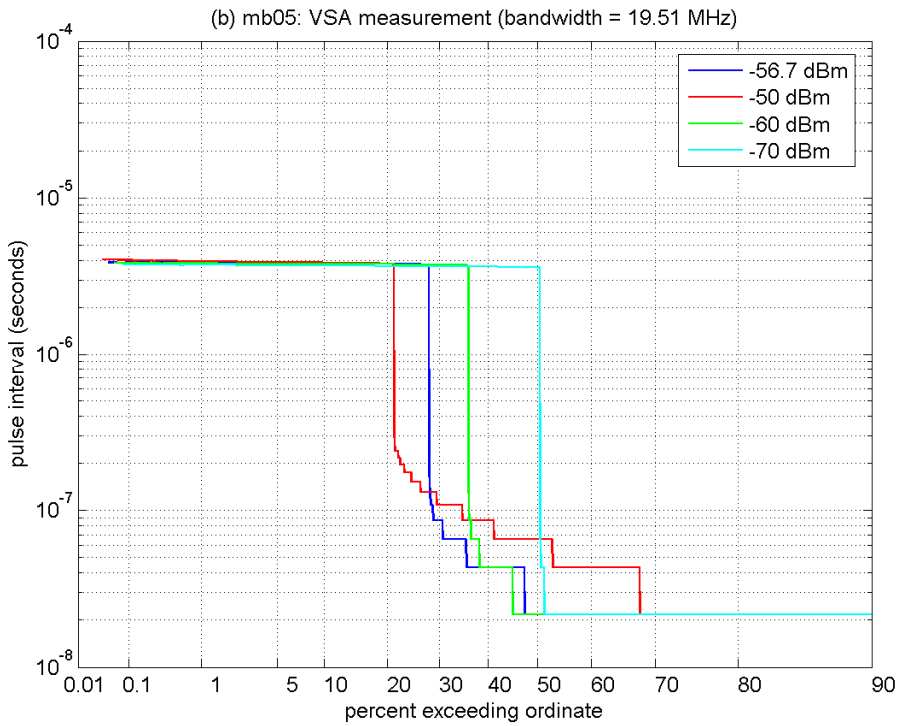

Figure B-20. RF temporal analyses of MB-05 ($b = 7$, $d = 2$).

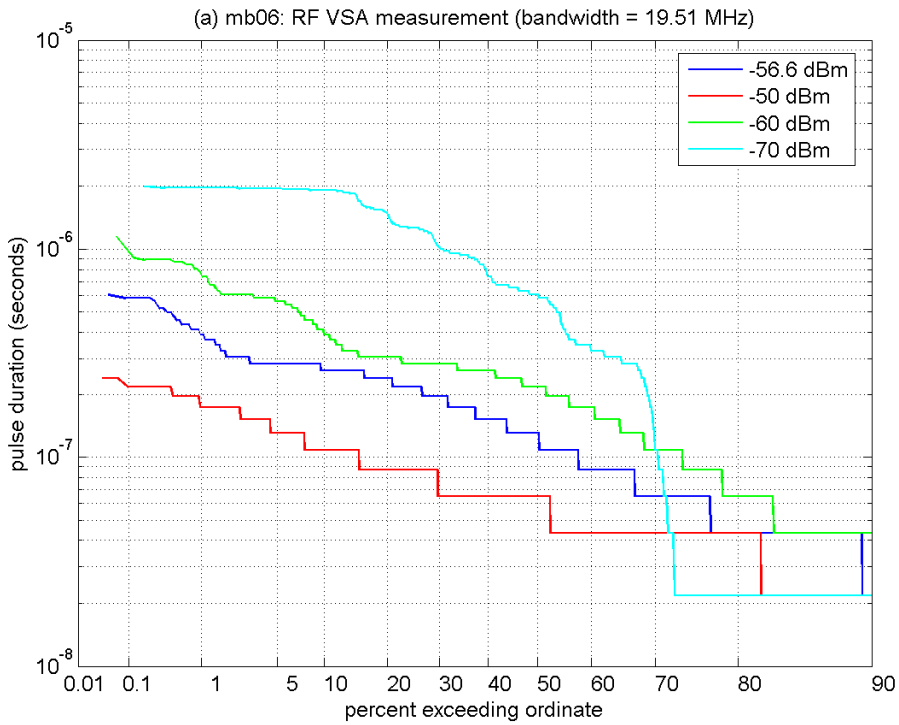

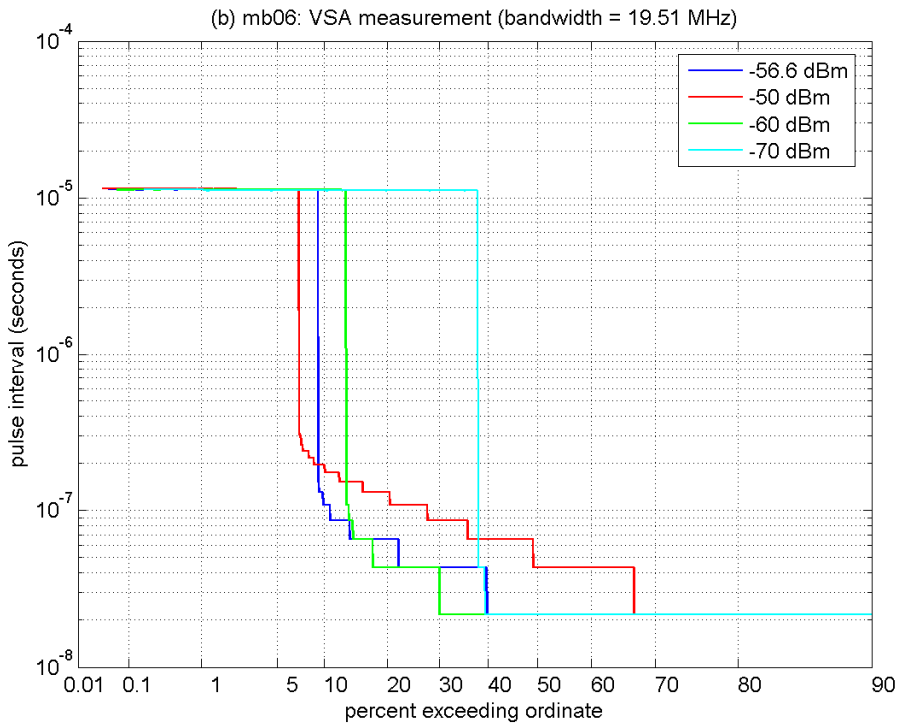

Figure B-21. RF temporal analyses of MB-06 ($b = 7$, $d = 6$).

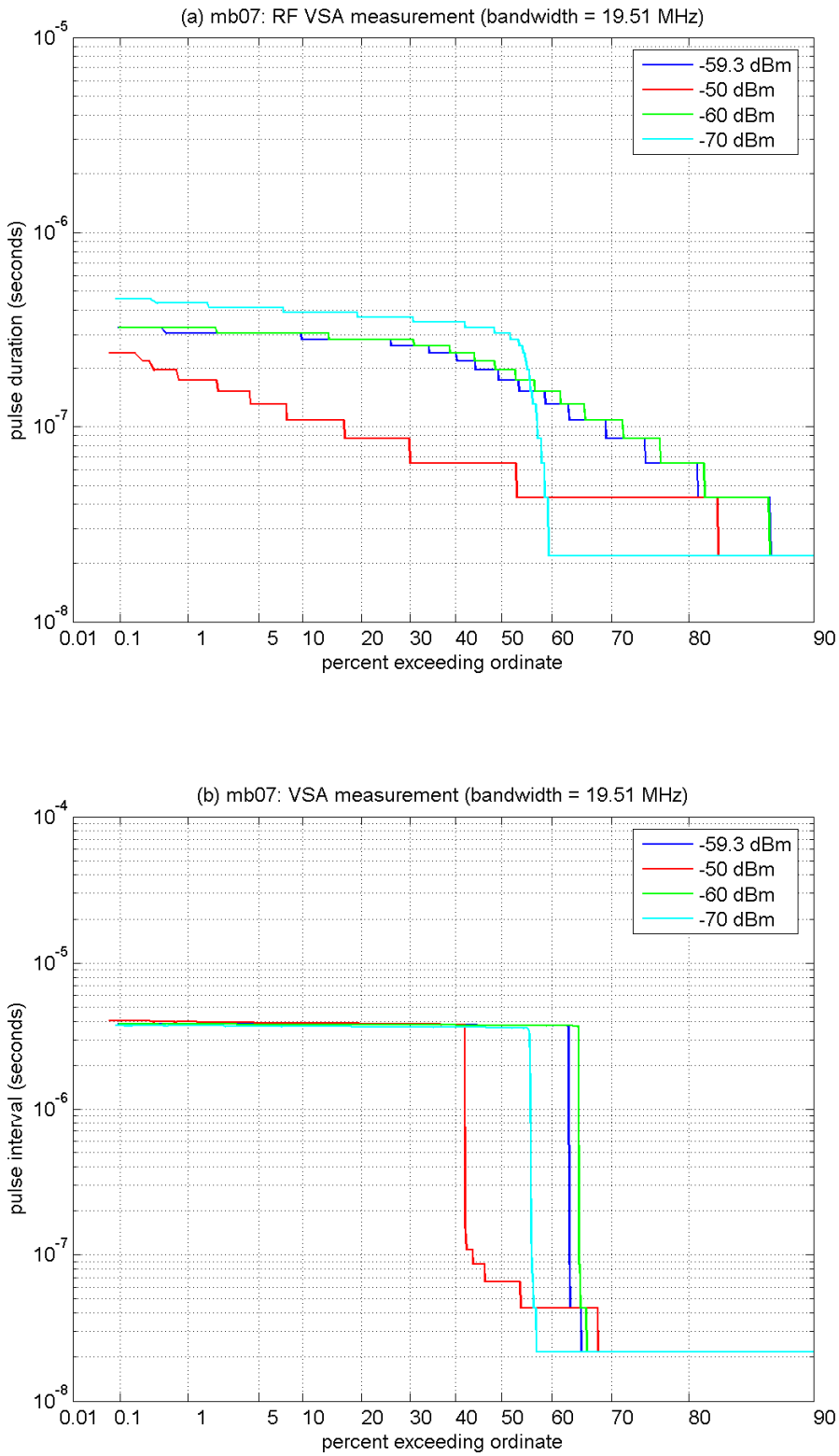

Figure B-22. RF temporal analyses of MB-07 (b = 13, d = 1).

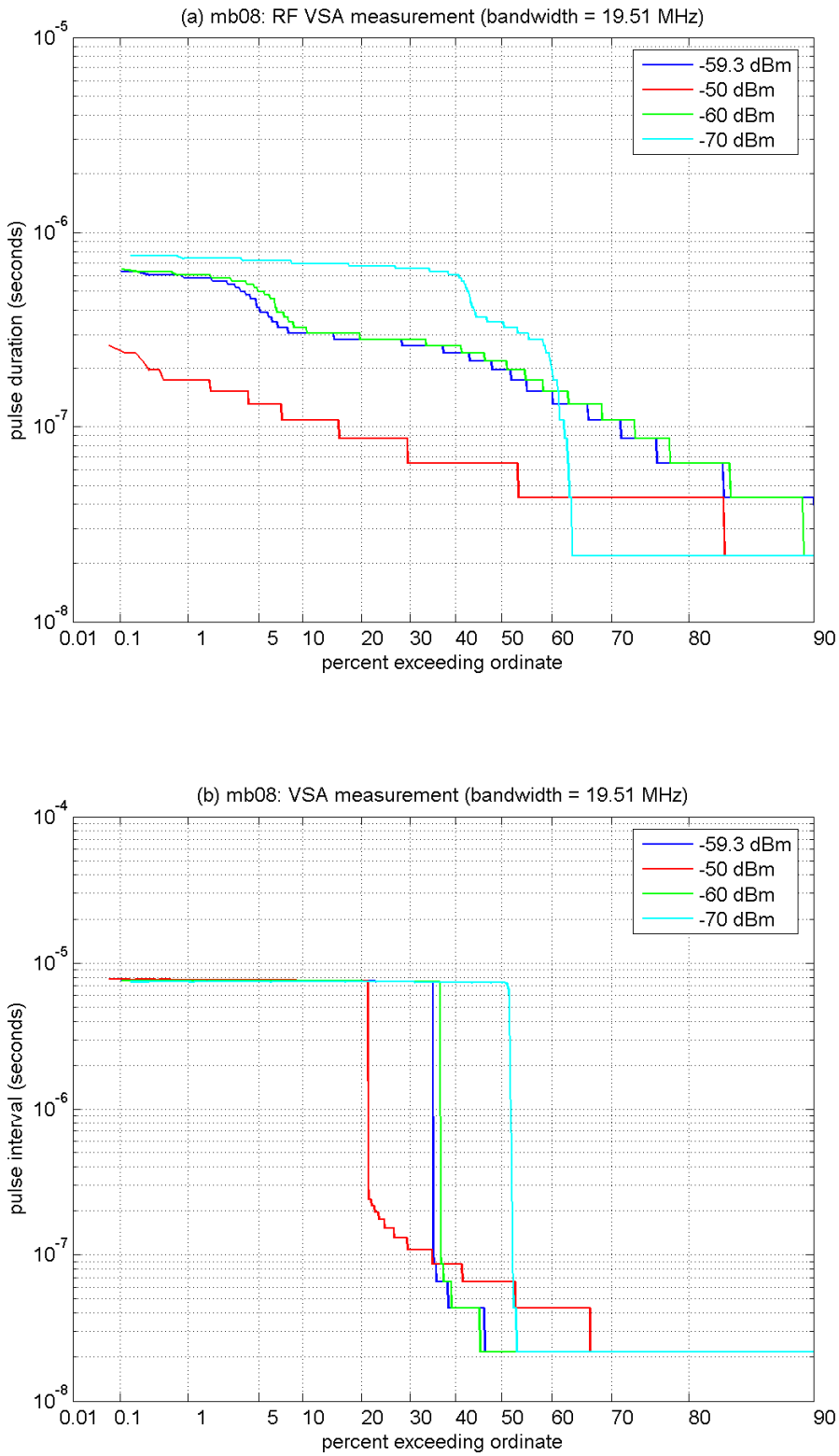

Figure B-23. RF temporal analyses of MB-08 (b = 13, d = 2).

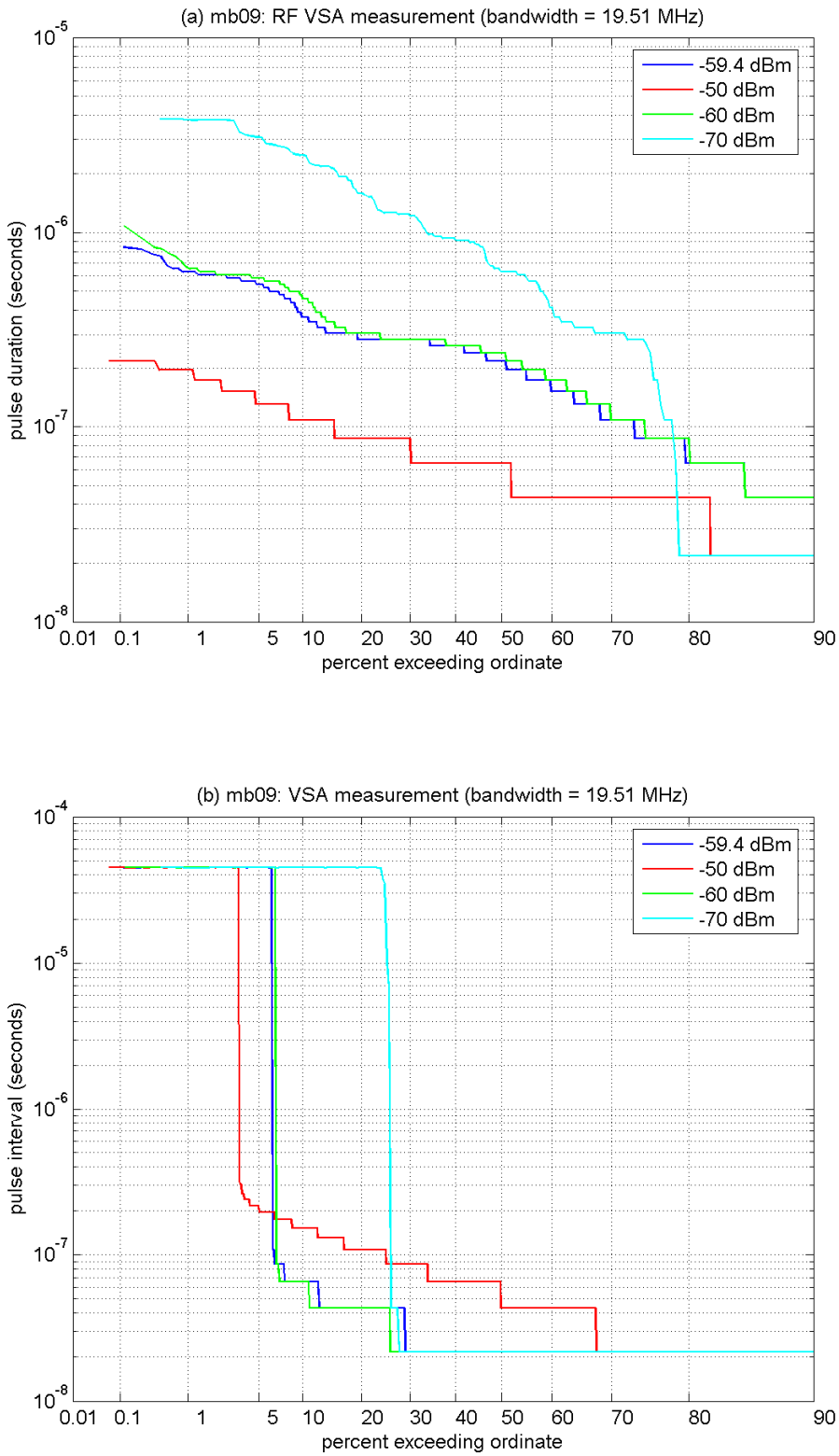

Figure B-24. RF temporal analyses of MB-09 (b = 13, d = 12).

B.3. Amplitude Analysis

This subsection provides measured time series and amplitude probability distributions (*APD*s) of the UWB signals. Odd numbered plots in Figures B-25 – B-62 provide RF measurement results organized as:

(a) Real time series measured with the DO and amplitude time series measured with the VSA and band-limited to B_{DTV} = 19.51 MHz.
(b) *APD*s measured with the VSA and band-limited to 36, B_{DTV}, 10, 1, and 0.1 MHz.

Even numbered plots in Figures B-25 – B-62 provide IF measurement results organized as:

(a) Amplitude time series measured with the VSA and band-limited to B_{DTV}.
(b) *APD*s measured with the VSA and band-limited to B_{DTV}.

Table B-3 provides peak-to-average (*P/A*) values for the UWB signals measured at RF and band-limited to various bandwidths in post-measurement processing. Table B-4 provides *P/A* values for the UWB signals measured at IF under TOV operational conditions and band-limited to B_{DTV} in post-measurement processing.

Table B-3. Measured RF *P/A* (dB) of UWB Signals Band-Limited to Different Bandwidths[‡]

Type	Index	36.0 MHz	B_{DTV}	10.0 MHz	1.0 MHz	0.1 MHz
DP	01	25.4	23.5	20.6	11.5	6.8
	02	15.7	13.8	11.0	6.1	9.4
	03	7.8	5.4	6.0	9.0	10.1
	04	7.7	8.1	9.0	9.4	9.4
DS	01	9.3	9.5	9.5	9.5	9.5
	02	8.8	9.0	9.5	9.8	9.6
	03	7.8	8.1	8.8	9.9	9.7
	04	6.8	6.6	8.0	9.6	9.6
	05	6.8	6.6	8.0	9.8	9.8
	06	6.6	6.8	8.3	9.5	9.8
MB	01	9.6	8.3	6.9	7.5	9.2
	02	13.5	12.8	11.1	5.6	8.6
	03	13.8	12.8	11.3	7.4	8.7
	04	16.9	16.2	14.7	6.4	8.1
	05	17.1	16.4	14.8	10.8	8.2
	06	17.2	16.3	15.0	14.8	10.0
	07	19.4	18.7	17.3	8.6	7.4
	08	19.4	18.9	17.3	13.3	7.6
	09	19.4	18.8	17.4	17.7	14.9

[‡] Shaded cells highlight Rayleigh-amplitude statistics.

Table B-4. Measured IF *P/A* (dB) of UWB Signals at INR_{TOV} and Band-Limited to B_{DTV} [§]

Type	Index	*SNR* = 9 dB	*SNR* = 12 dB	*SNR* = 15 dB
DP	01	23.4	?	?
	02	13.2	14.0	14.1
	03	8.9	7.9	7.2
	04	9.3	8.9	8.7
DS	01	9.6	9.4	9.4
	02	9.5	9.0	9.1
	03	9.1	8.8	8.6
	04	9.1	8.1	7.8
	05	8.9	8.4	7.7
	06	9.4	8.9	8.4
MB	01	9.6	9.3	9.0
	02	11.7	12.7	12.8
	03	11.9	12.4	12.5
	04	13.6	15.1	15.6
	05	12.8	14.5	15.2
	06	12.4	14.0	15.2
	07	15.0	16.6	17.8
	08	14.0	16.0	17.2
	09	12.7	14.6	16.2

[§] Shaded cells highlight Rayleigh-amplitude statistics. Question marks indicate uncertainty in the measurement due to exceedingly high signal voltages overdriving the VSA.

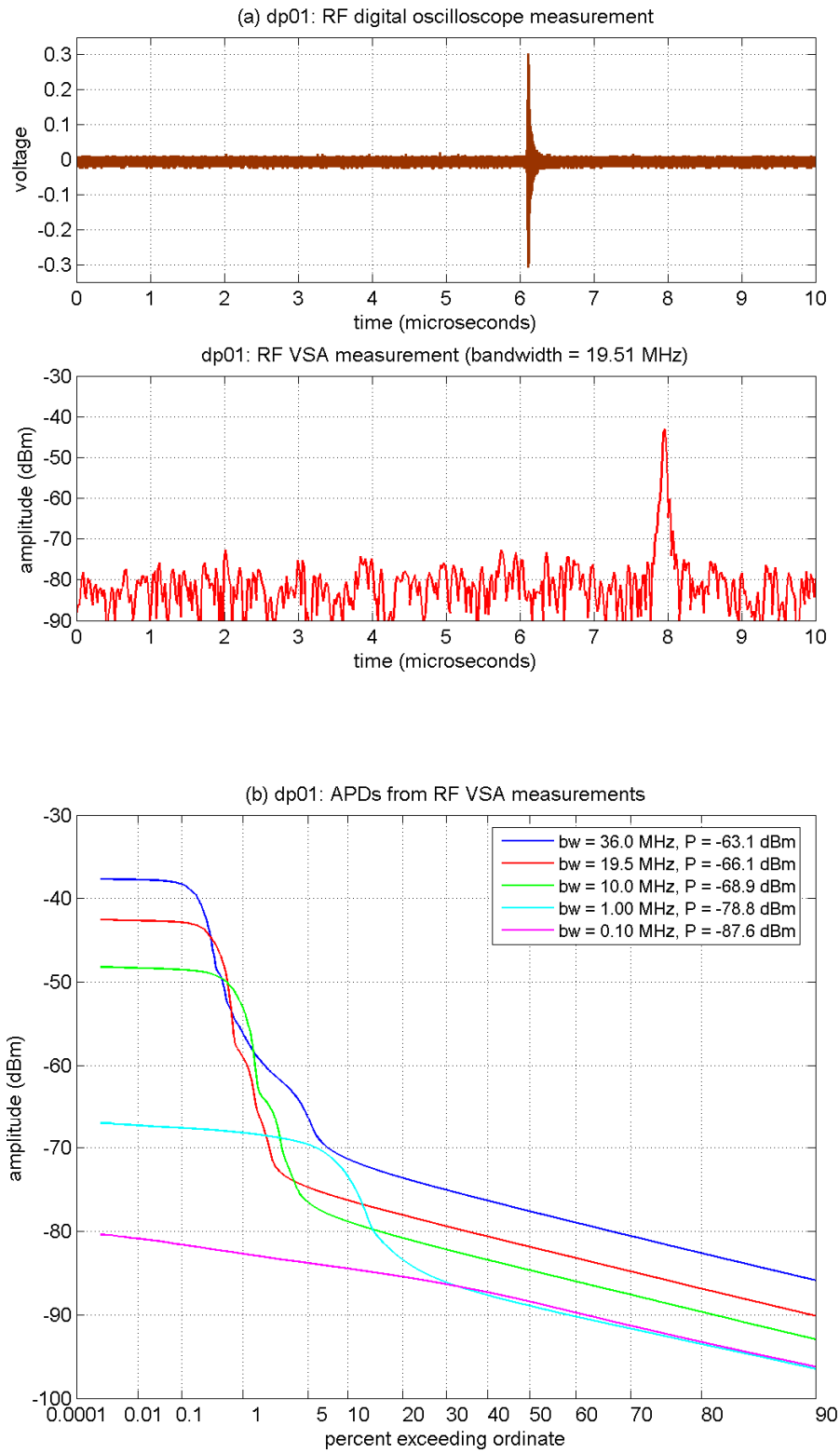

Figure B-25. RF amplitude analyses of DP-01 (T_{pulse} = 10,000 ns, w = 0.094 ns, f_D = 0.5).

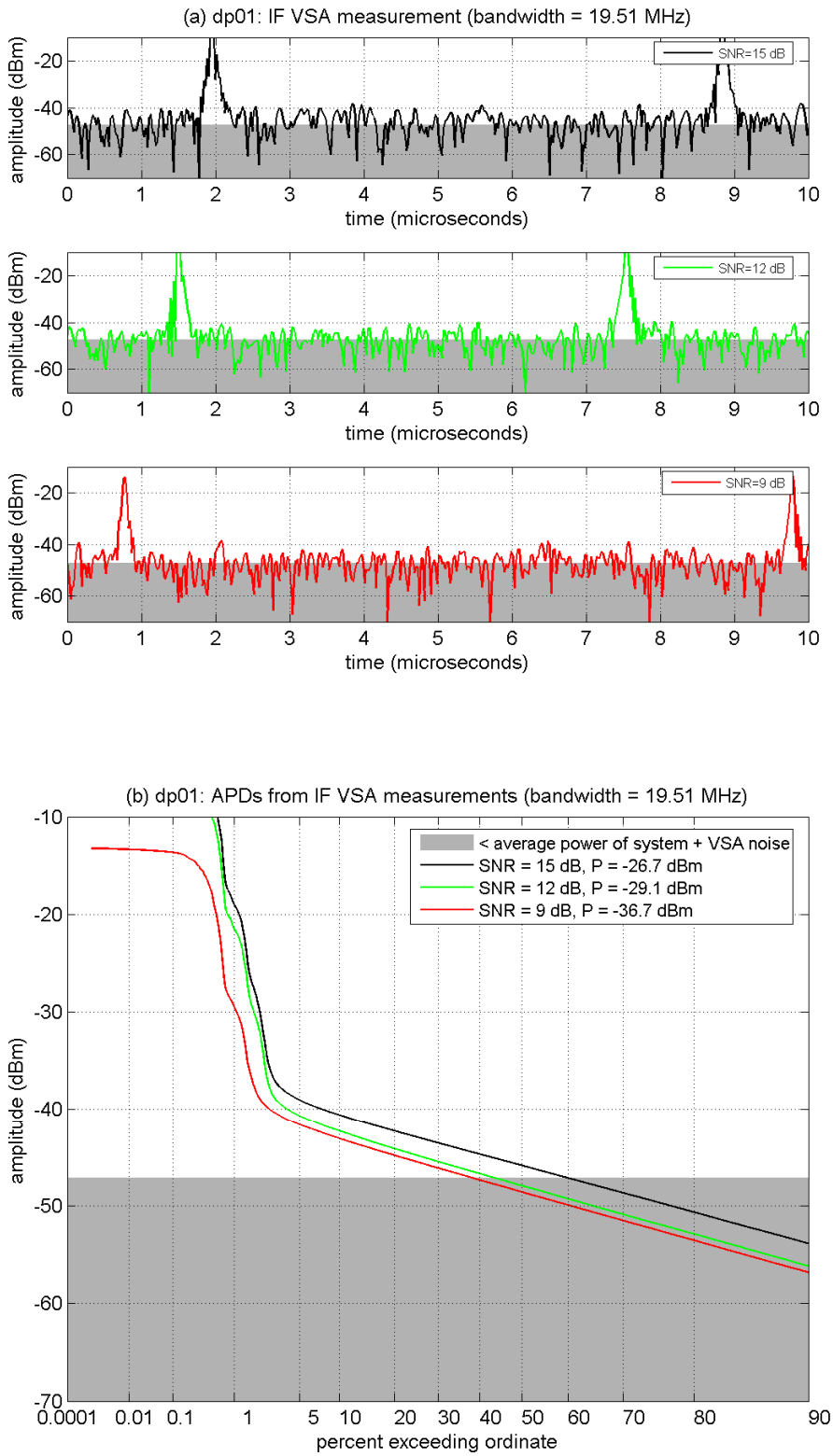

Figure B-26. IF amplitude analyses of DP-01 at INR_{TOV}.

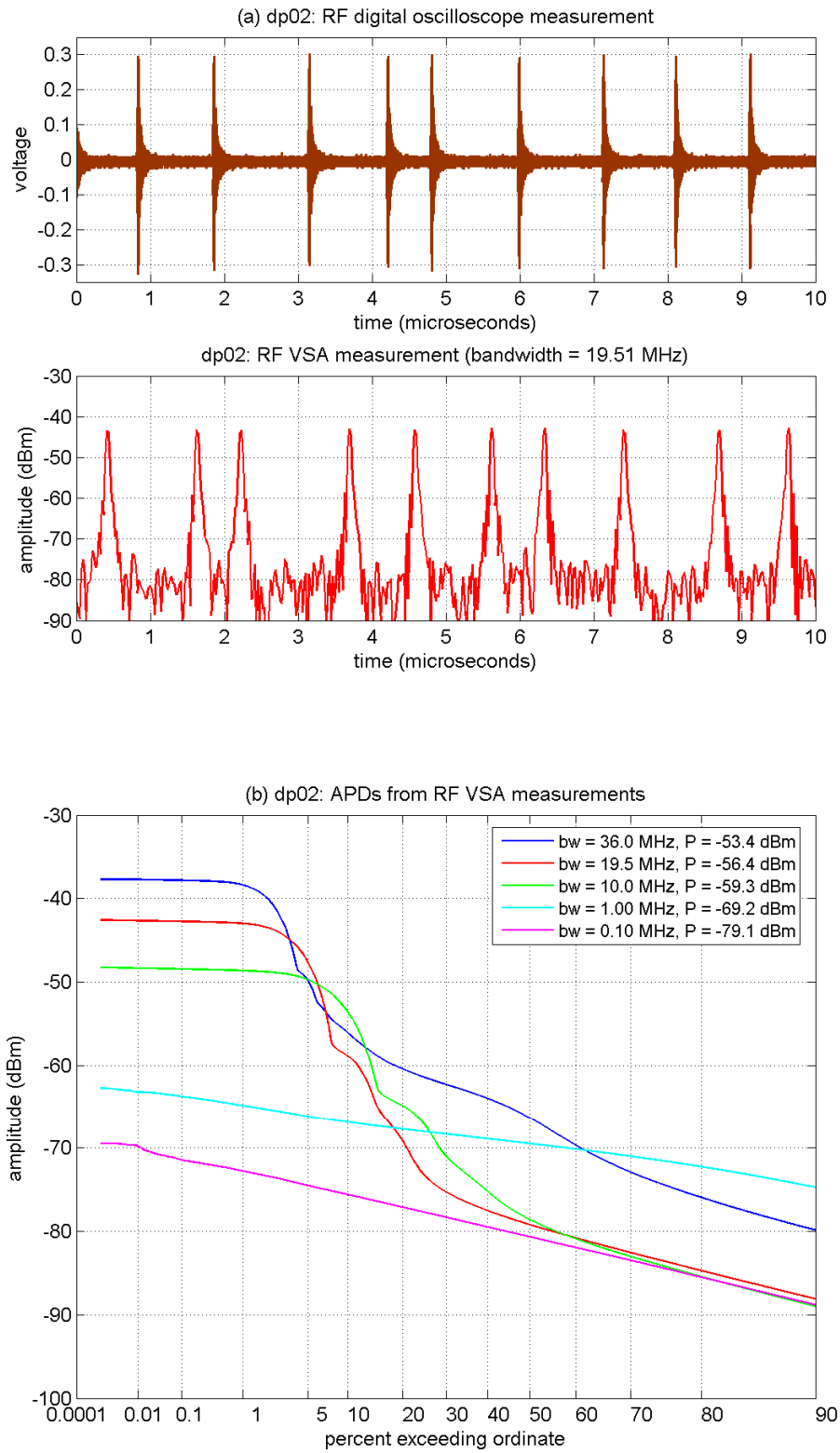

Figure B-27. RF amplitude analyses of DP-02 (T_{pulse} = 1000 ns, w = 0.094 ns, f_D = 0.5).

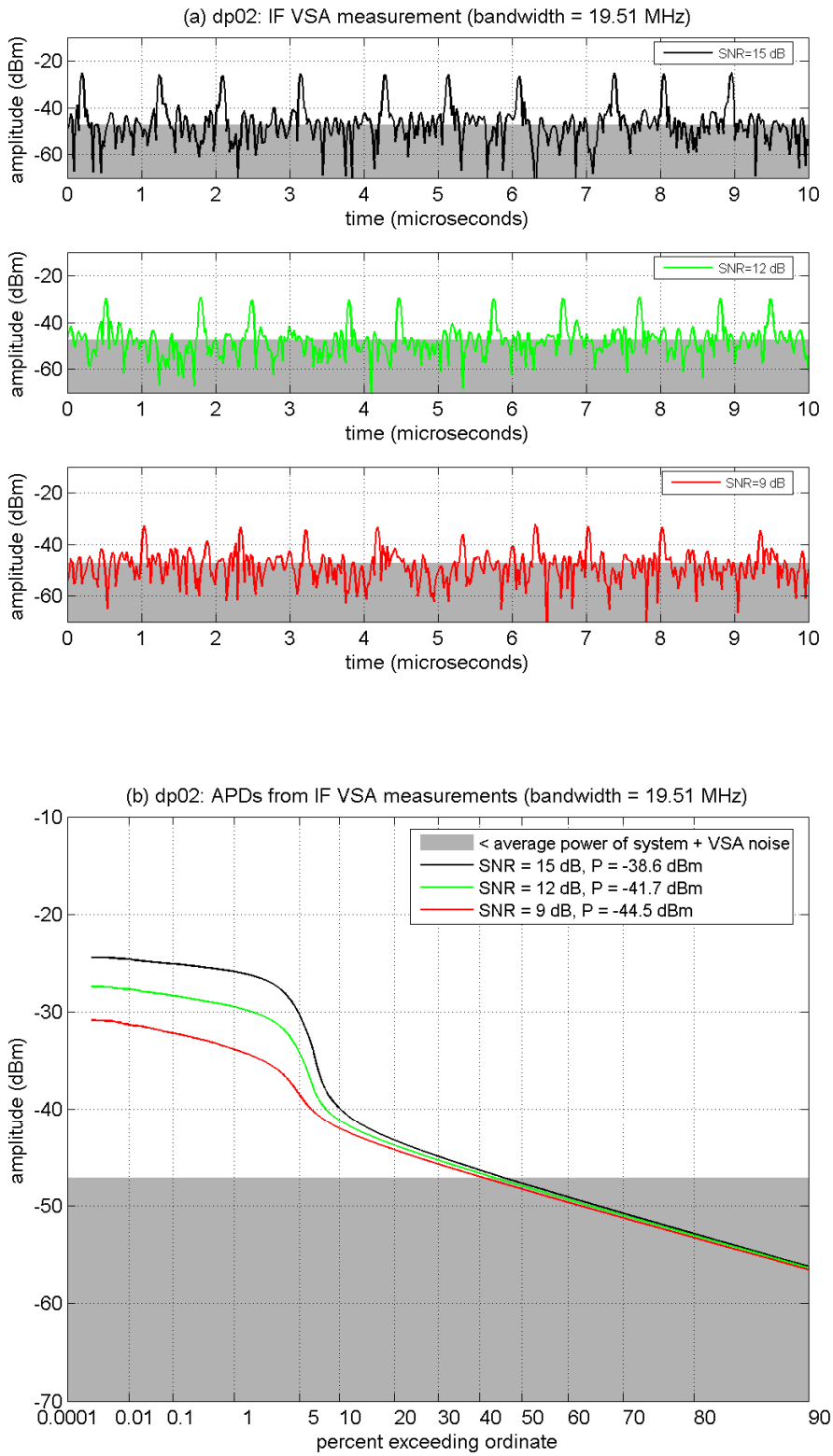

Figure B-28. IF amplitude analyses of DP-02 at INR_{TOV}.

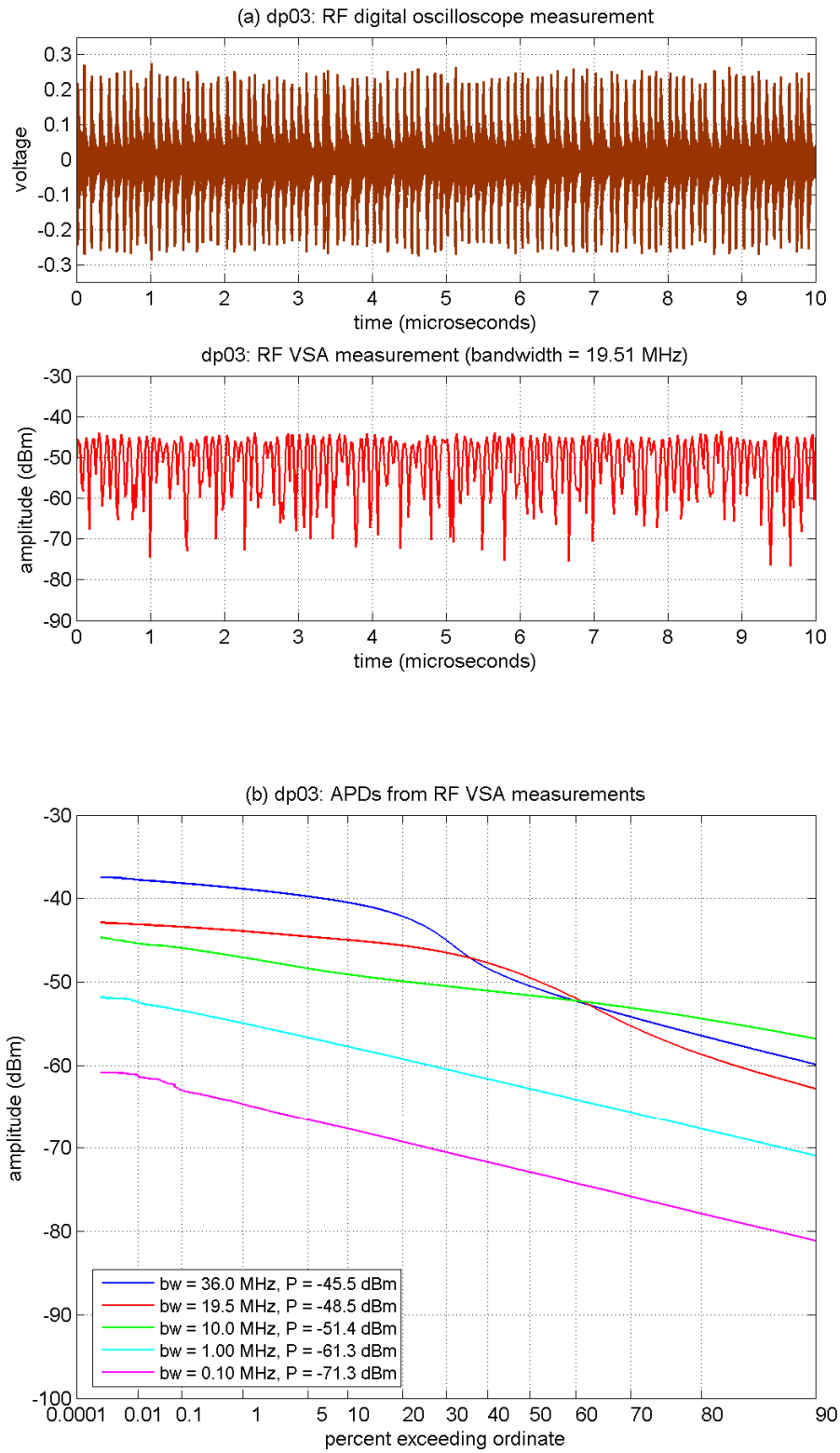

Figure B-29. RF amplitude analyses of DP-03 (T_{pulse} = 100 ns, w = 0.094 ns, f_D = 0.5).

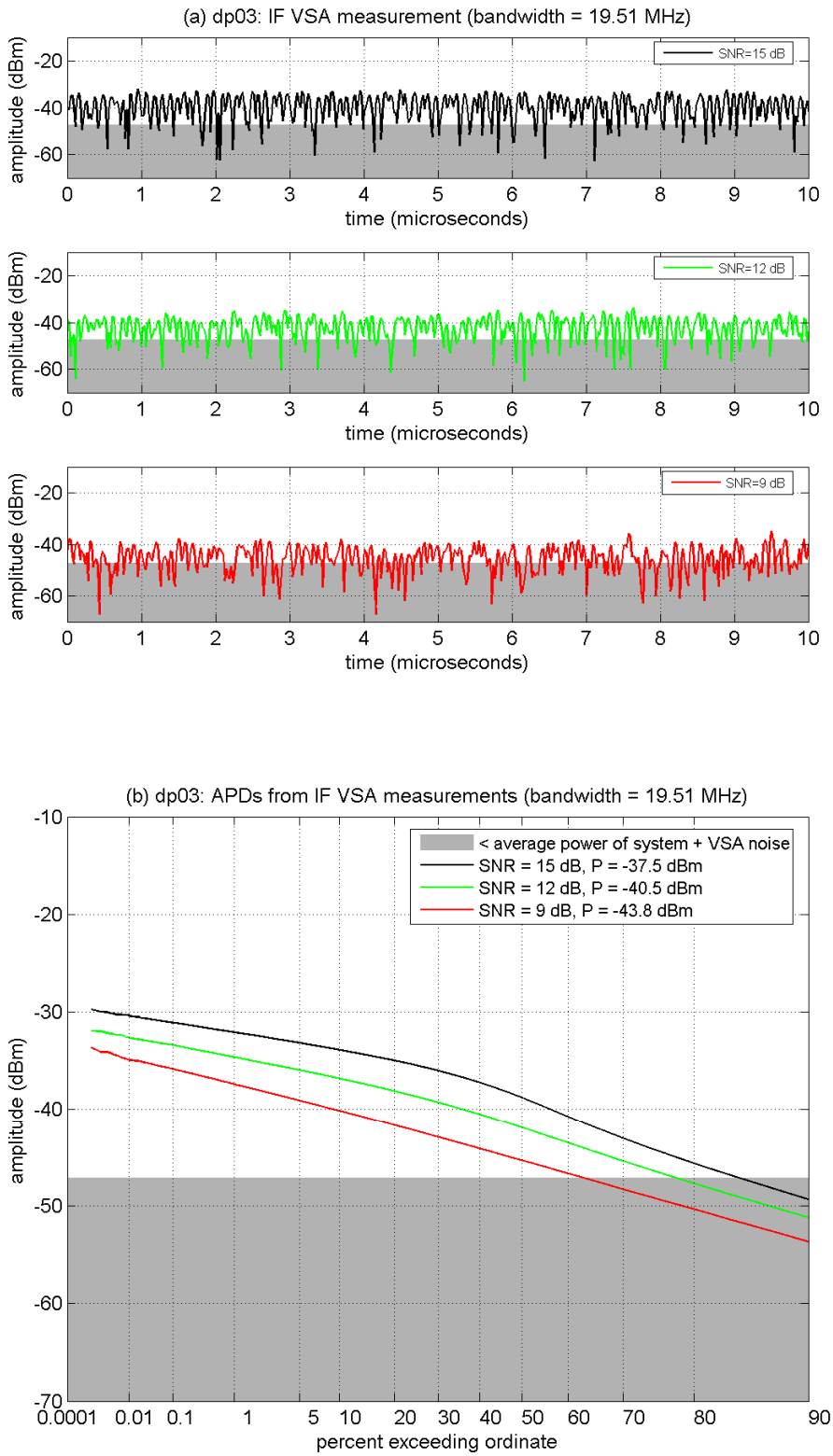

Figure B-30. IF amplitude analyses of DP-03 at INR_{TOV}.

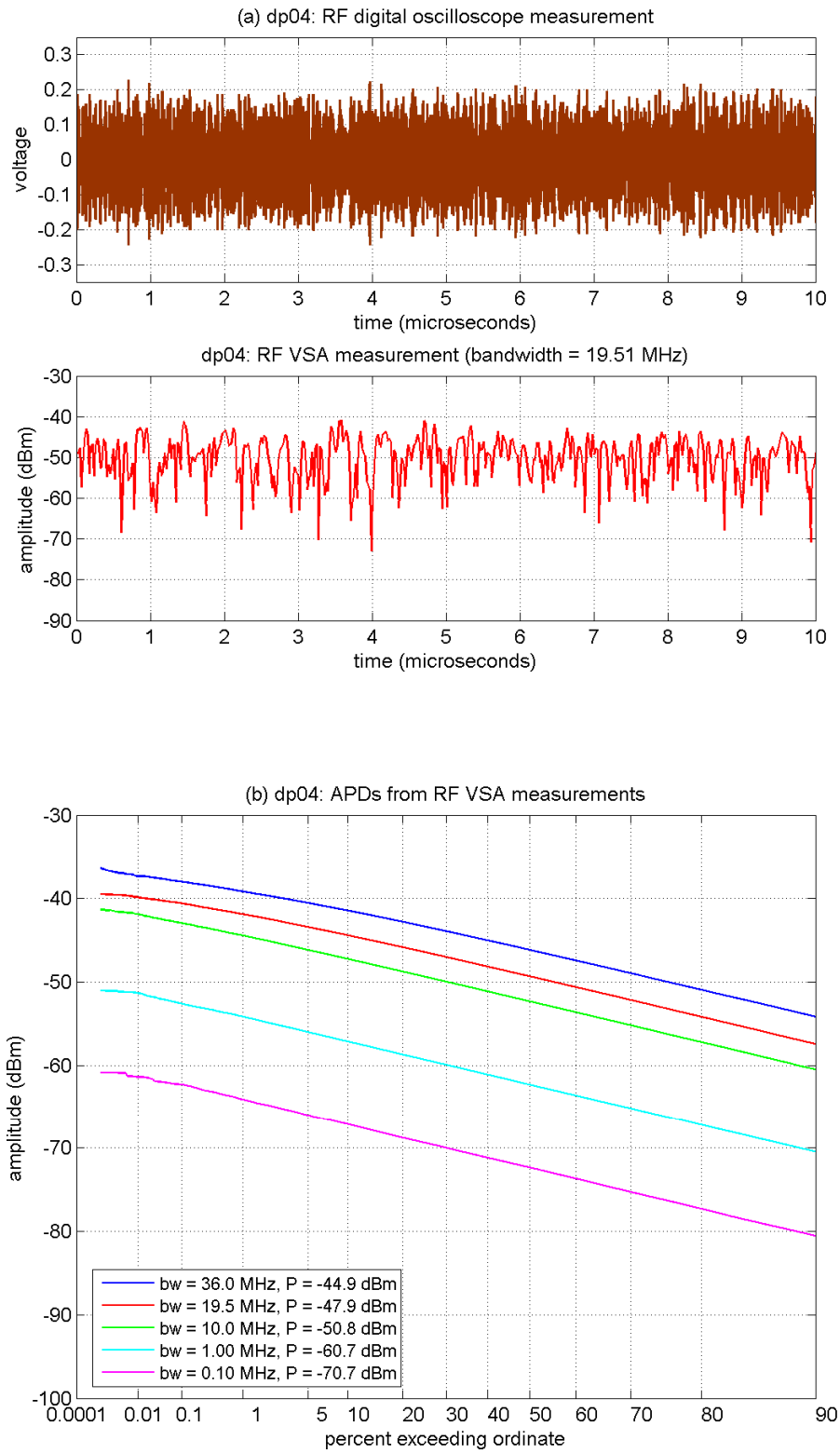

Figure B-31. RF amplitude analyses of DP-04 (T_{pulse} = 10 ns, w = 0.094 ns, f_D = 0.5).

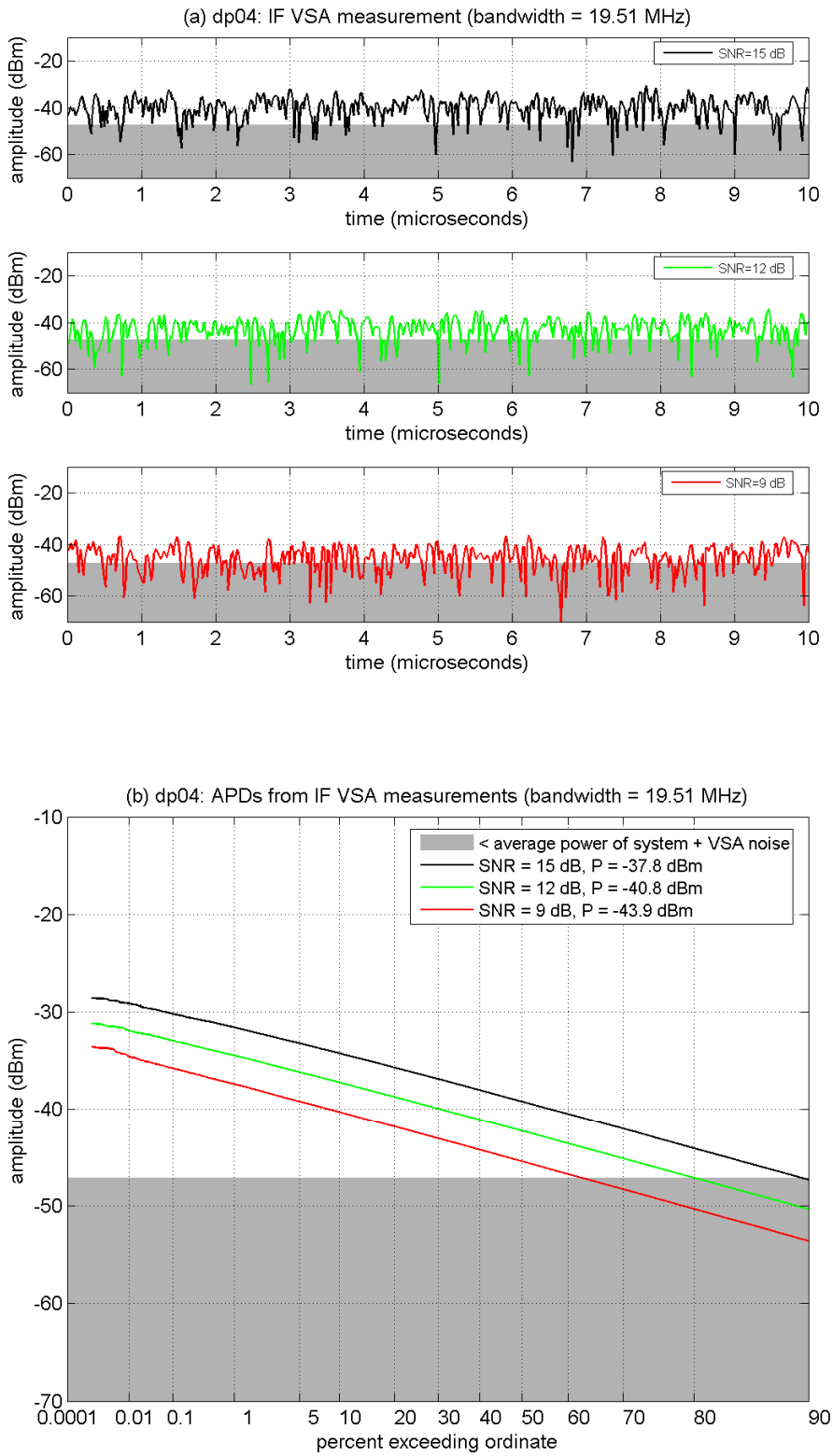

Figure B-32. IF amplitude analyses of DP-04 at INR_{TOV}.

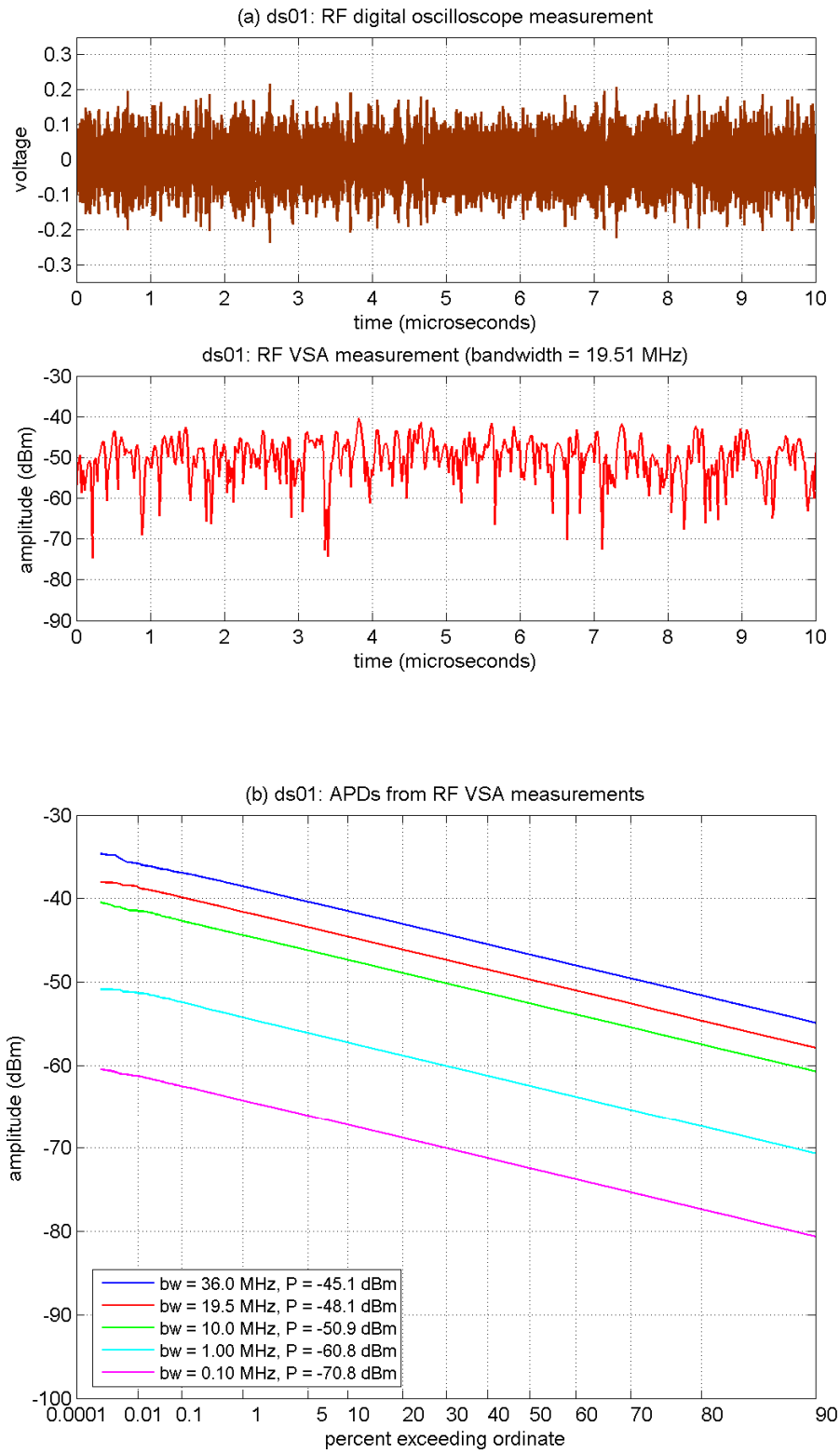

Figure B-33. RF amplitude analyses of DS-01 (L = 1).

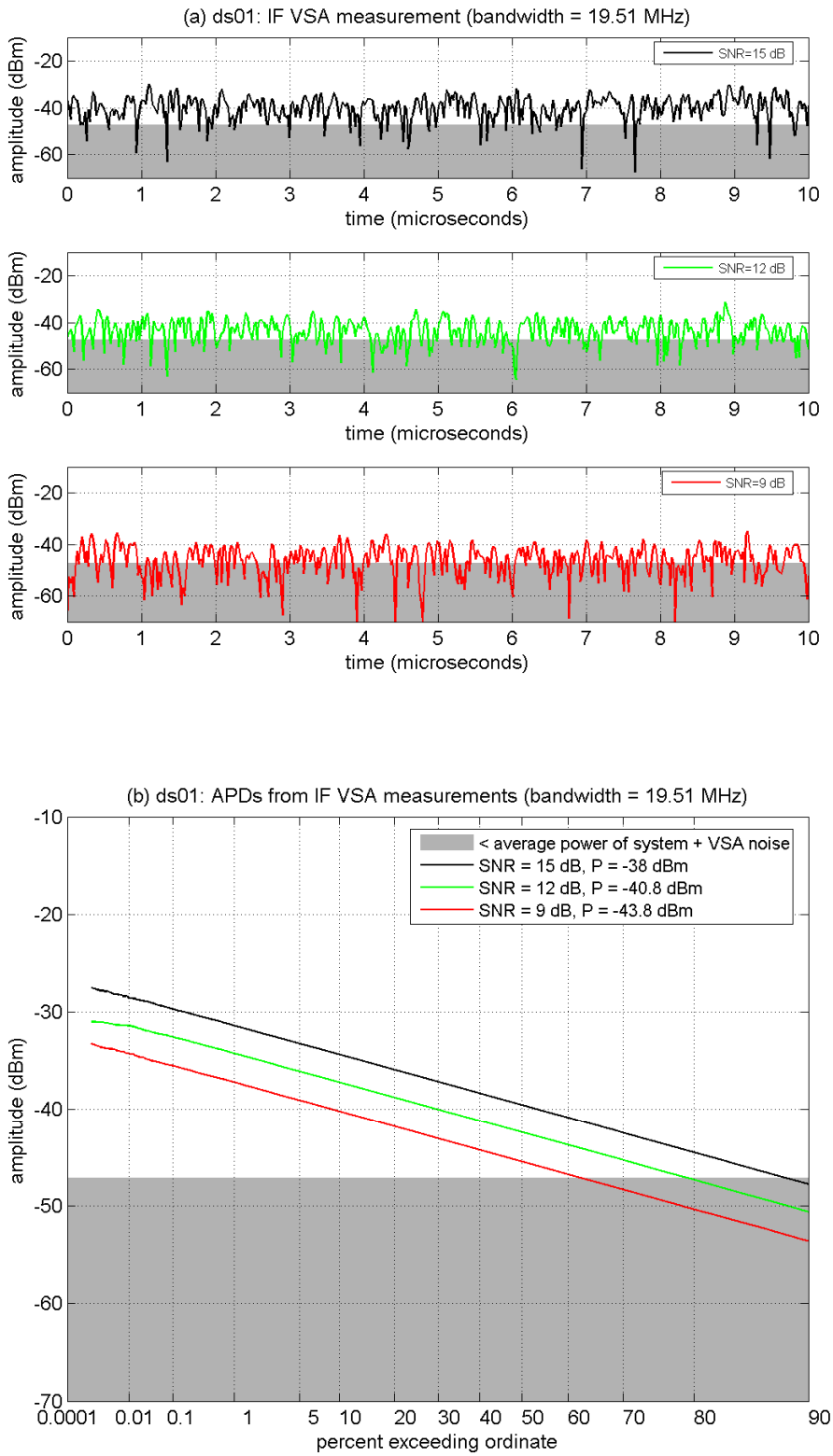

Figure B-34. IF amplitude analyses of DS-01 at INR_{TOV}.

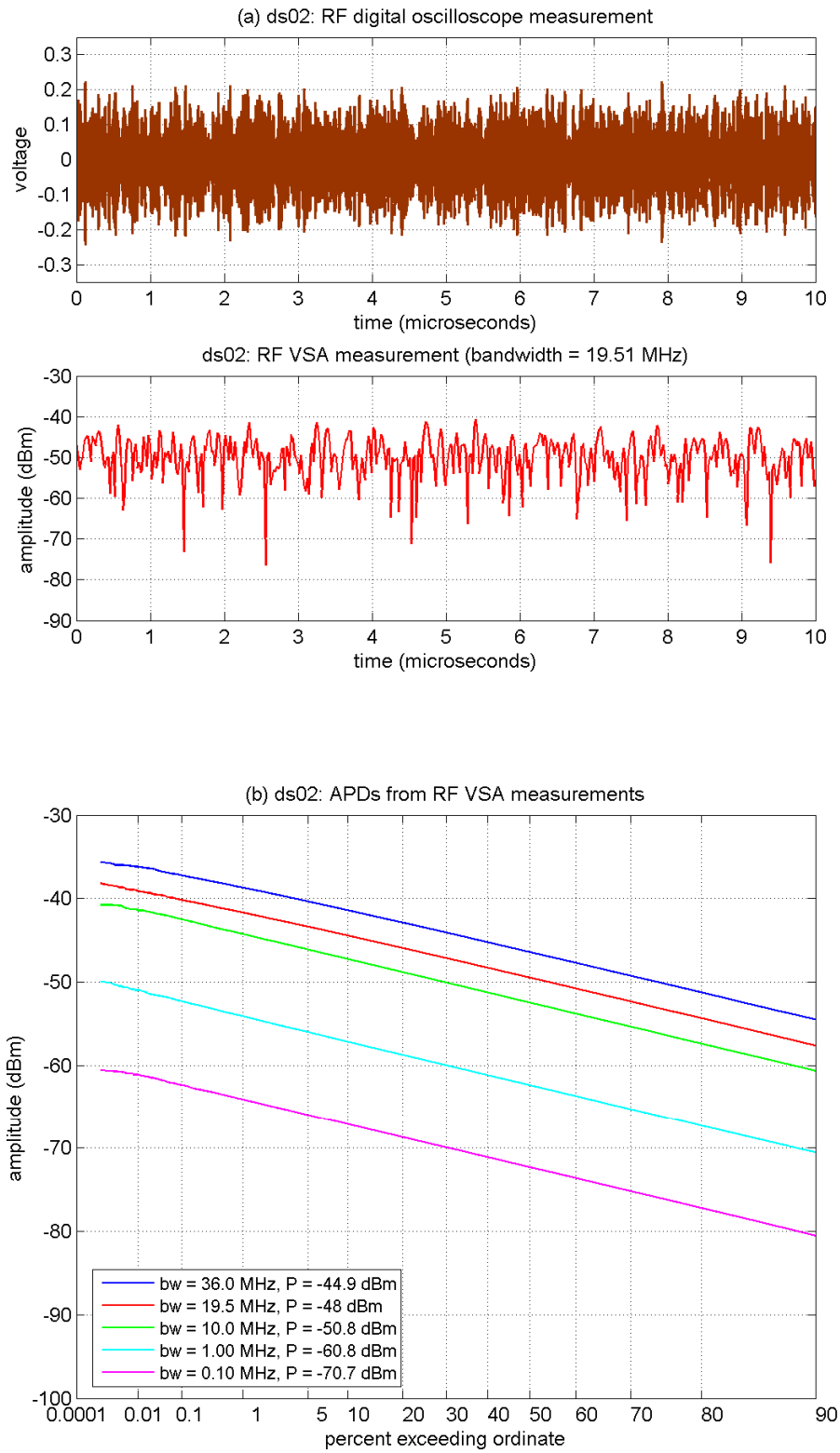

Figure B-35. RF amplitude analyses of DS-02 (L = 3, sparse code).

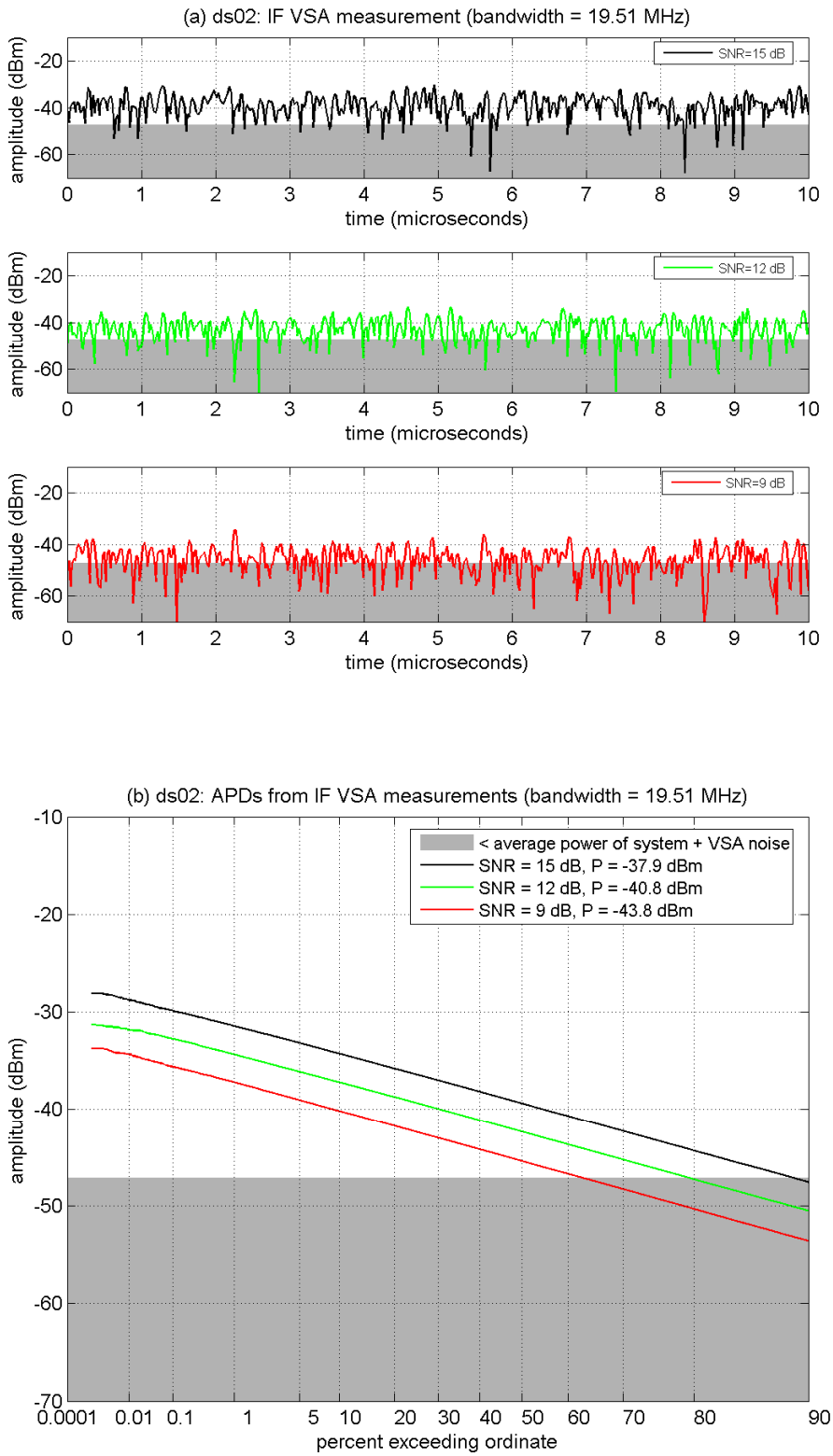

Figure B-36. IF amplitude analyses of DS-02 at INR_{TOV}.

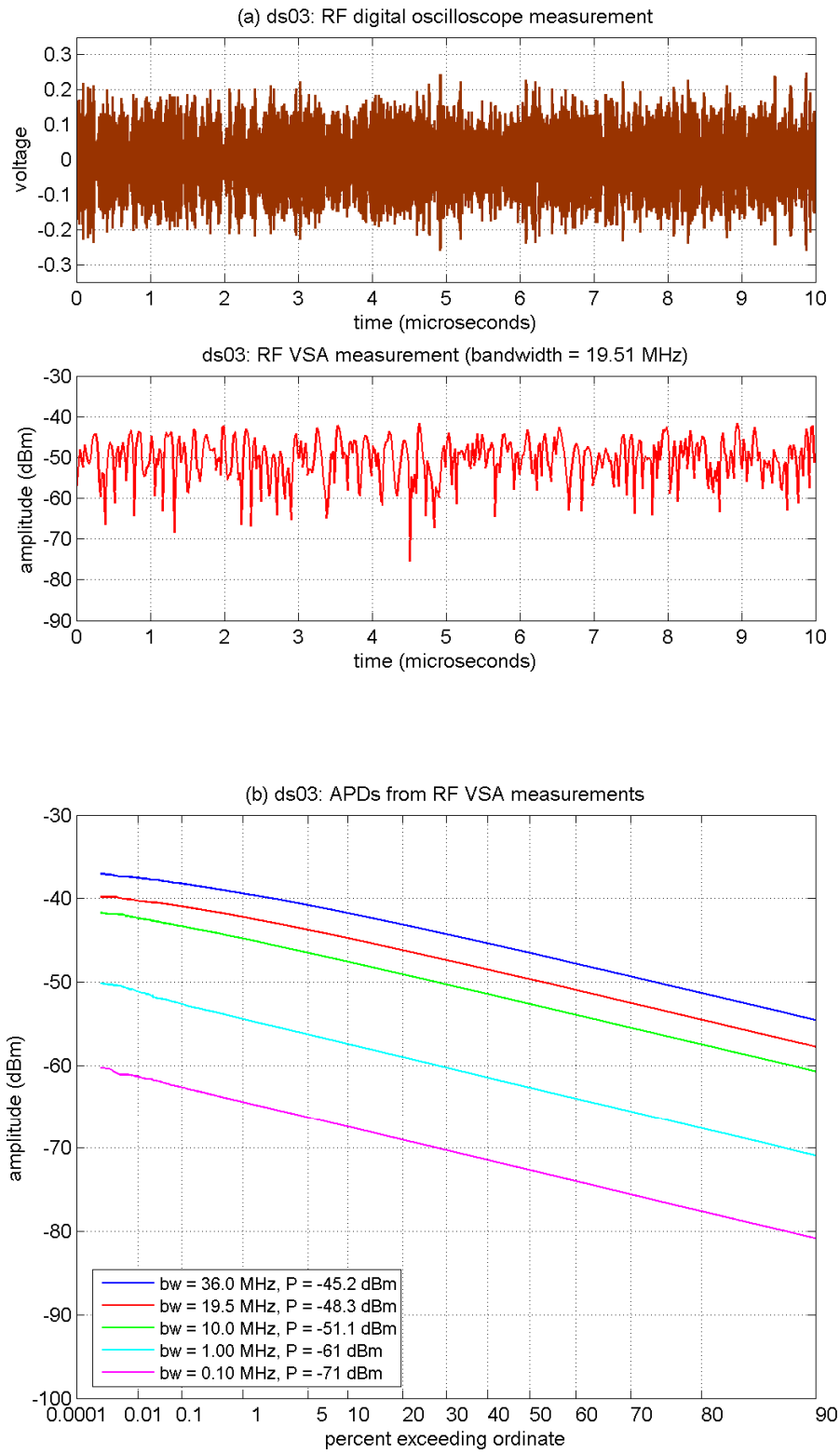

Figure B-37. RF amplitude analyses of DS-03 (L = 6, sparse code).

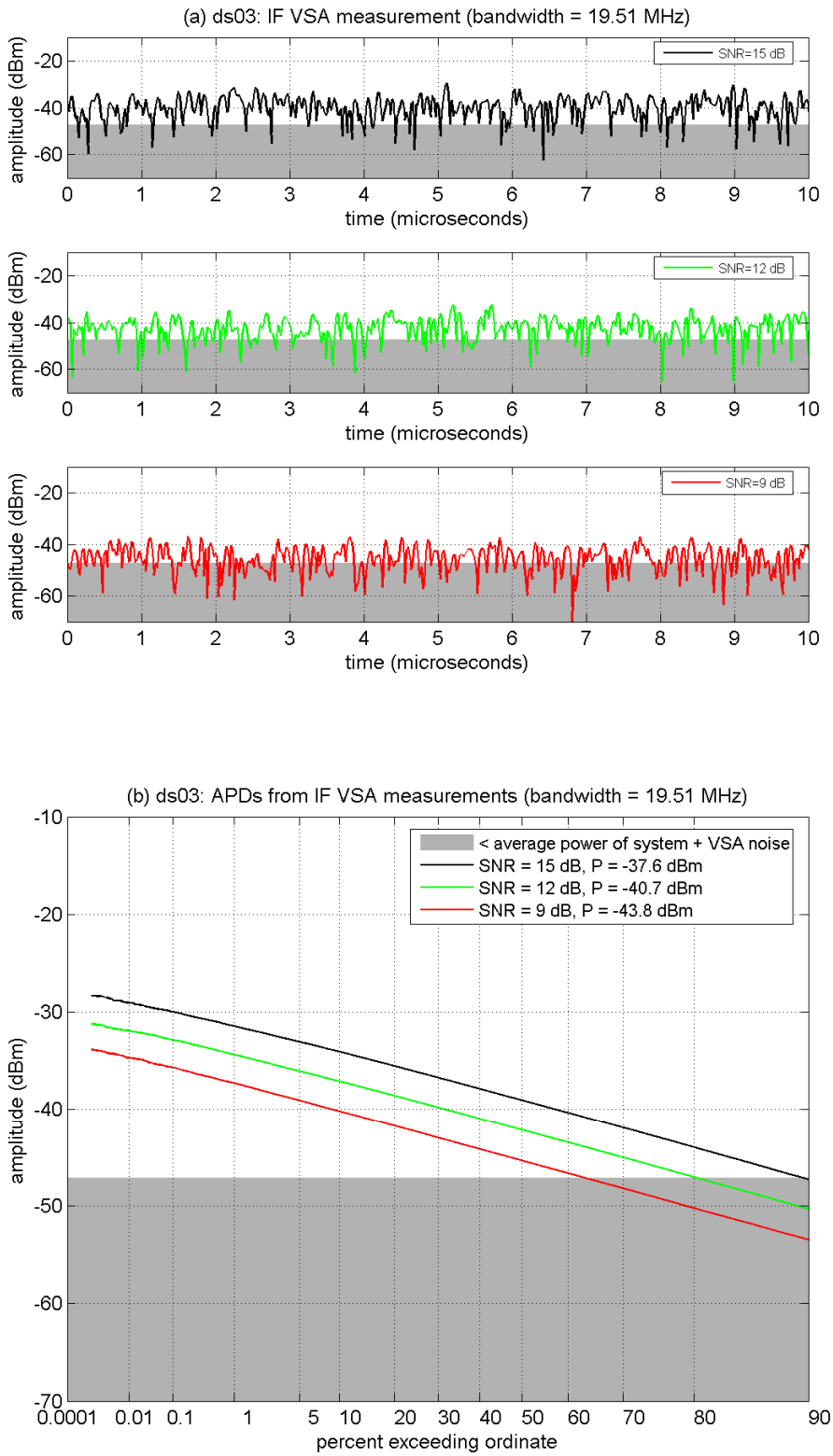

Figure B-38. IF amplitude analyses of DS-03 at INR_{TOV}.

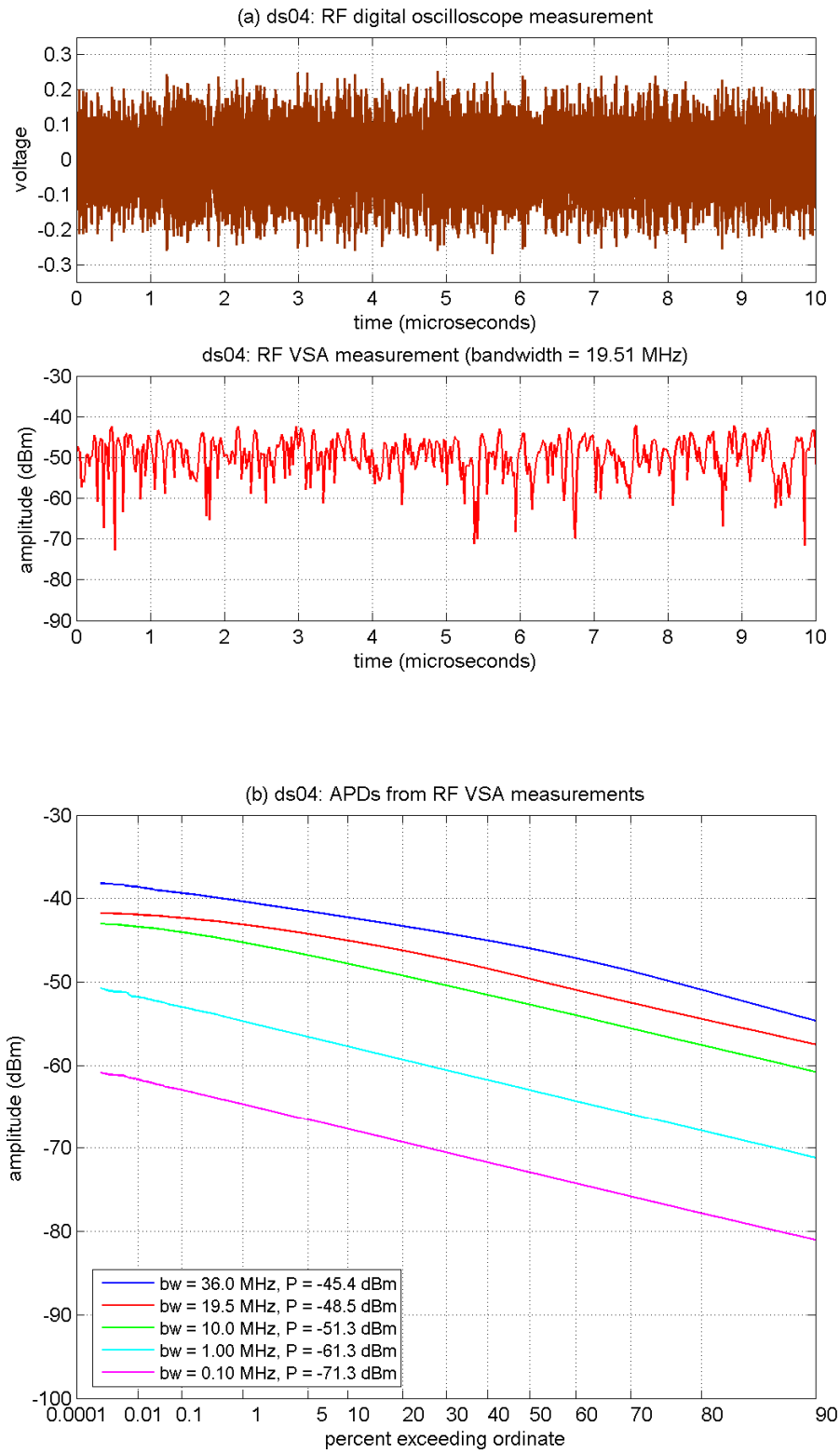

Figure B-39. RF amplitude analyses of DS-04 (L = 12, DS code).

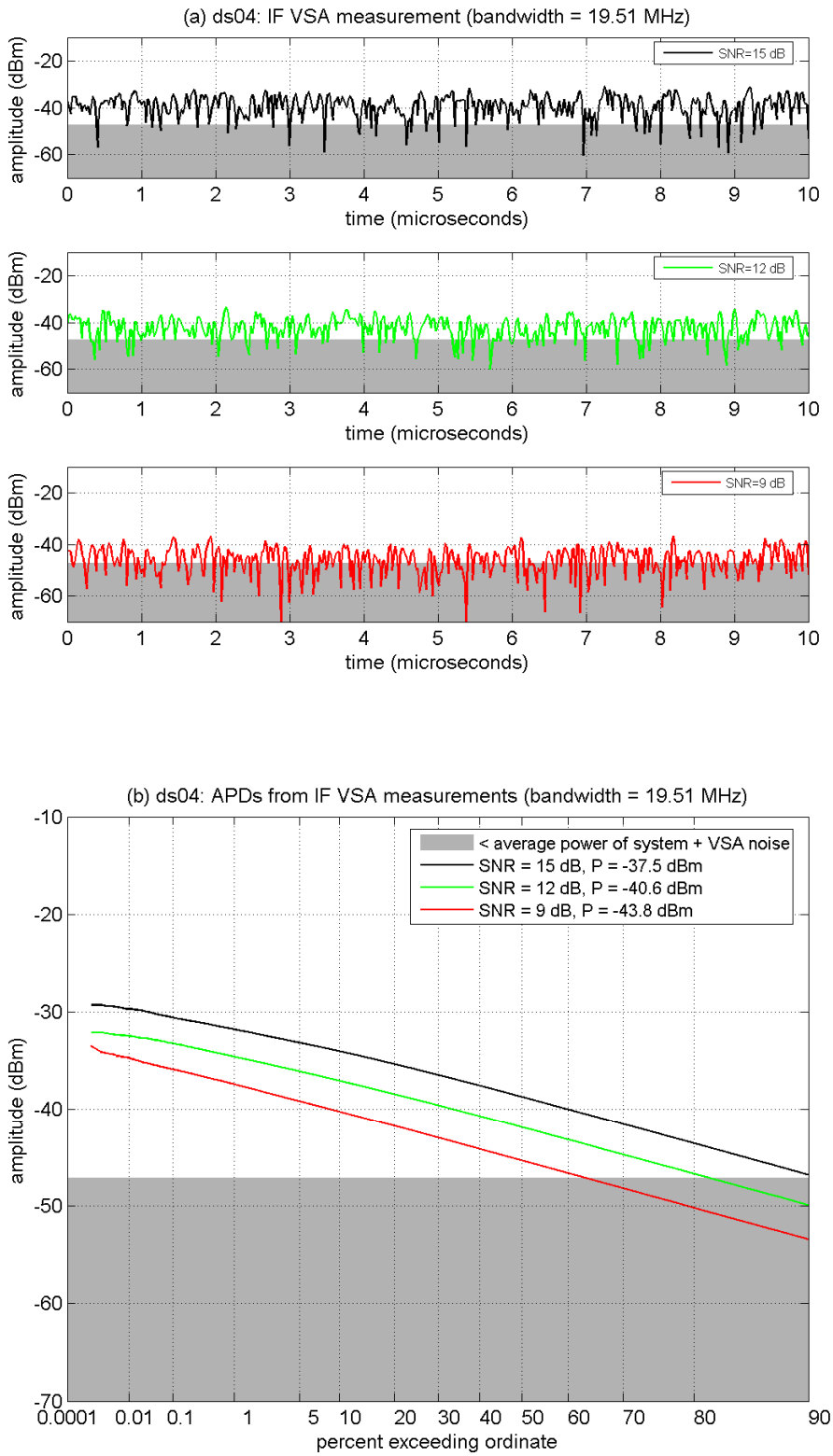

Figure B-40. IF amplitude analyses of DS-04 at INR_{TOV}.

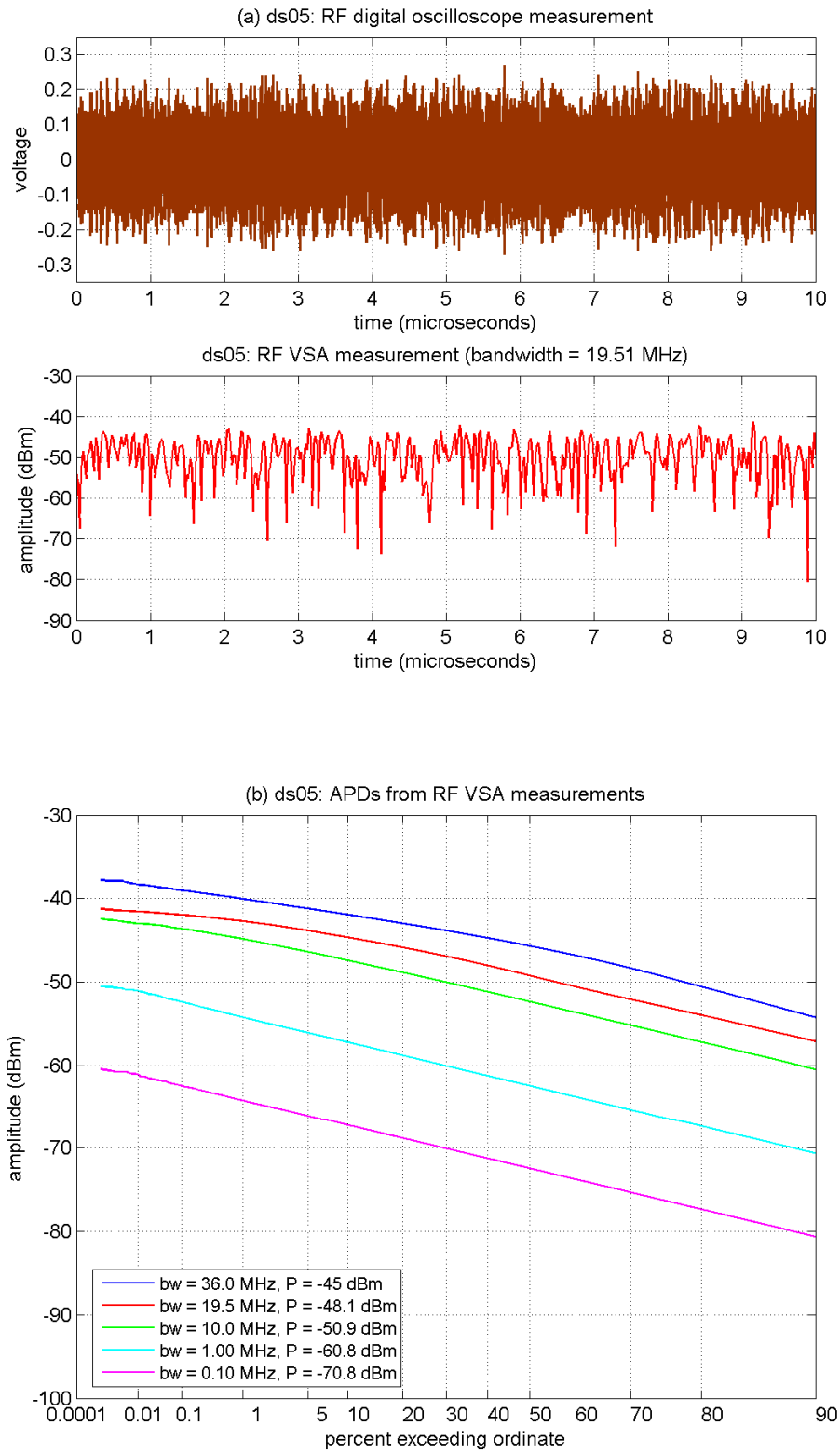

Figure B-41. RF amplitude analyses of DS-05 (L = 12, sparse code).

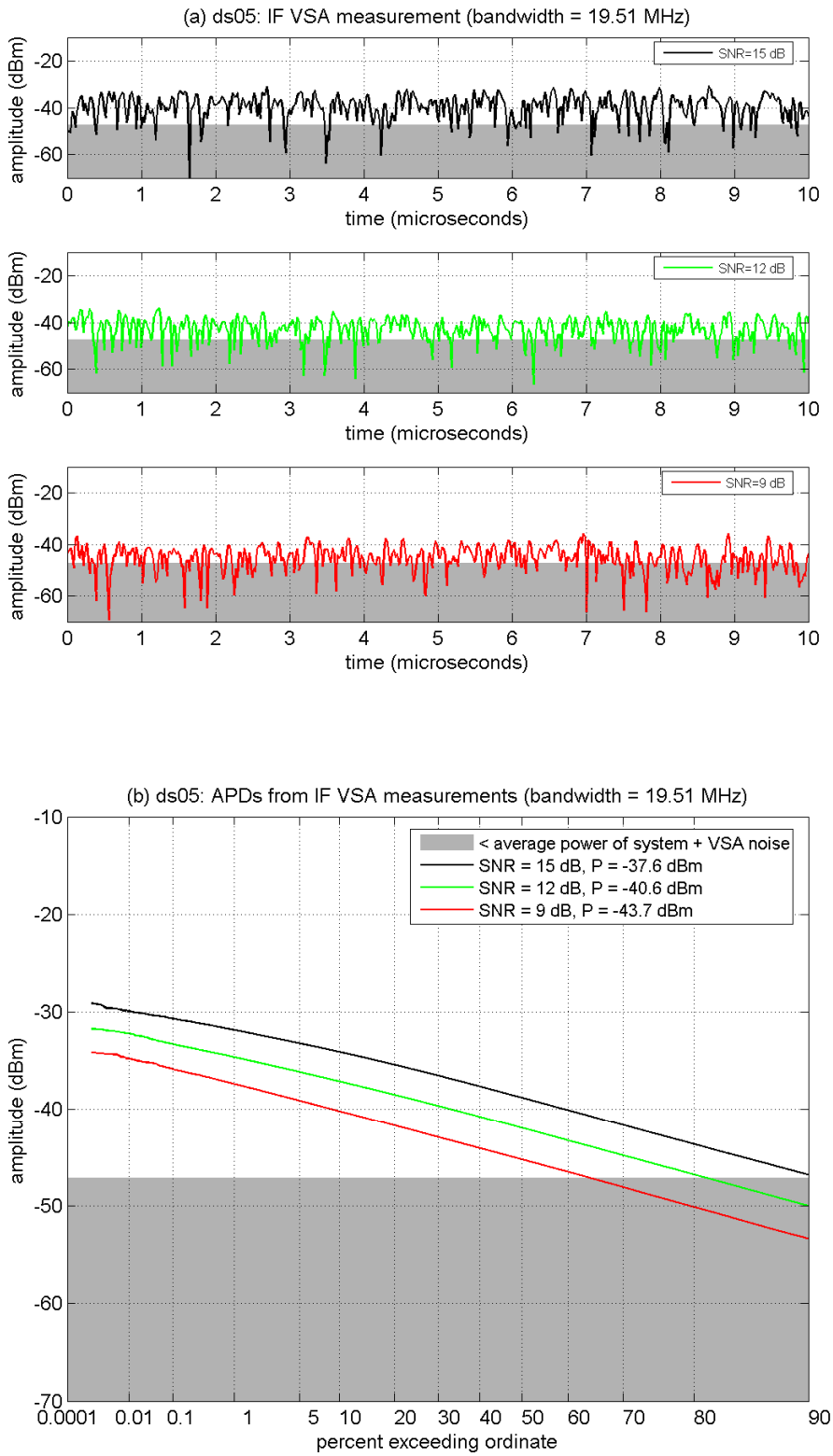

Figure B-42. IF amplitude analyses of DS-05 at INR_{TOV}.

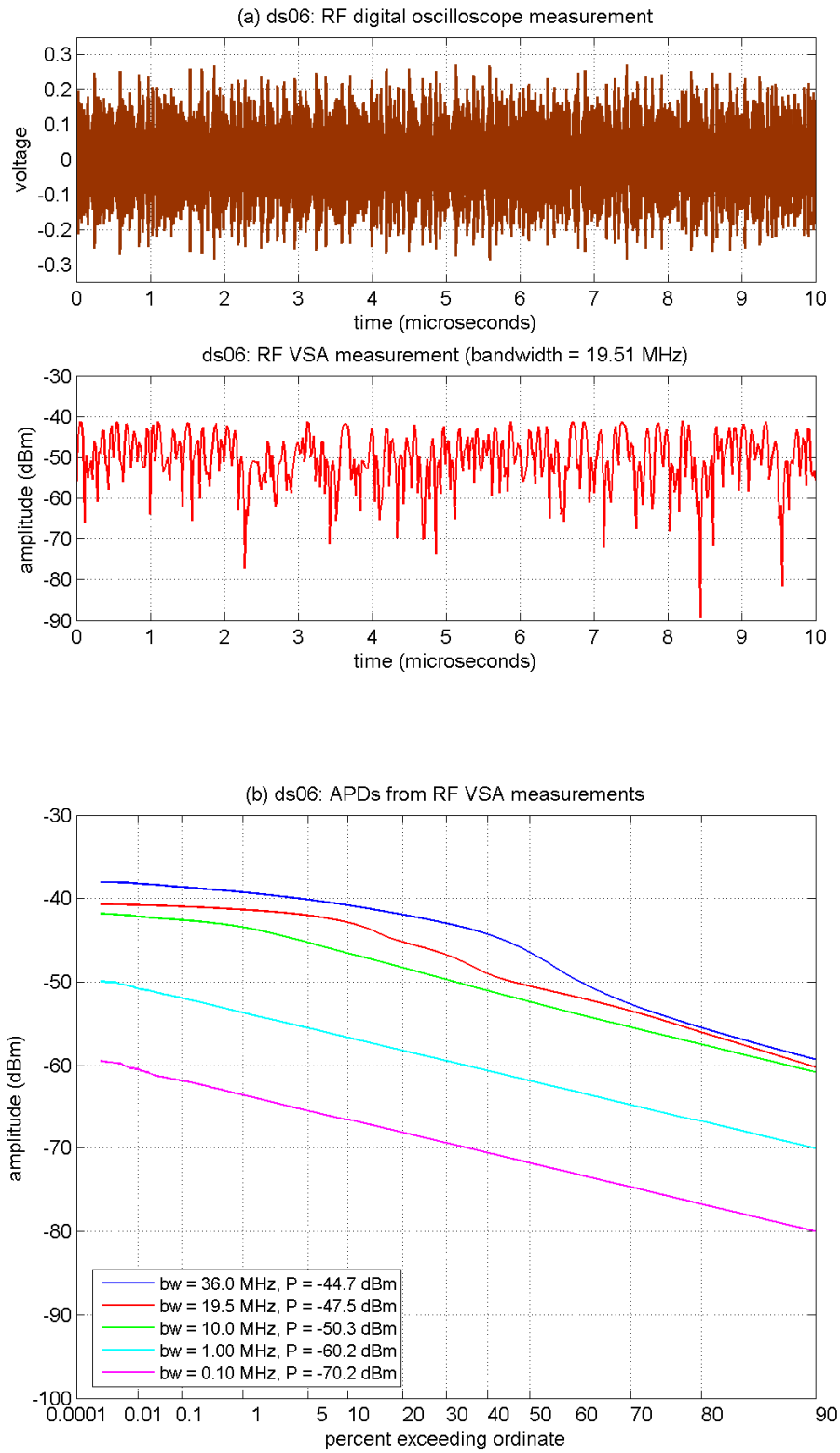

Figure B-43. RF amplitude analyses of DS-06 (L = 24, DS code).

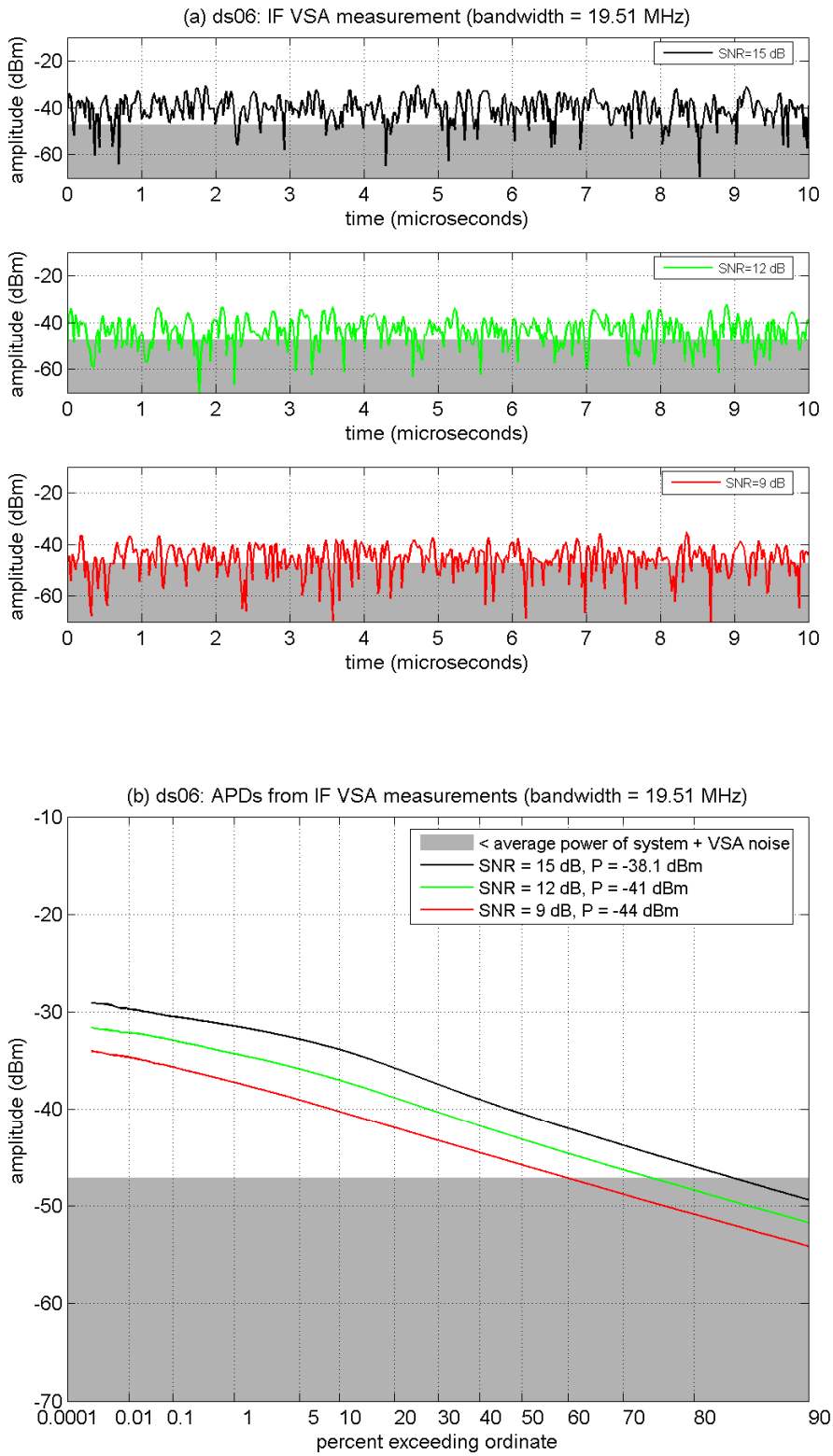

Figure B-44. IF amplitude analyses of DS-06 at INR_{TOV}.

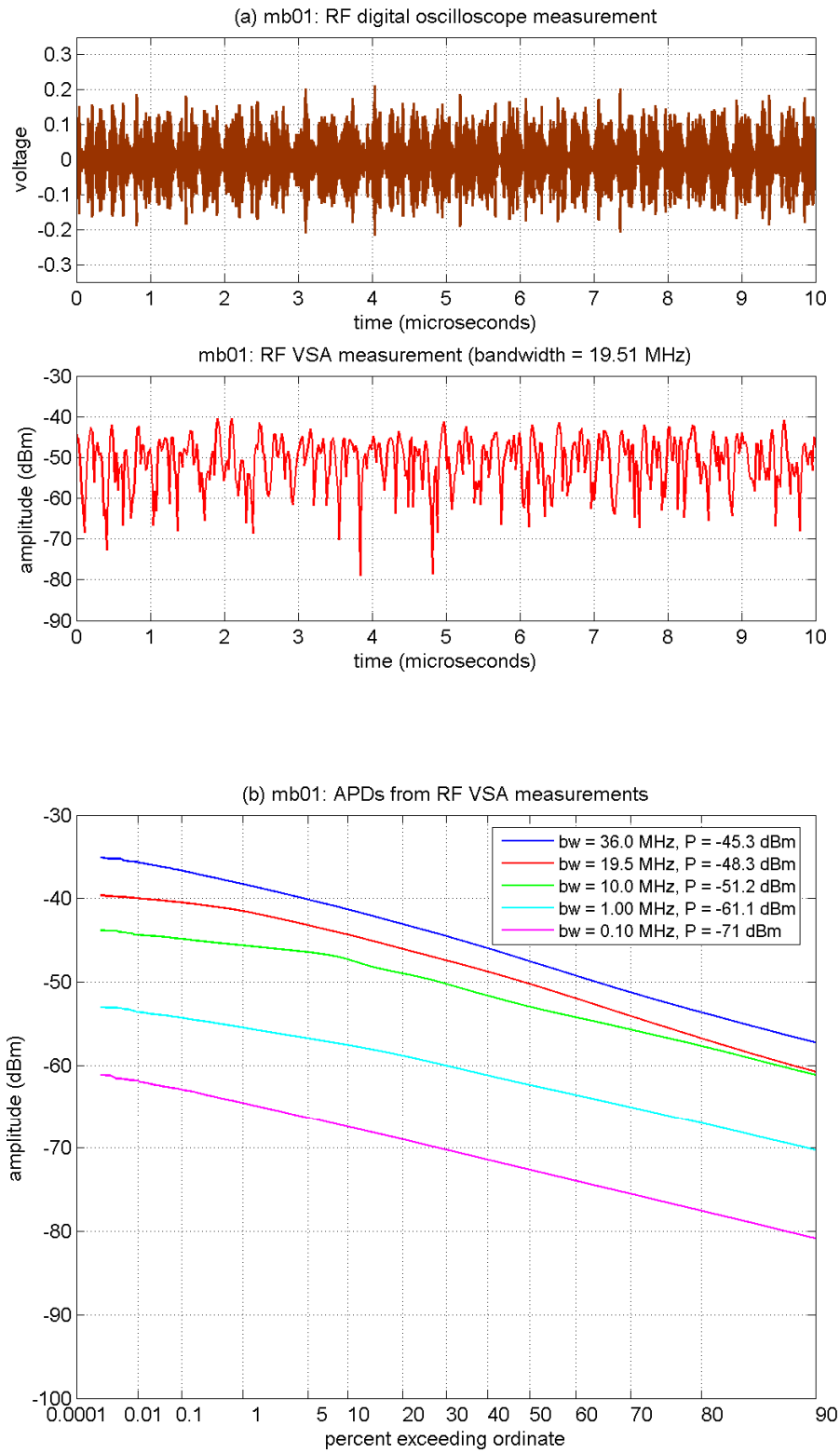

Figure B-45. RF amplitude analyses of MB-01 (b = 1).

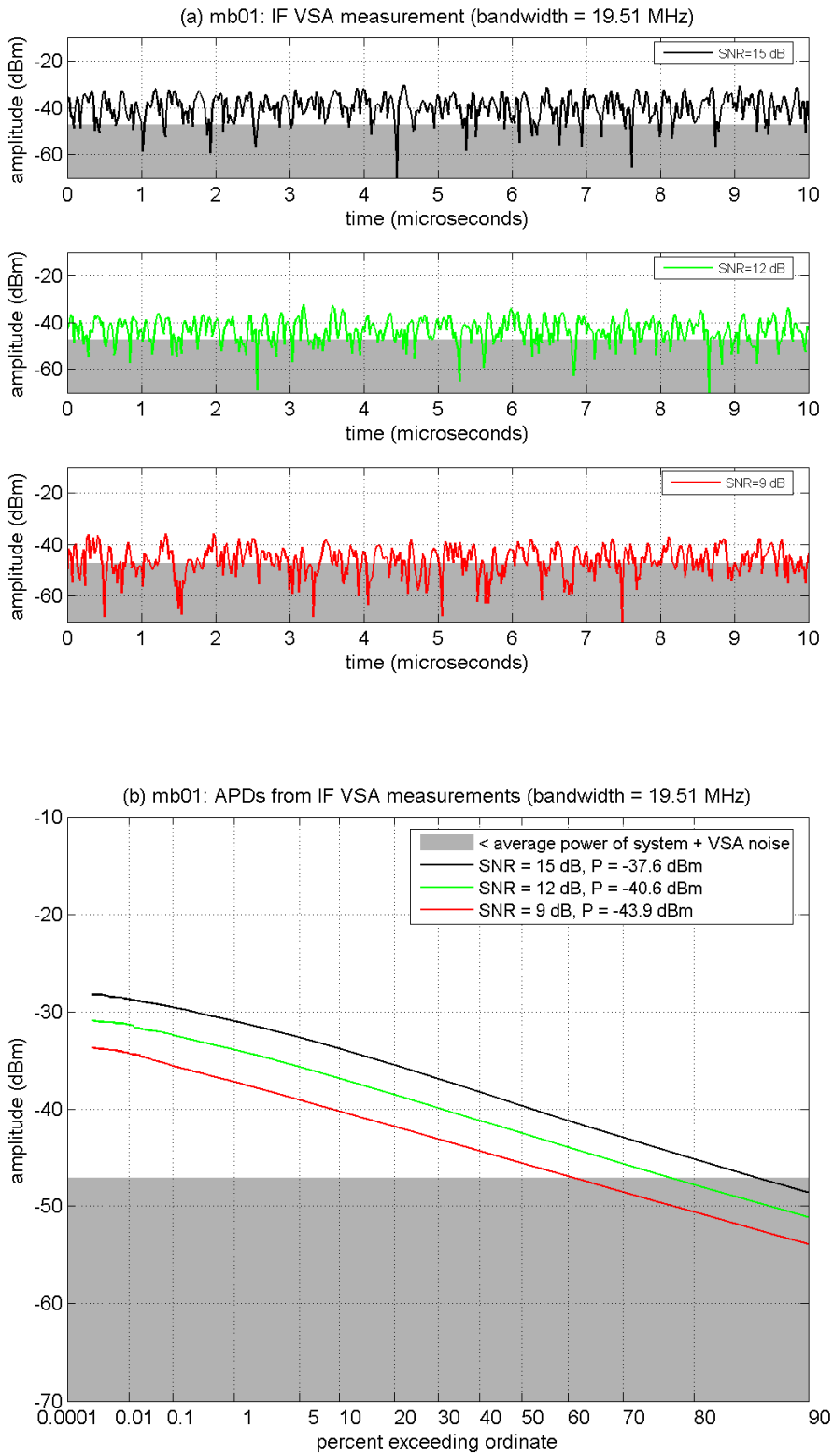

Figure B-46. IF amplitude analyses of MB-01 at INR_{TOV}.

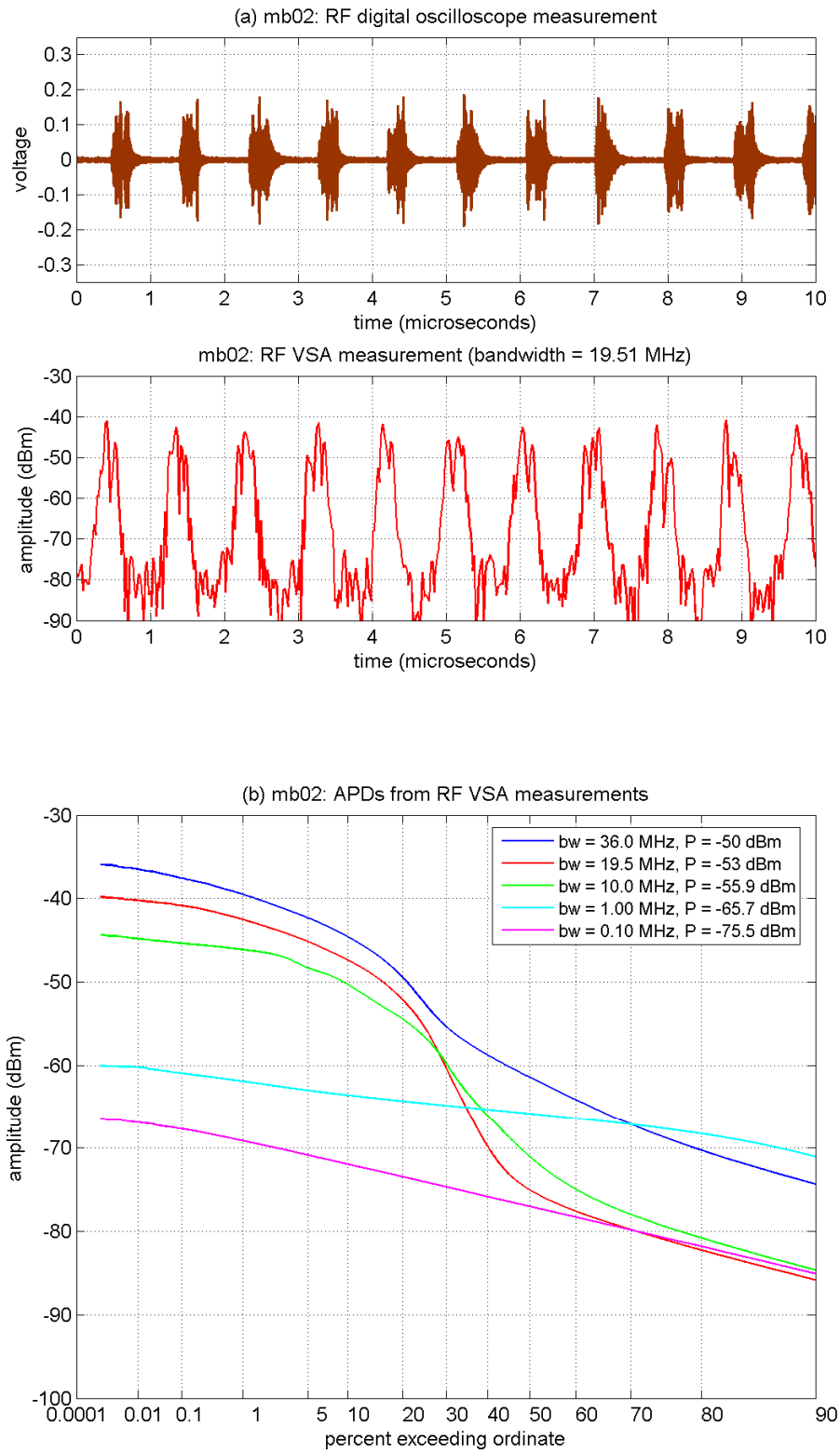

Figure B-47. RF amplitude analyses of MB-02 ($b = 3$, $d = 1$).

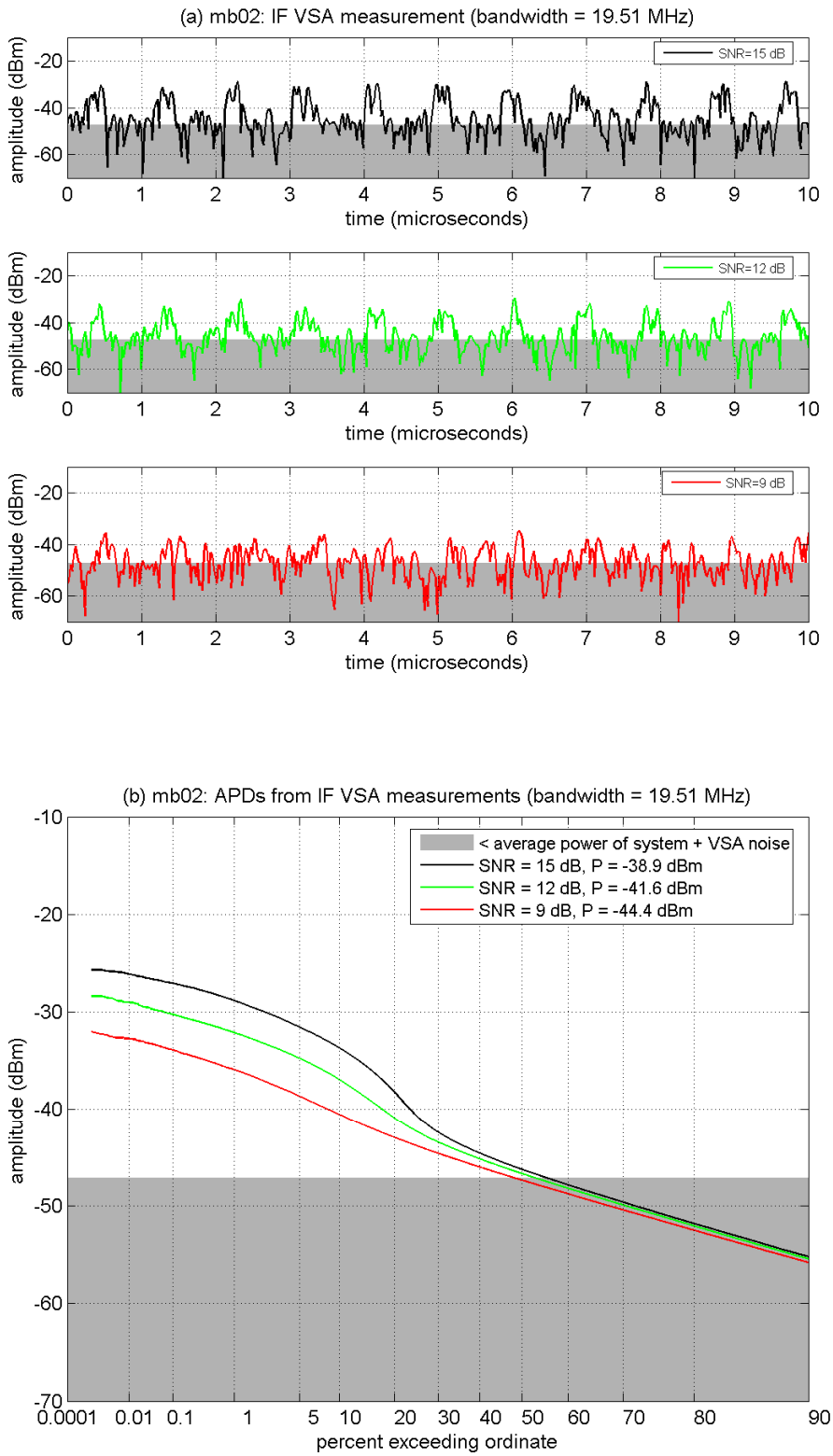

Figure B-48. IF amplitude analyses of MB-02 at INR_{TOV}.

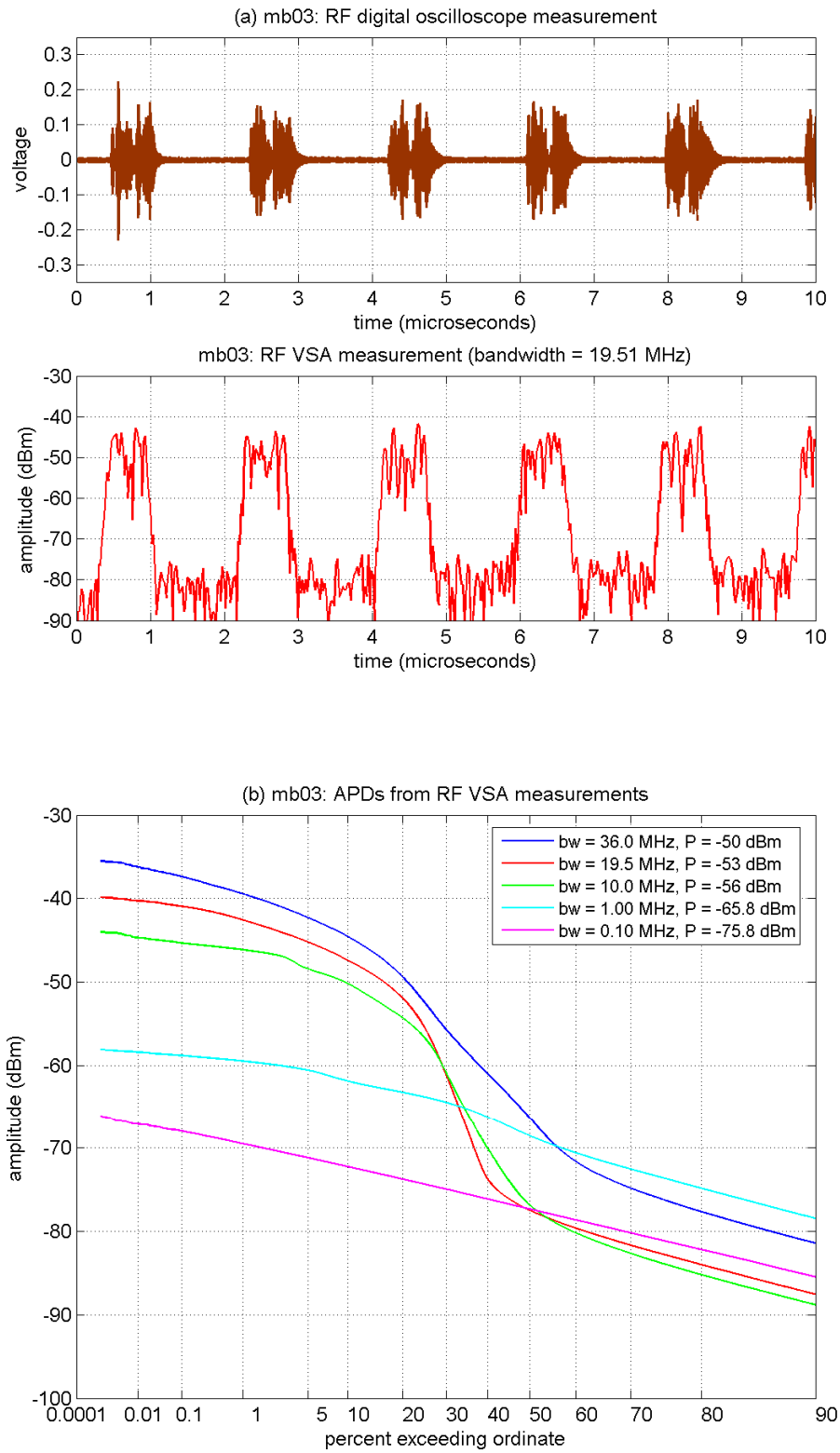

Figure B-49. RF amplitude analyses of MB-03 ($b = 3$, $d = 2$).

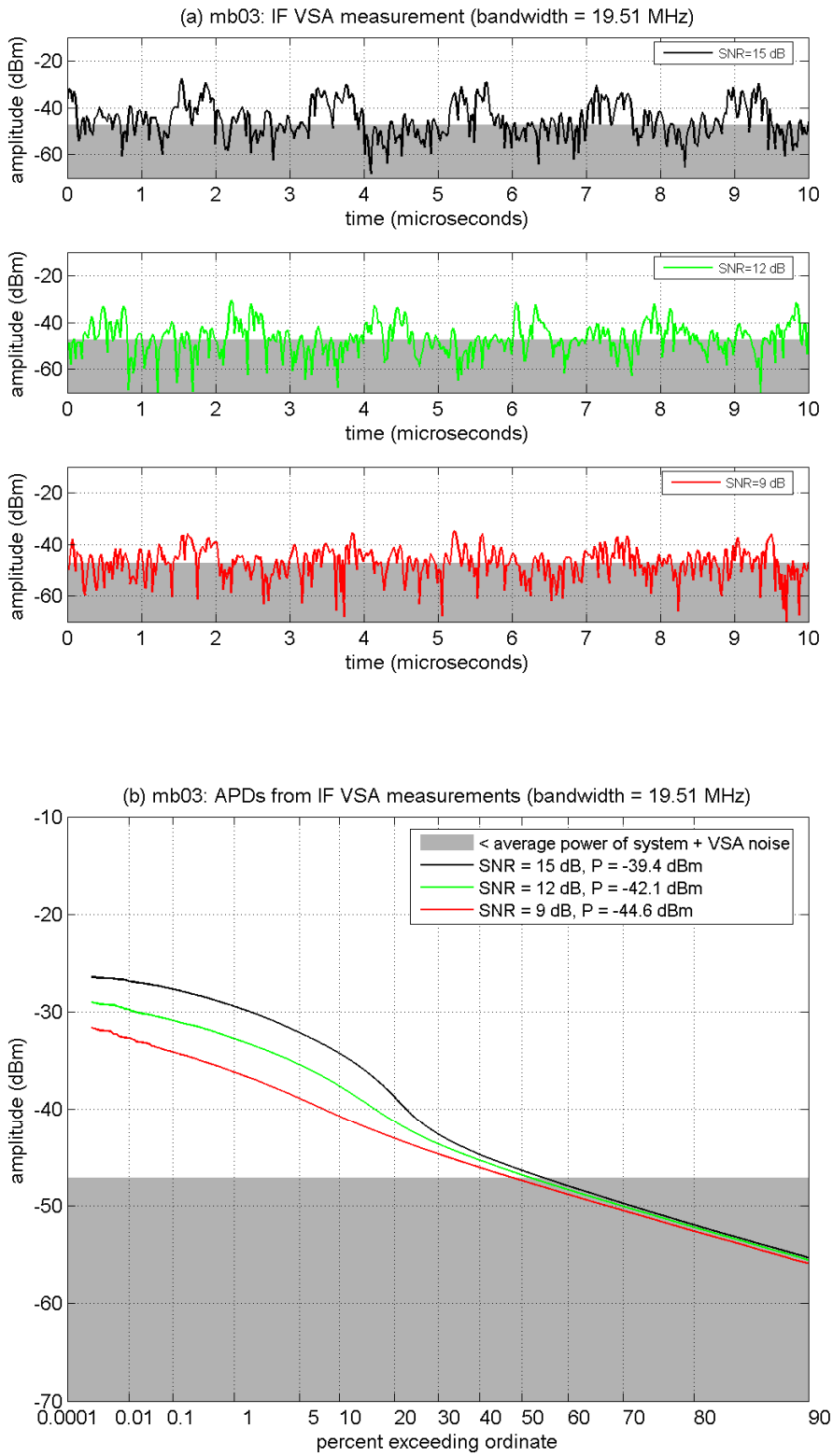

Figure B-50. IF amplitude analyses of MB-03 at INR_{TOV}.

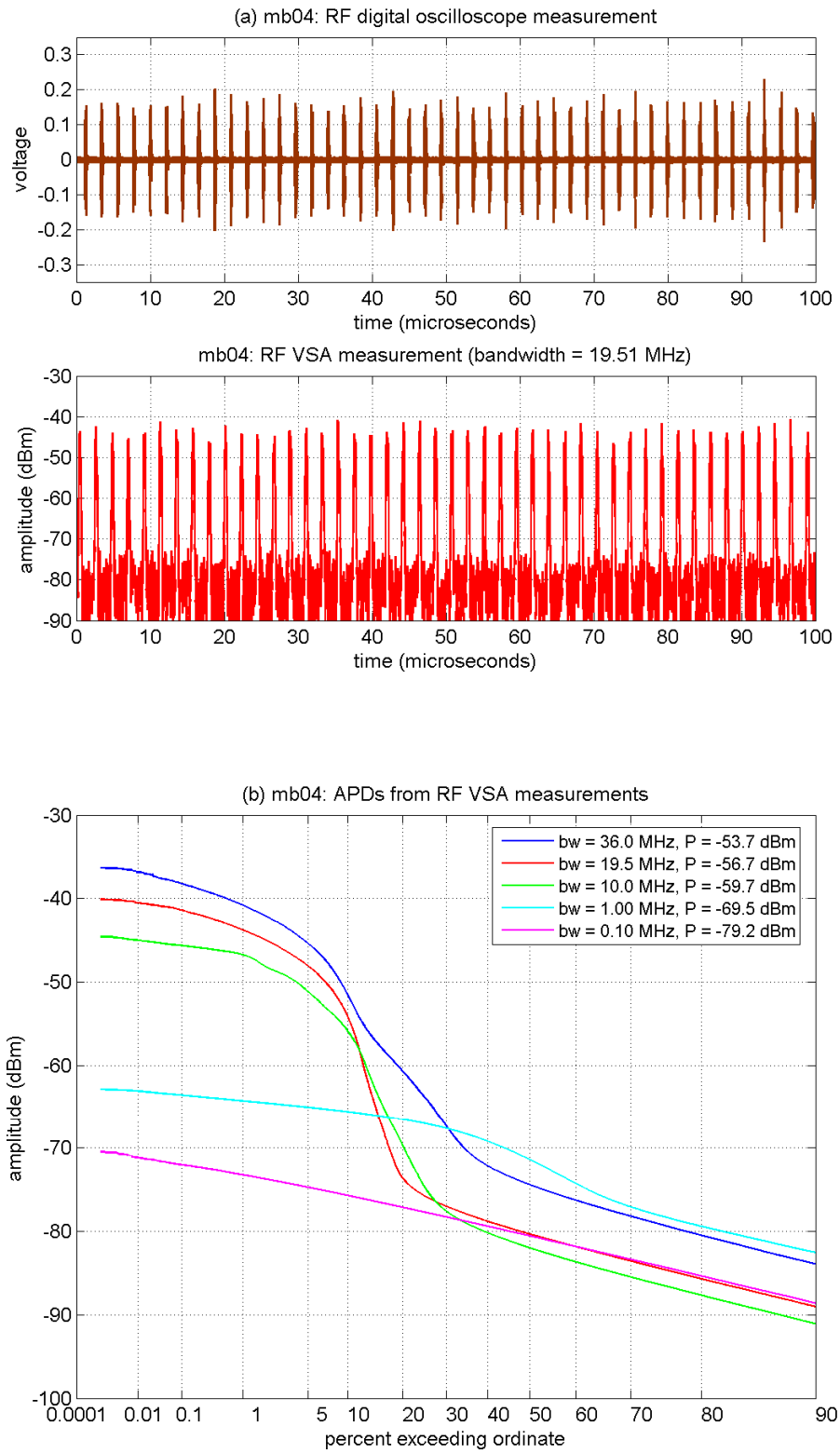

Figure B-51. RF amplitude analyses of MB-04 ($b = 7$, $d = 1$).

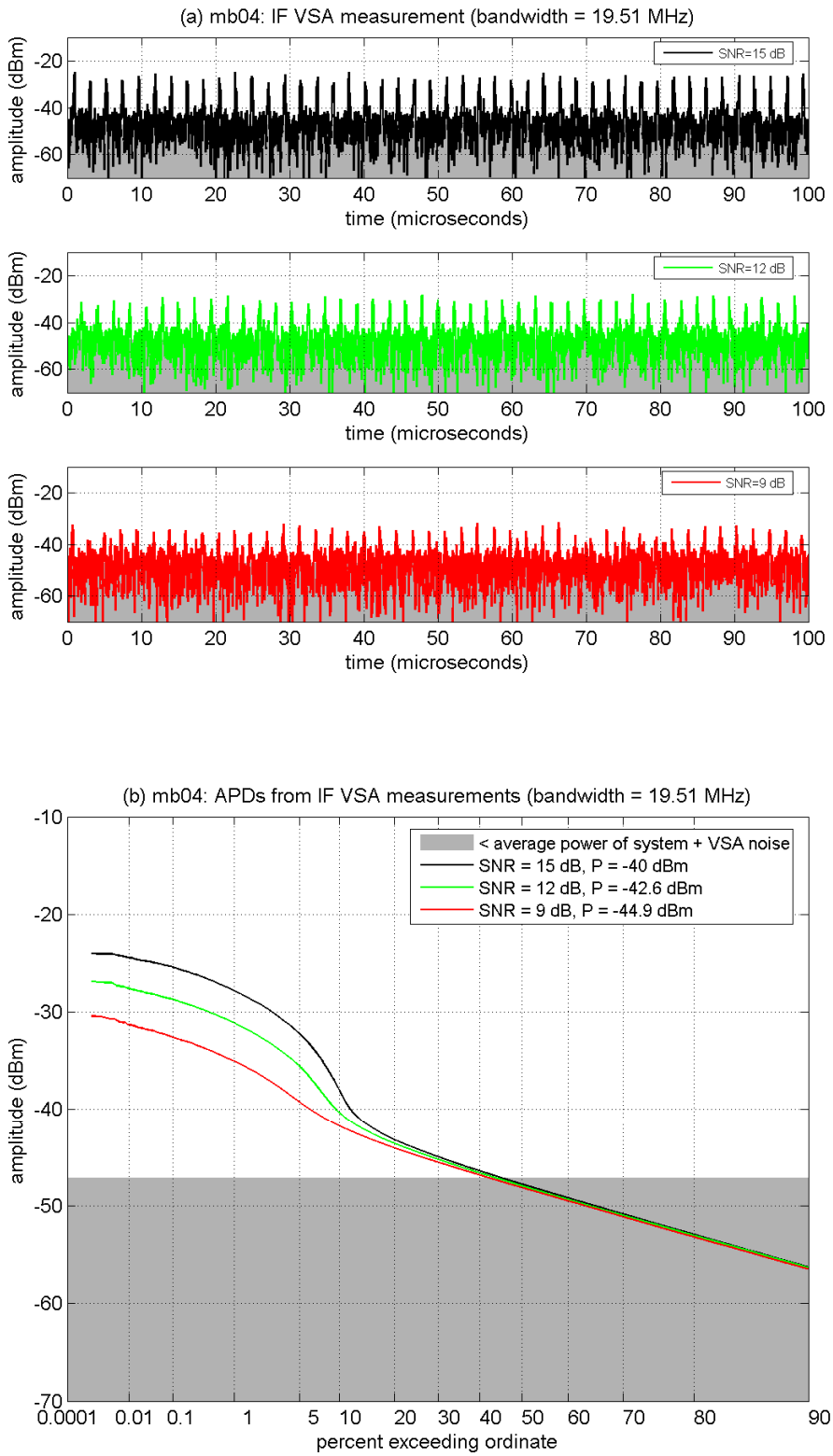

Figure B-52. IF amplitude analyses of MB-04 at INR_{TOV}.

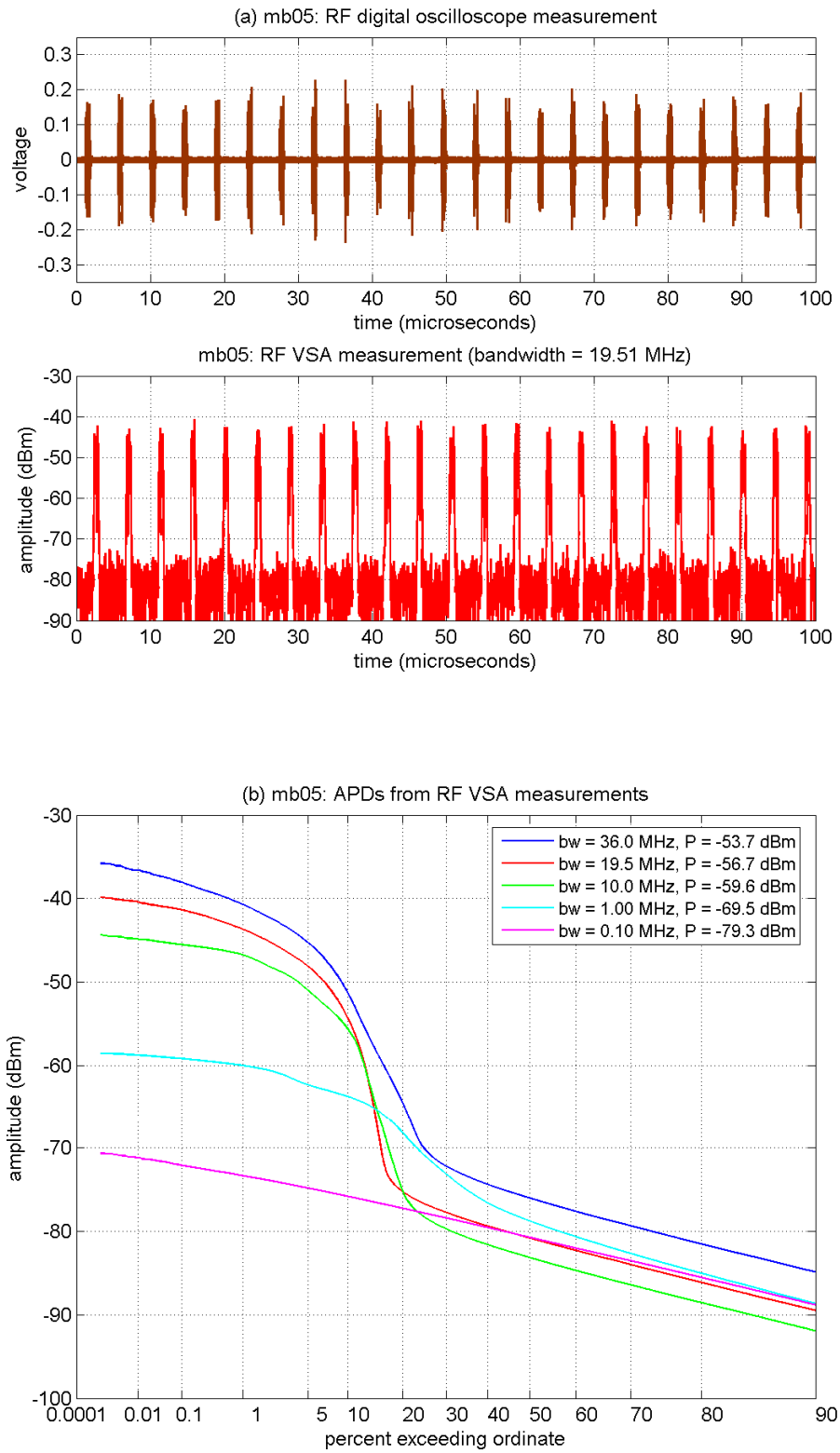

Figure B-53. RF amplitude analyses of MB-05 ($b = 7$, $d = 2$).

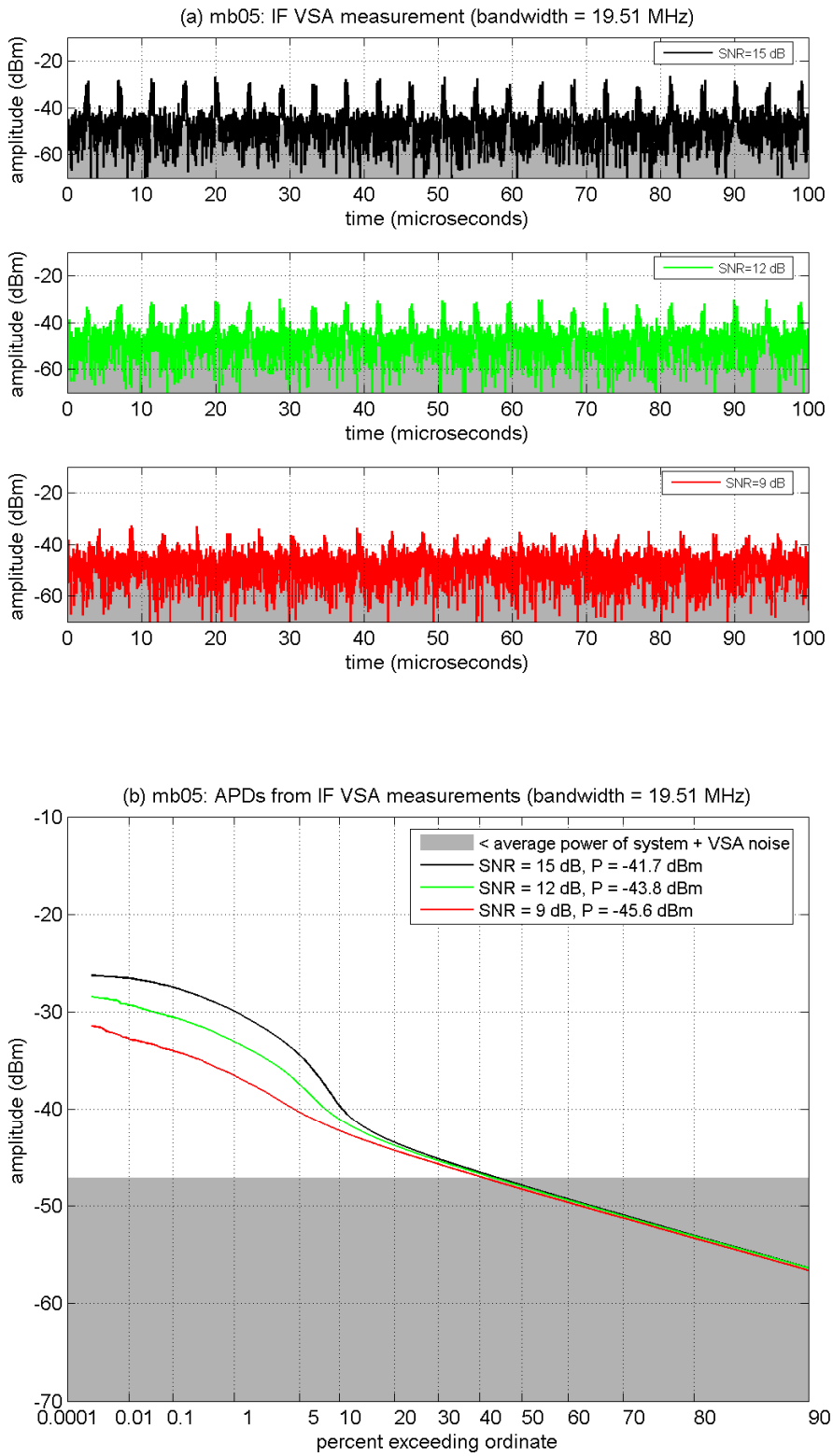

Figure B-54. IF amplitude analyses of MB-05 at INR_{TOV}.

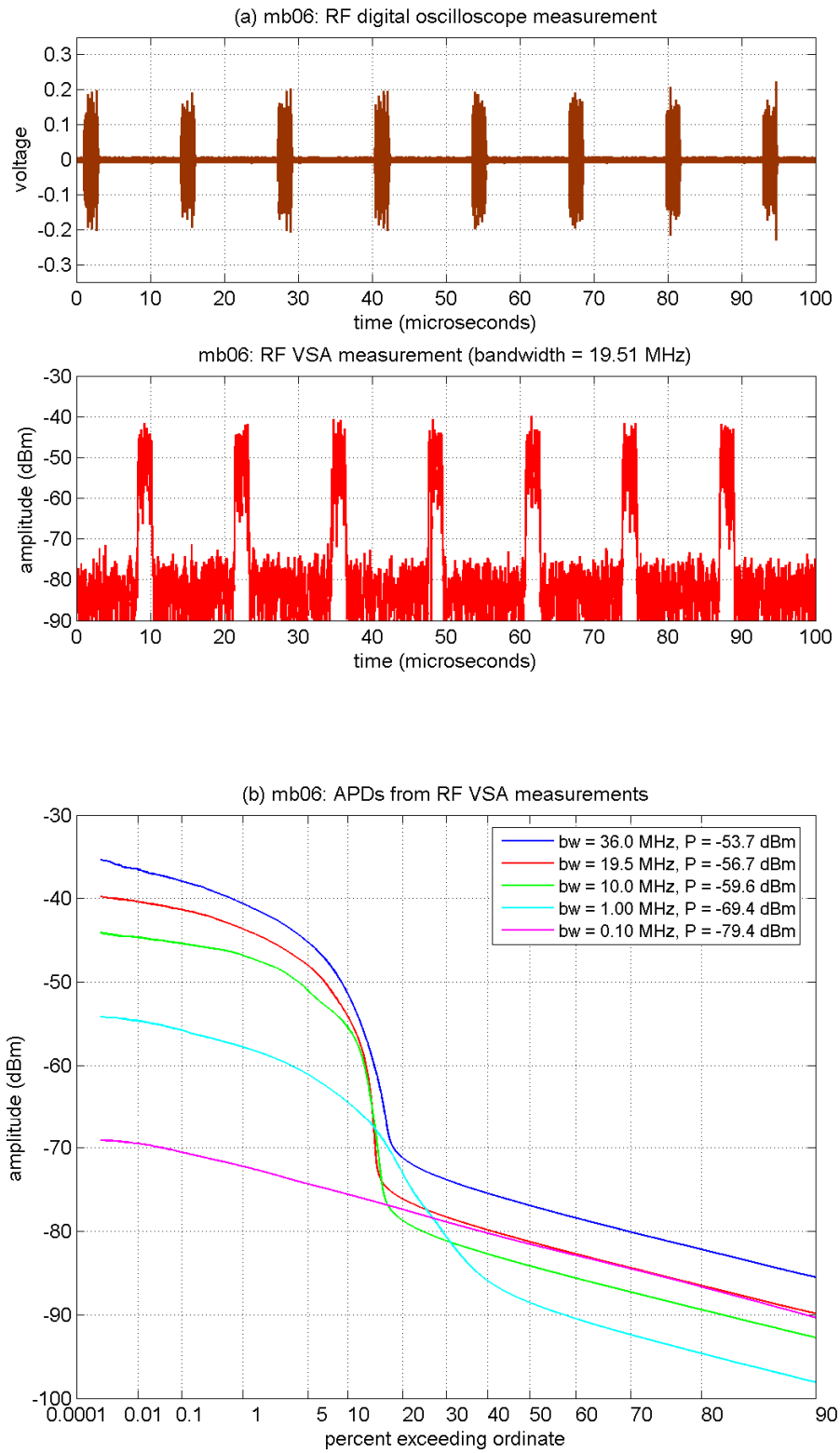

Figure B-55. RF amplitude analyses of MB-06 ($b = 7$, $d = 6$).

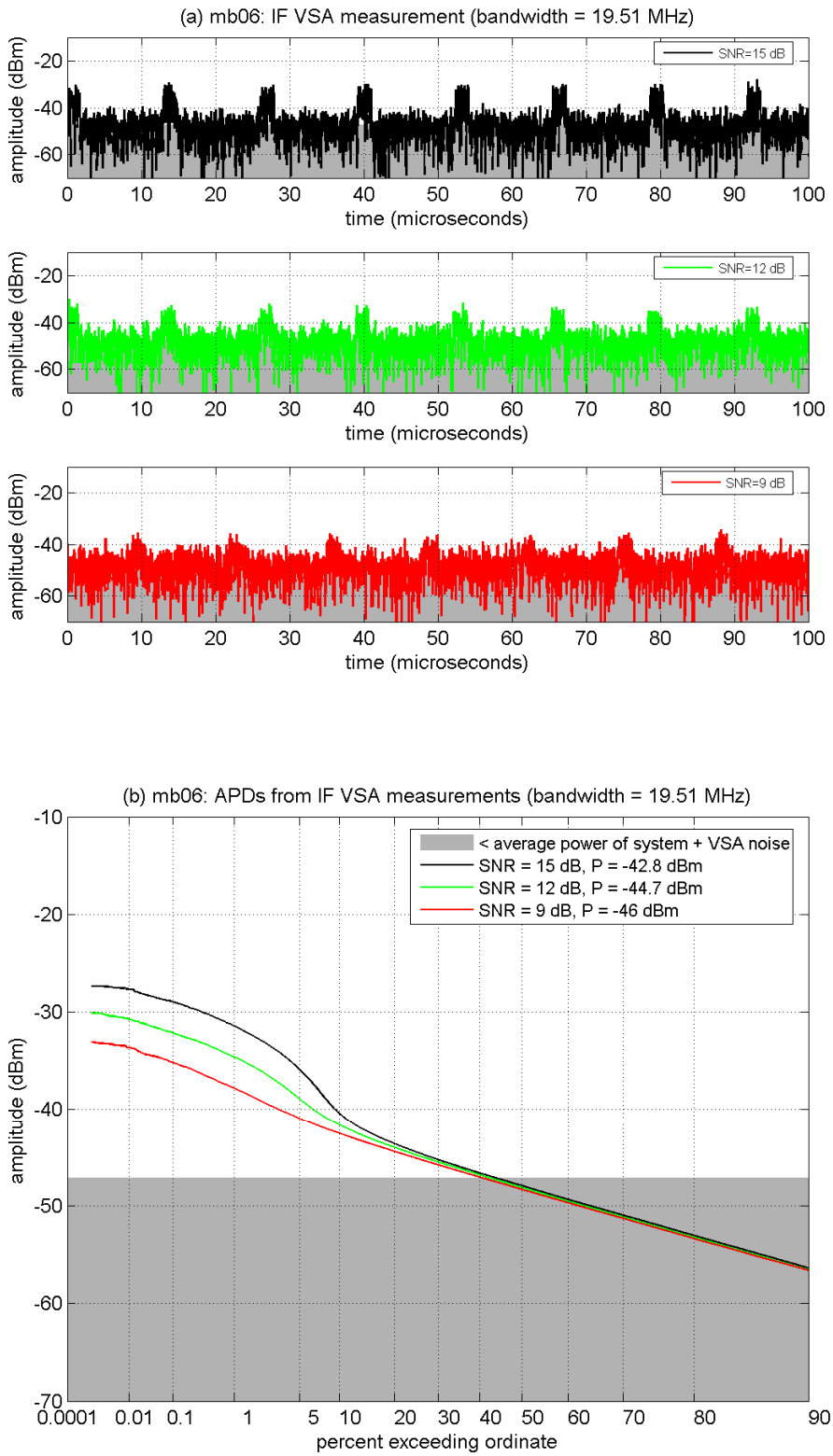

Figure B-56. IF amplitude analyses of MB-06 at INR_{TOV}.

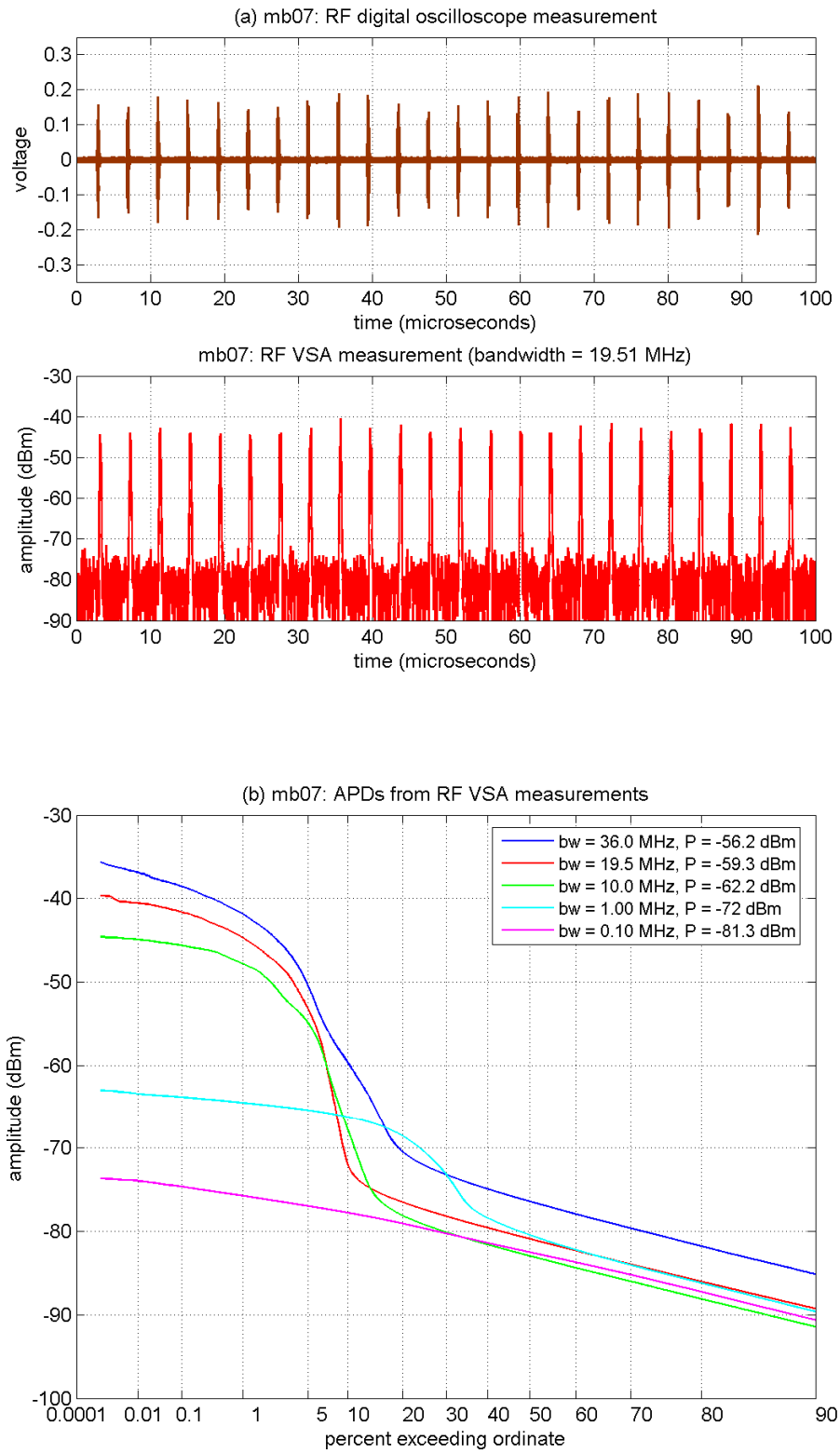

Figure B-57. RF amplitude analyses of MB-07 (b = 13, d = 1).

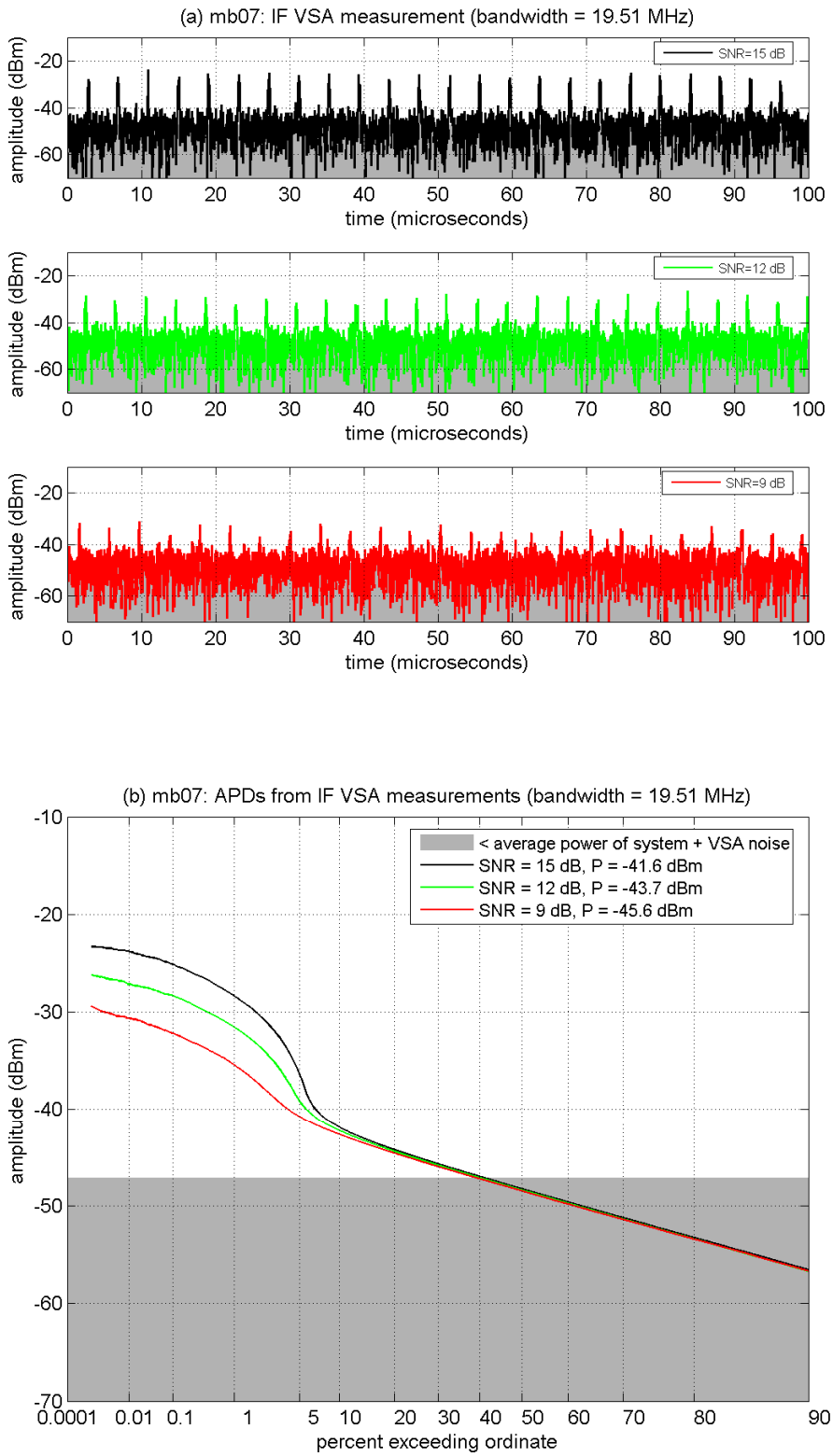

Figure B-58. IF amplitude analyses of MB-07 at INR_{TOV}.

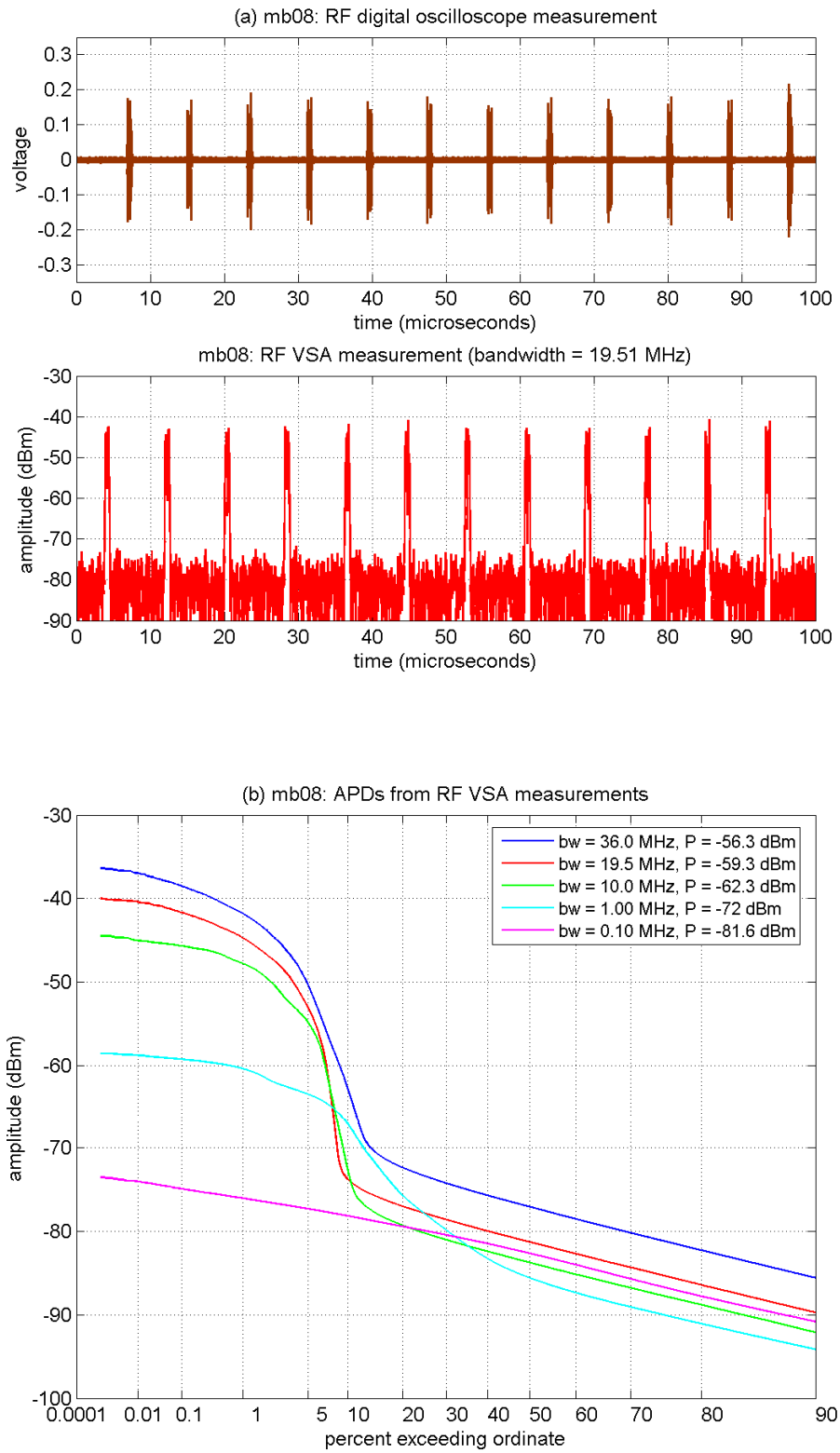

Figure B-59. RF amplitude analyses of MB-08 (b = 13, d = 2).

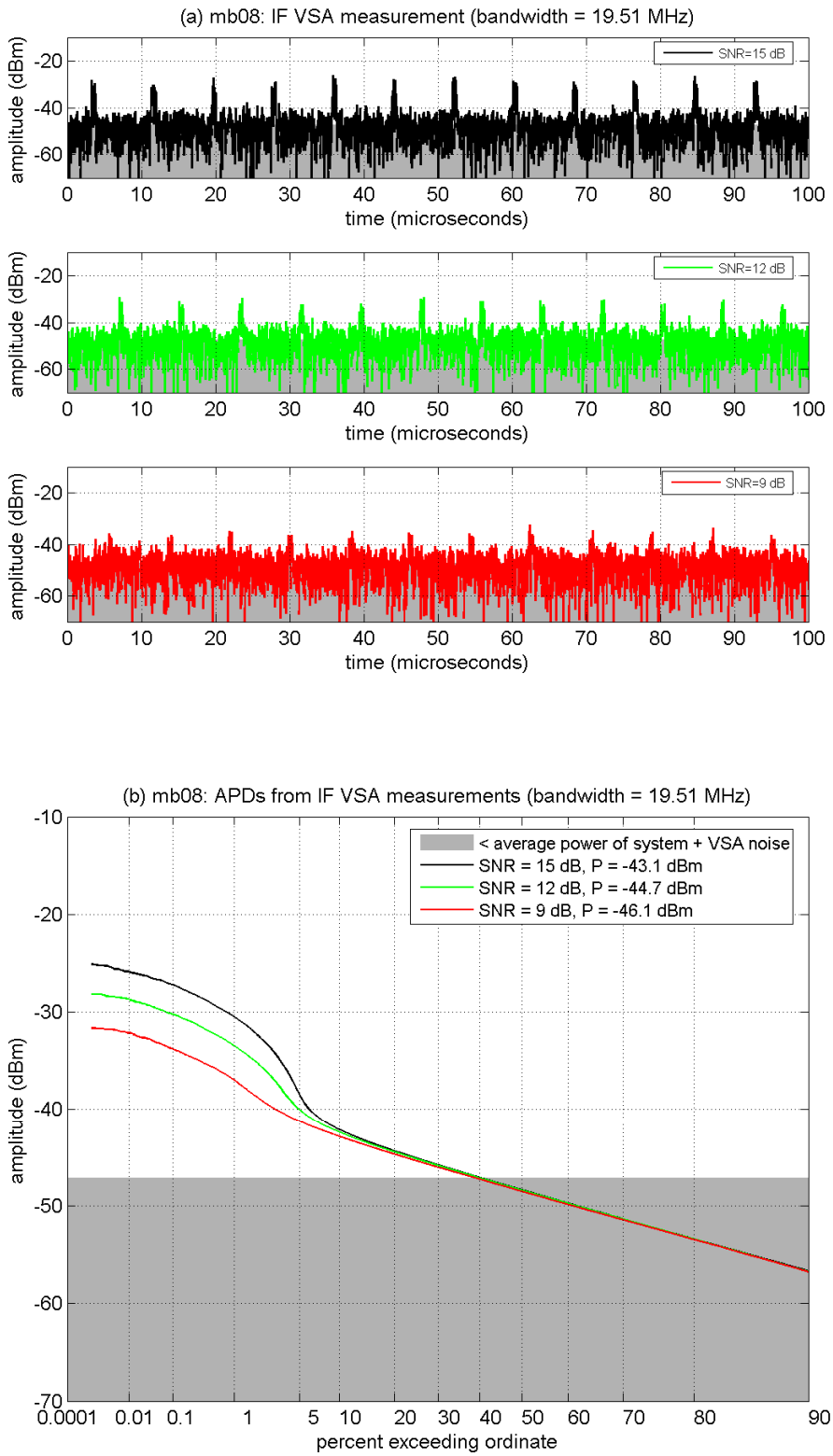

Figure B-60. IF amplitude analyses of MB-08 at INR_{TOV}.

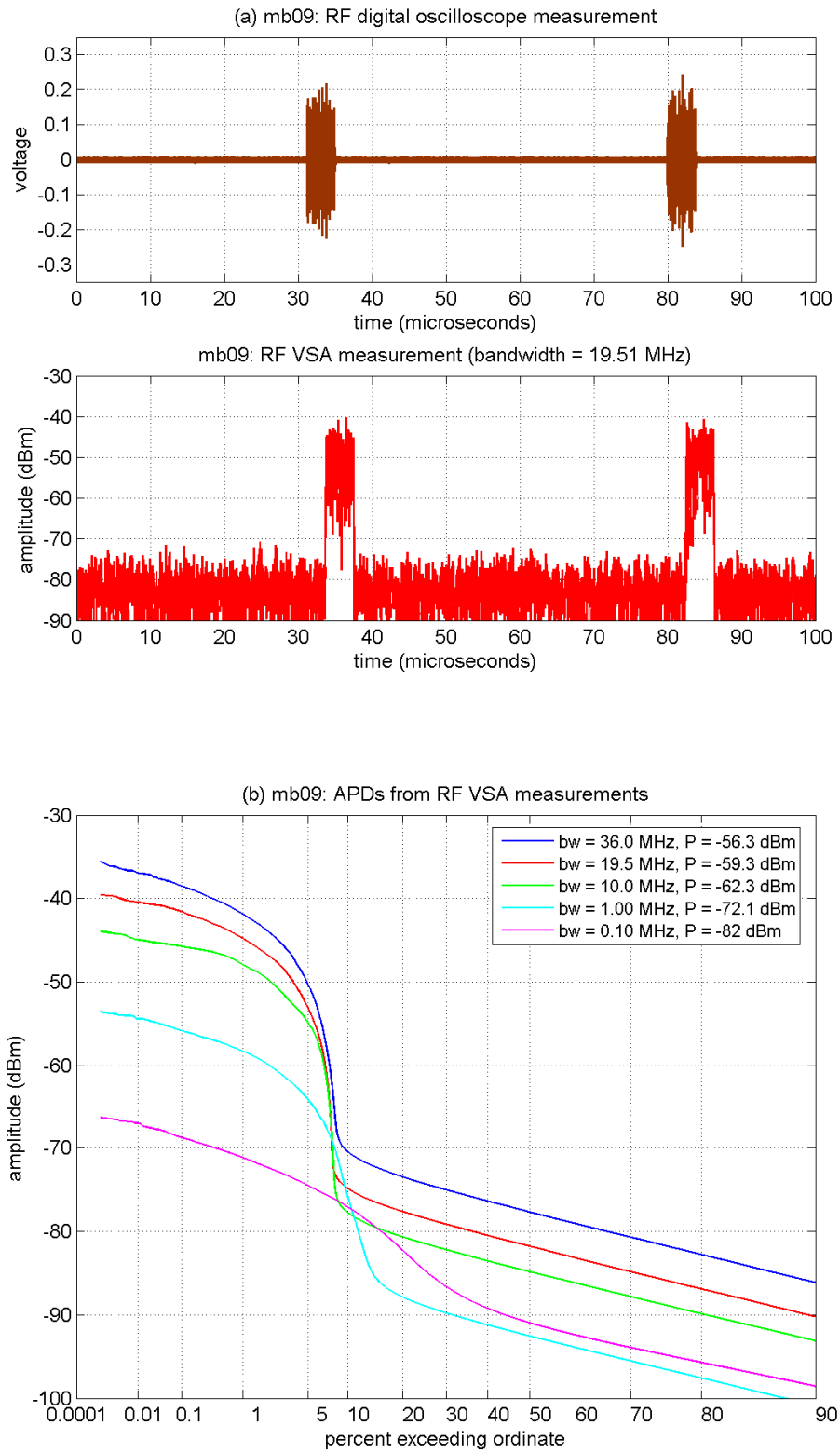

Figure B-61. RF amplitude analyses of MB-09 (b = 13, d = 12).

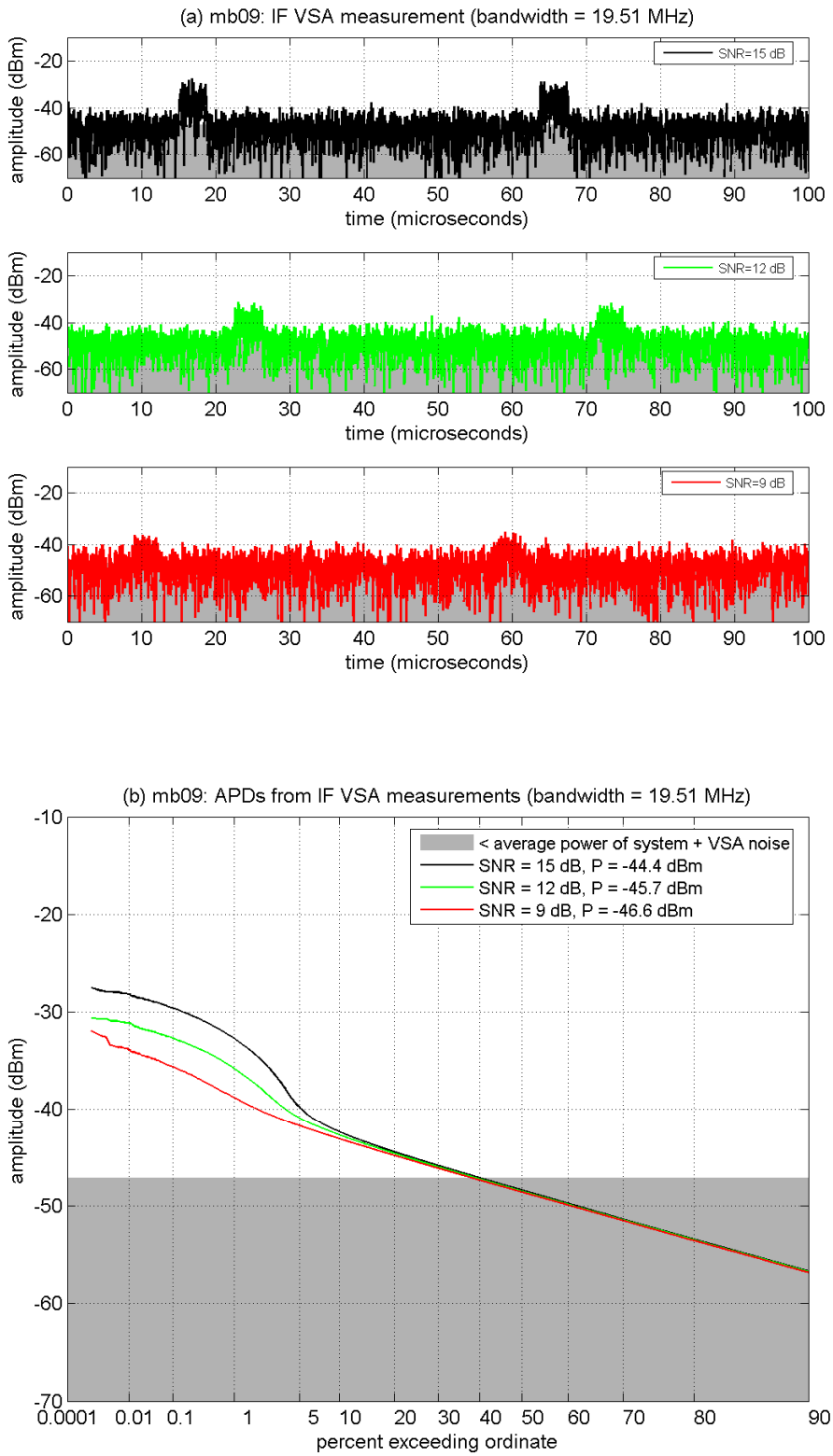

Figure B-62. IF amplitude analyses of MB-09 at INR_{TOV}.

B.4. Spectral Analyses

The spectral analyses provided in this subsection were derived from VSA measurements and intended to emulate the swept spectrum analyzer (SA) measurements described in Table B-5. Complex samples measured in a 36-MHz VSA span were frequency shifted so that the frequency of interest was centered at 0 Hz. Next, the signal was band-limited to a resolution bandwidth (*RBW*) of 1 MHz or 0.1 MHz using a root-raised cosine filter with $\alpha = 0.35$. Mean, median, and peak statistics were computed for the resulting band-limited complex-baseband data.

Table B-5. Spectrum Analyzer Settings for Characterizing UWB Signals

Center Frequency (MHz)	Span (MHz)	Resolution Bandwidth (MHz)	Video Bandwidth (MHz)	Number of Frequency Steps	Sweep Time (seconds)	Detector
3950 3820	600 40	1 0.1	50	3600 2400	10.8 72.0	Rms, peak

These *RBW*s are smaller than that of the victim digital television channel; however, results provide mean and peak estimates relevant to possible narrowband circuitry within the receiver. Frequencies of interest spanned the bandwidth of the satellite channel with a frequency step size set to one tenth of *RBW* to ensure that spectrum details were not missed.

Figures B-63 – B-81 provide spectral statistics for the UWB signals: Figures B-63 – B-66 correspond to DP-01 – DP-04, Figures B-67 – B-72 correspond to DS-01 – DS-06, and Figures B-73 – B-81 correspond to MB-01 – MB-09. SA measurements were made and show agreement with the VSA measurement results; SA measurements are not included in this report.

The most notable trend was frequency-dependent variation in the MB peak amplitude statistics. This behavior is related to the location and modulation of the data and pilot tones of the MB signals, and is the primary difference between MB and GN(MB) signals. GN(MB) peak statistics are flat versus frequency as demonstrated theoretically in Section C.2 in Part 2 [7].

A notable example of this trend is MB-02 in a 0.1-MHz *RBW*. The pilot tone in the band of interest, located at -4.375 MHz, caused spikes in the peak spectra at intervals of ½ the reciprocal gating repetition rate, i.e., 0.533 MHz. Although this feature is evident in the 1-MHz *RBW*, the more prominent feature is the cyclic variation of all peak statistics. Interestingly, the nulls in the cyclic variation correspond to center frequencies of the data and pilot tones.

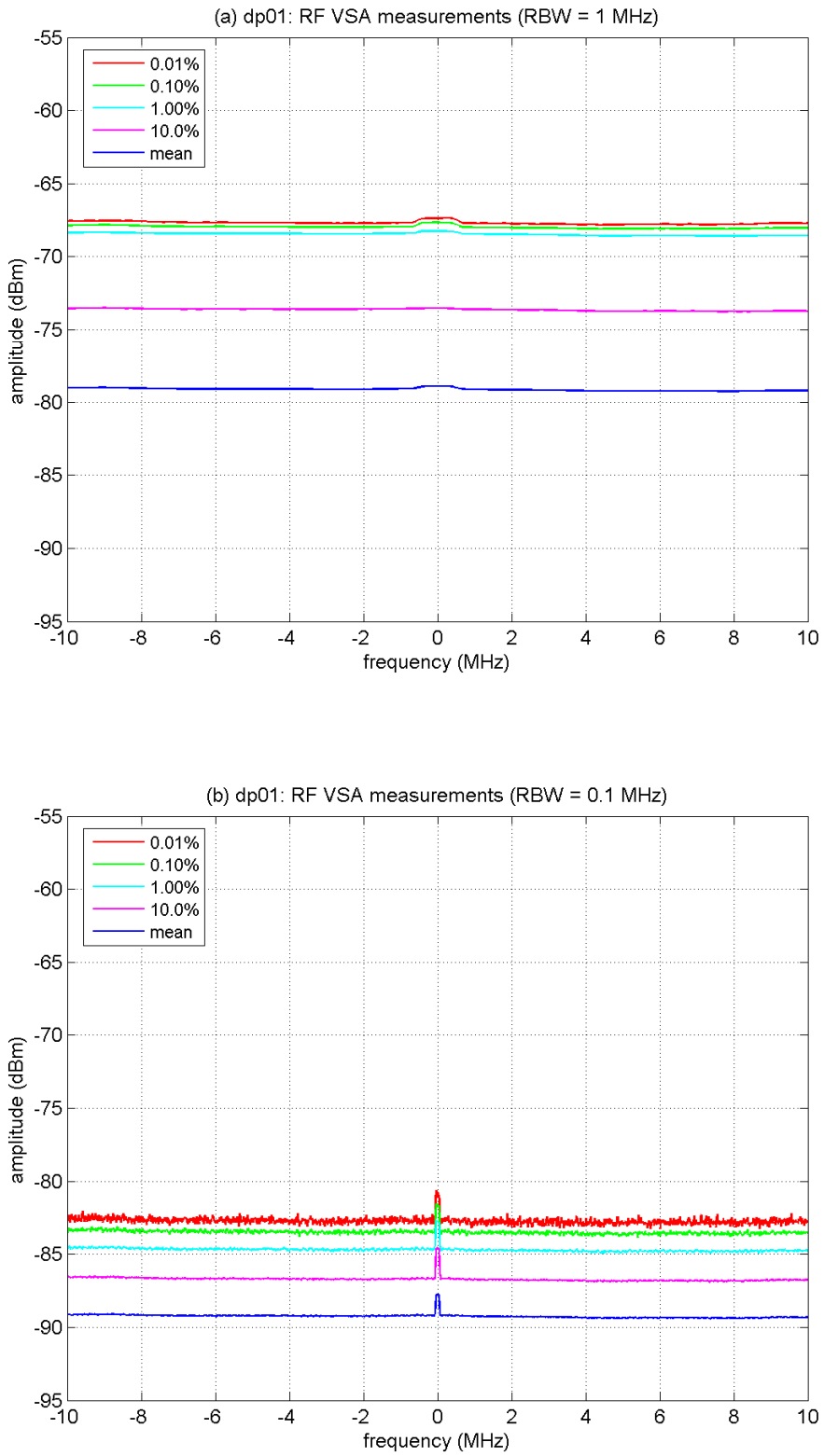

Figure B-63. RF spectral analyses of DP-01 (T_{pulse} = 10,000 ns, w = 0.094 ns, f_D = 0.5).

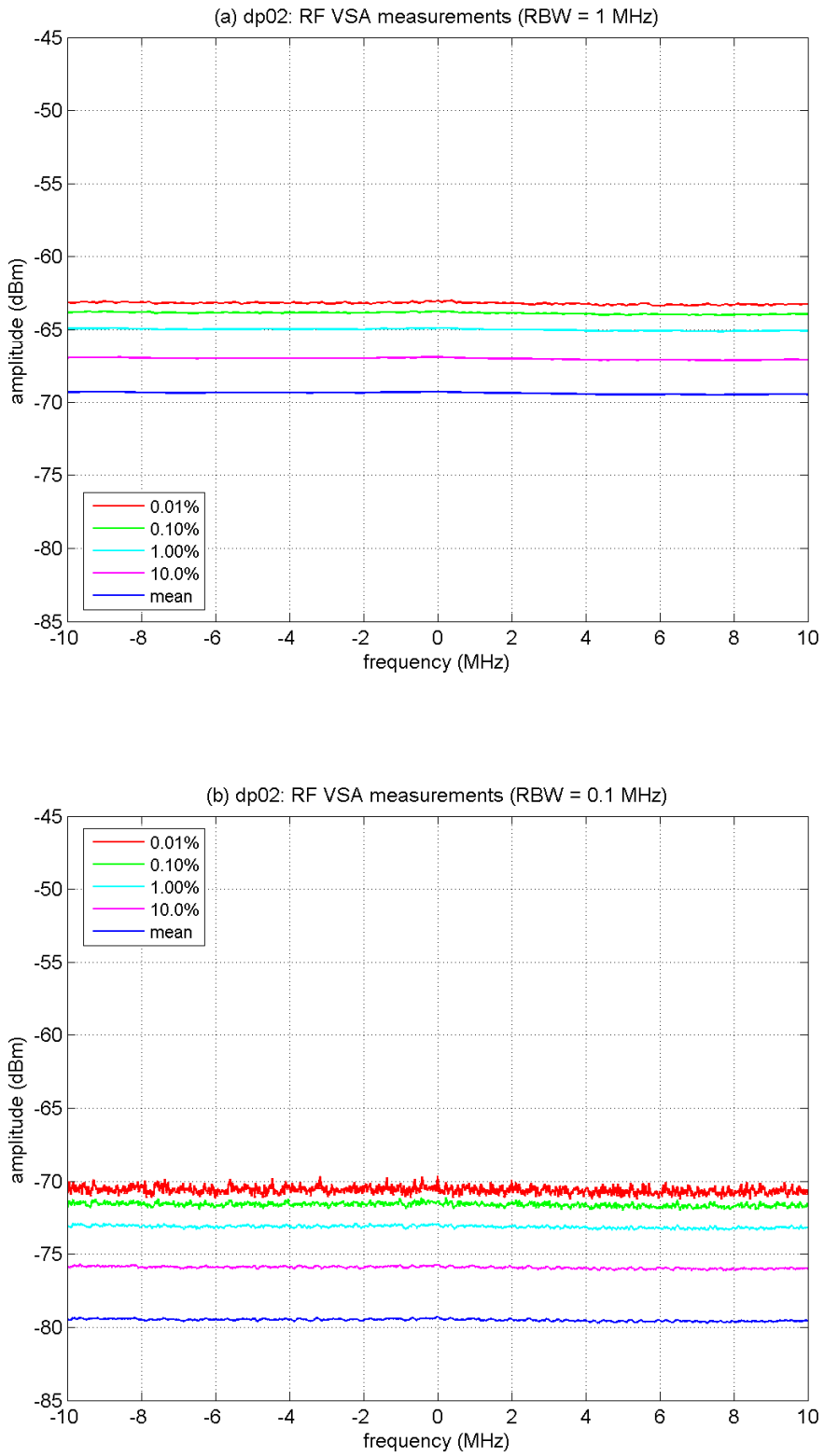

Figure B-64. RF spectral analyses of DP-02 (T_{pulse} = 1000 ns, w = 0.094 ns, f_D = 0.5).

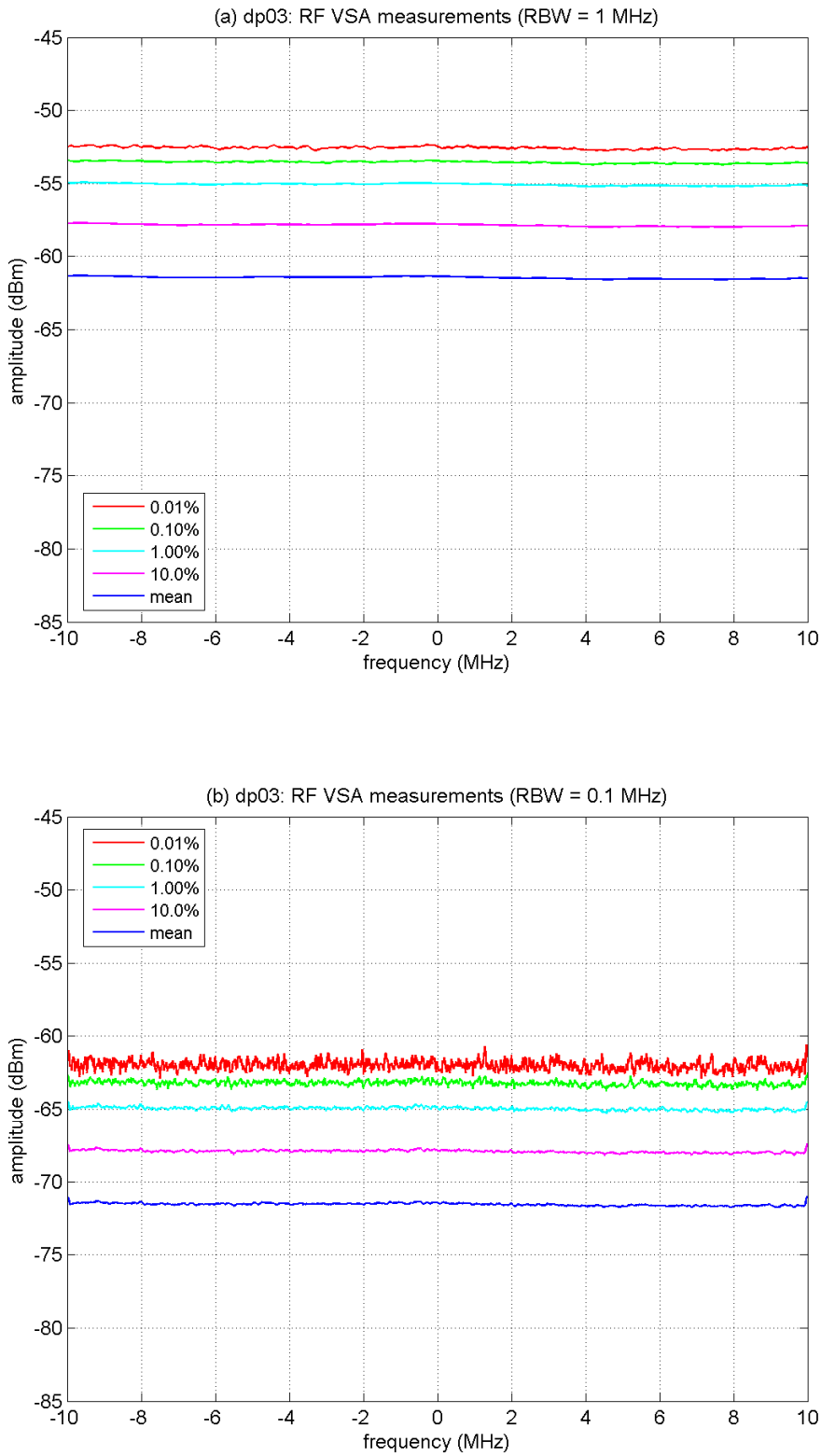

Figure B-65. RF spectral analyses of DP-03 (T_{pulse} = 100 ns, w = 0.094 ns, f_D = 0.5).

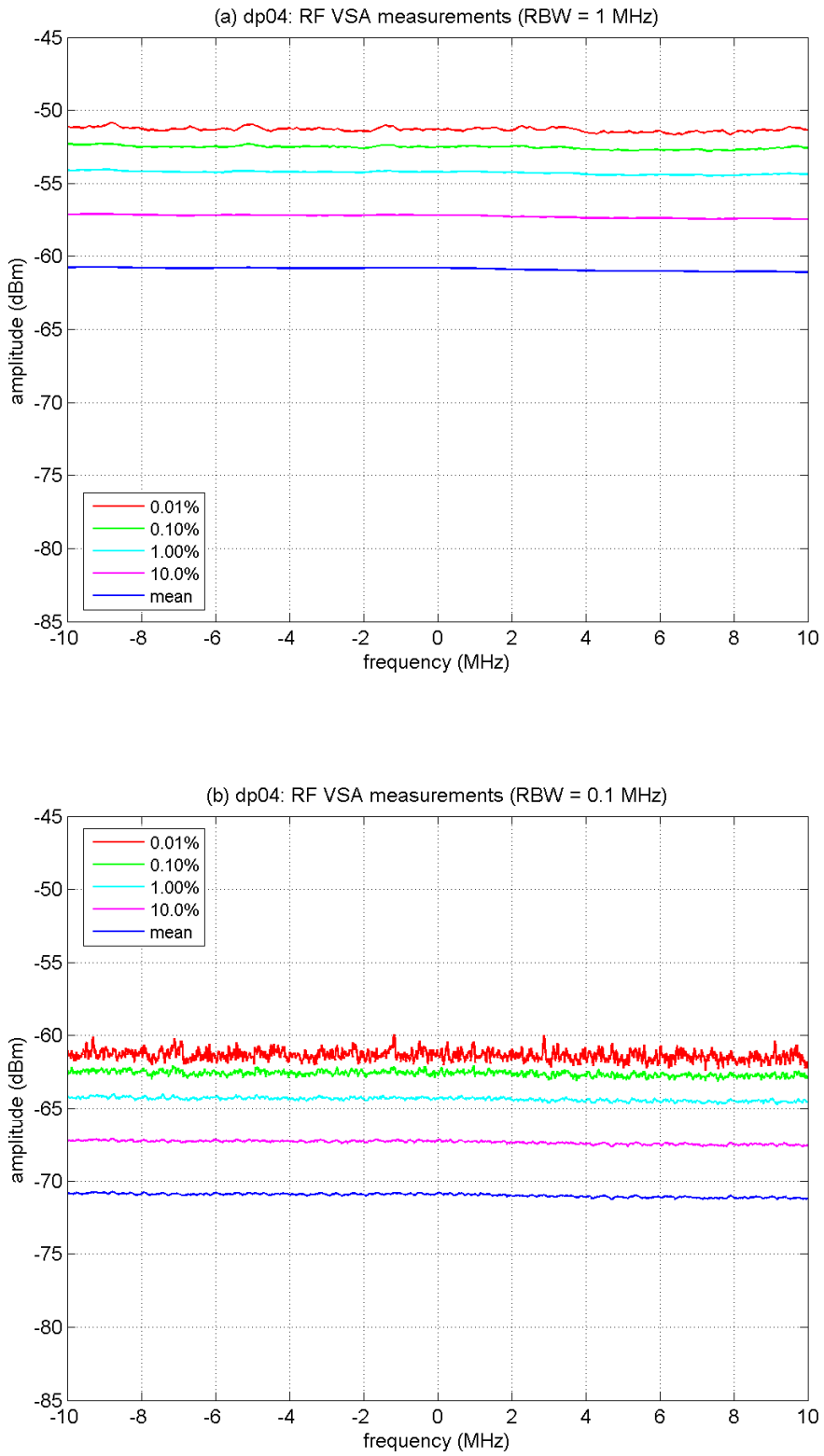

Figure B-66. RF spectral analyses of DP-04 (T_{pulse} = 10 ns, w = 0.094 ns, f_D = 0.5).

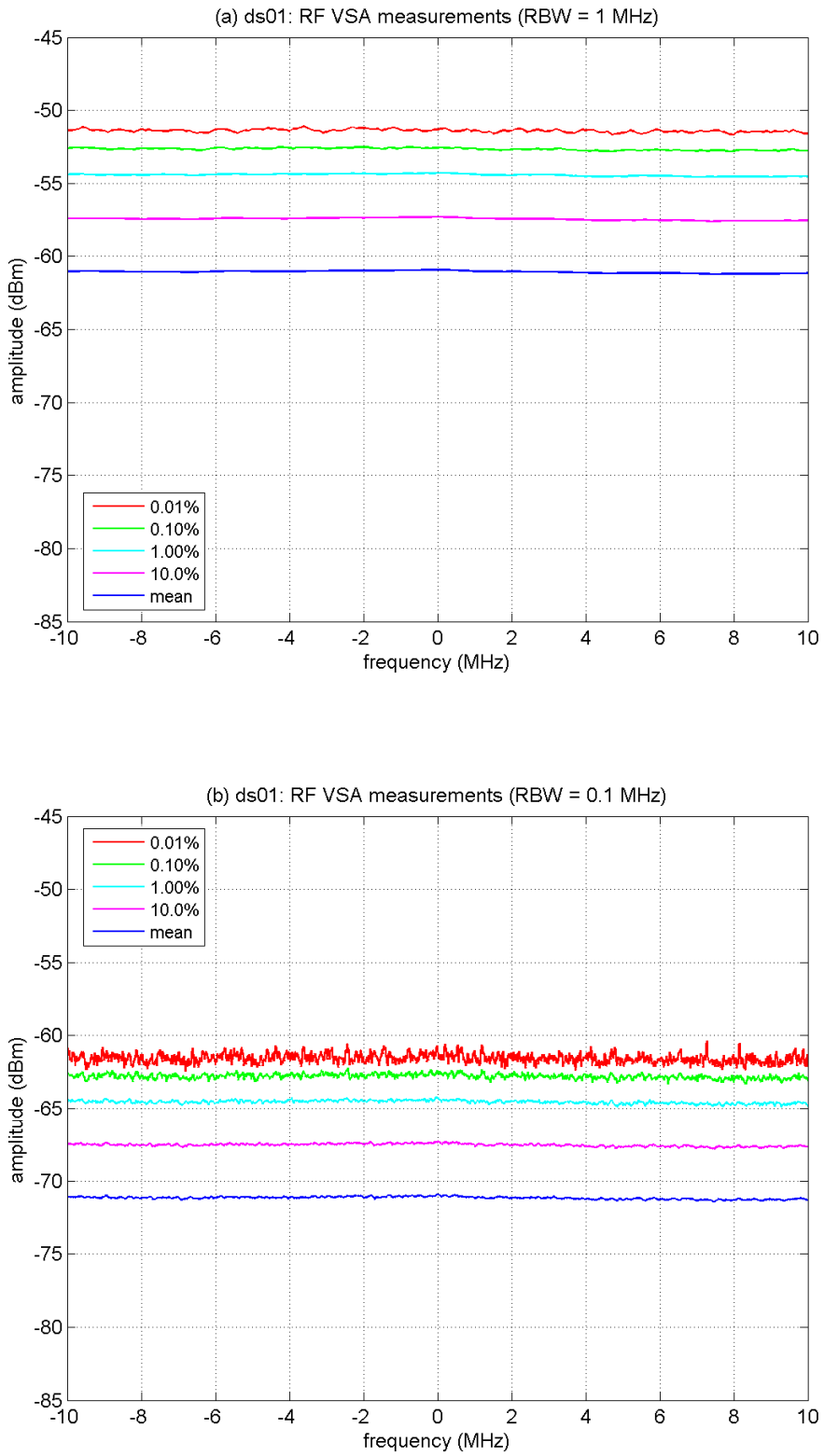

Figure B-67. RF spectral analyses of DS-01 (L = 1).

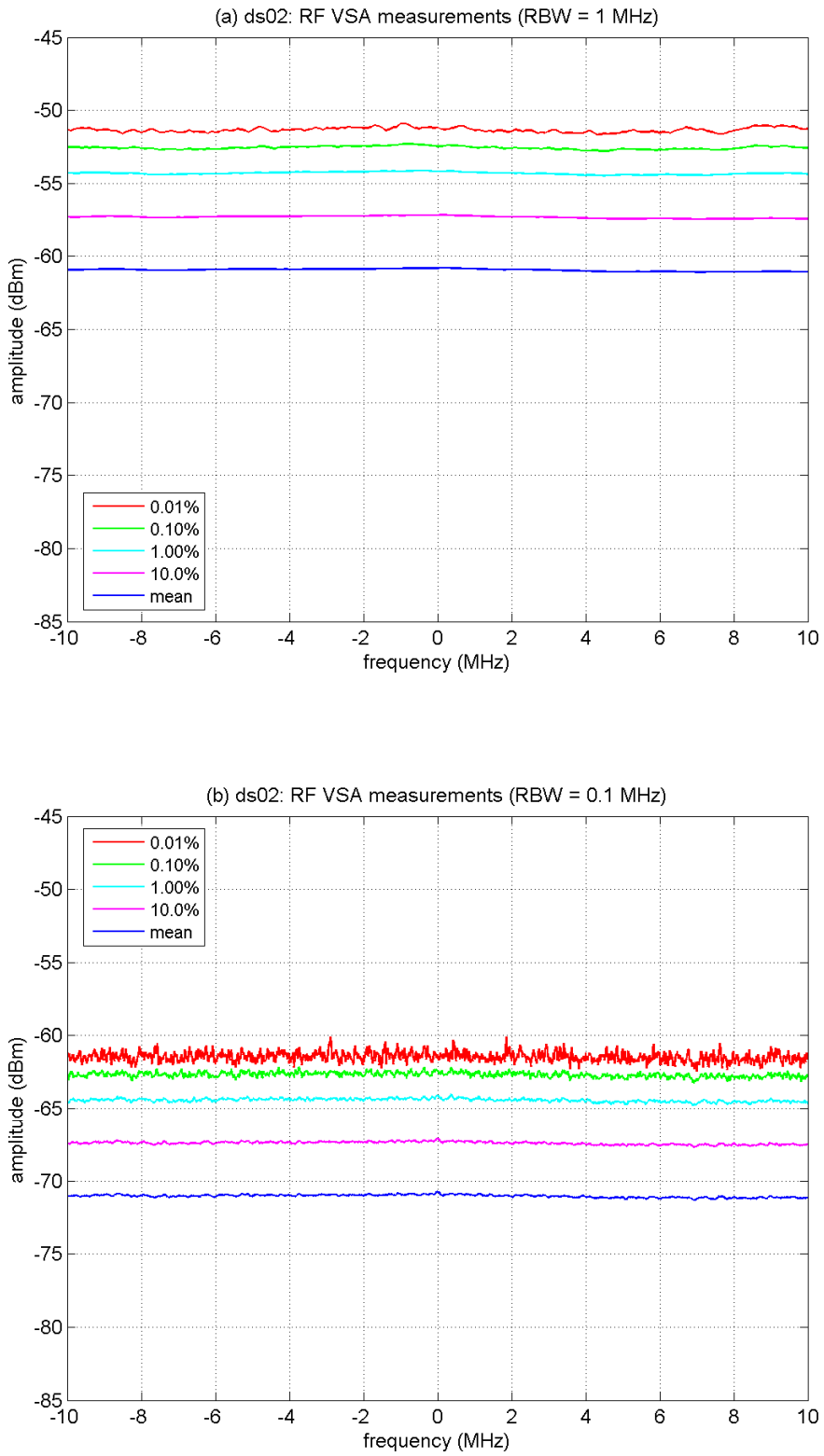

Figure B-68. RF spectral analyses of DS-02 (L = 3, sparse code).

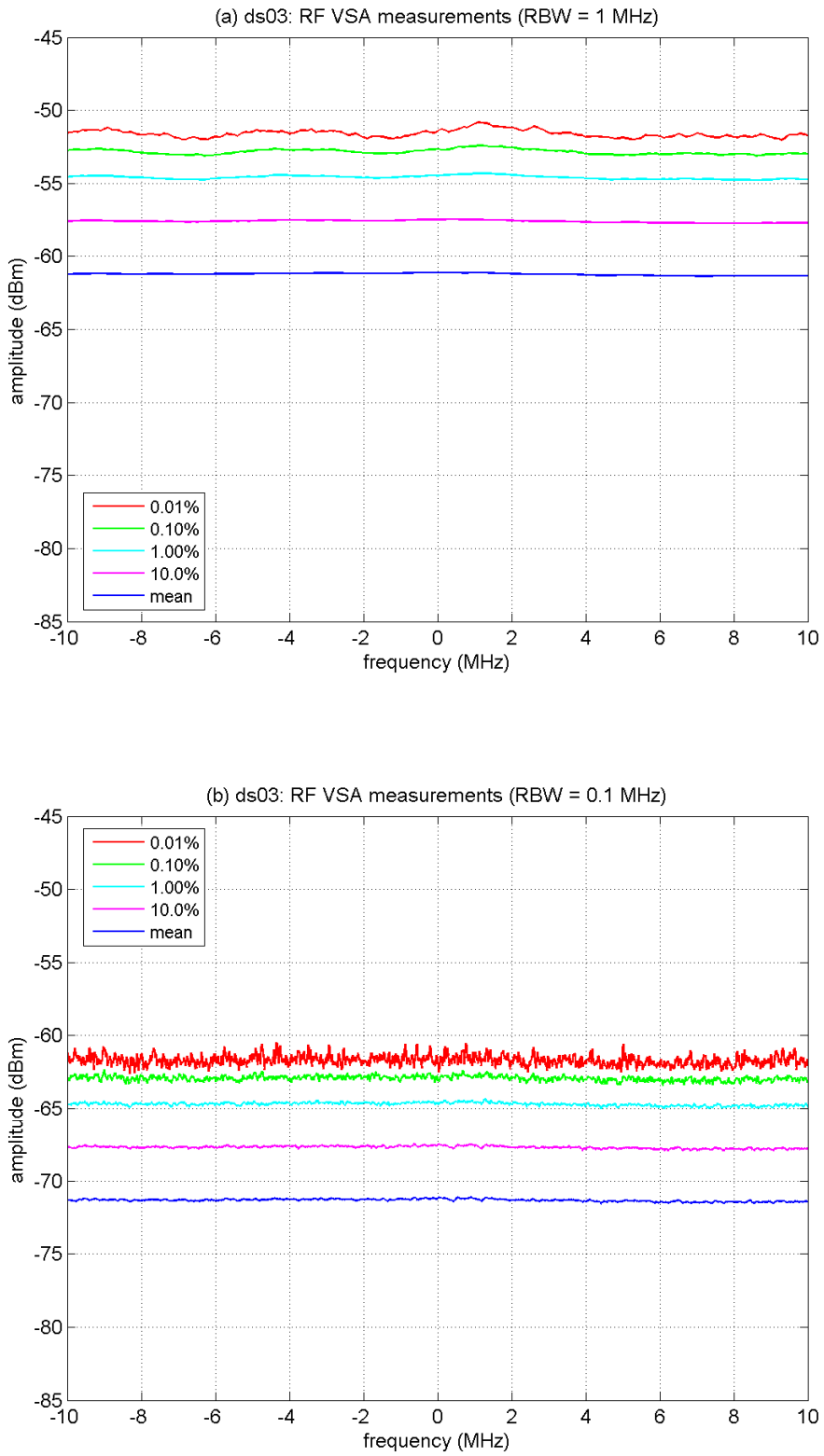

Figure B-69. RF spectral analyses of DS-03 (L = 6, sparse code).

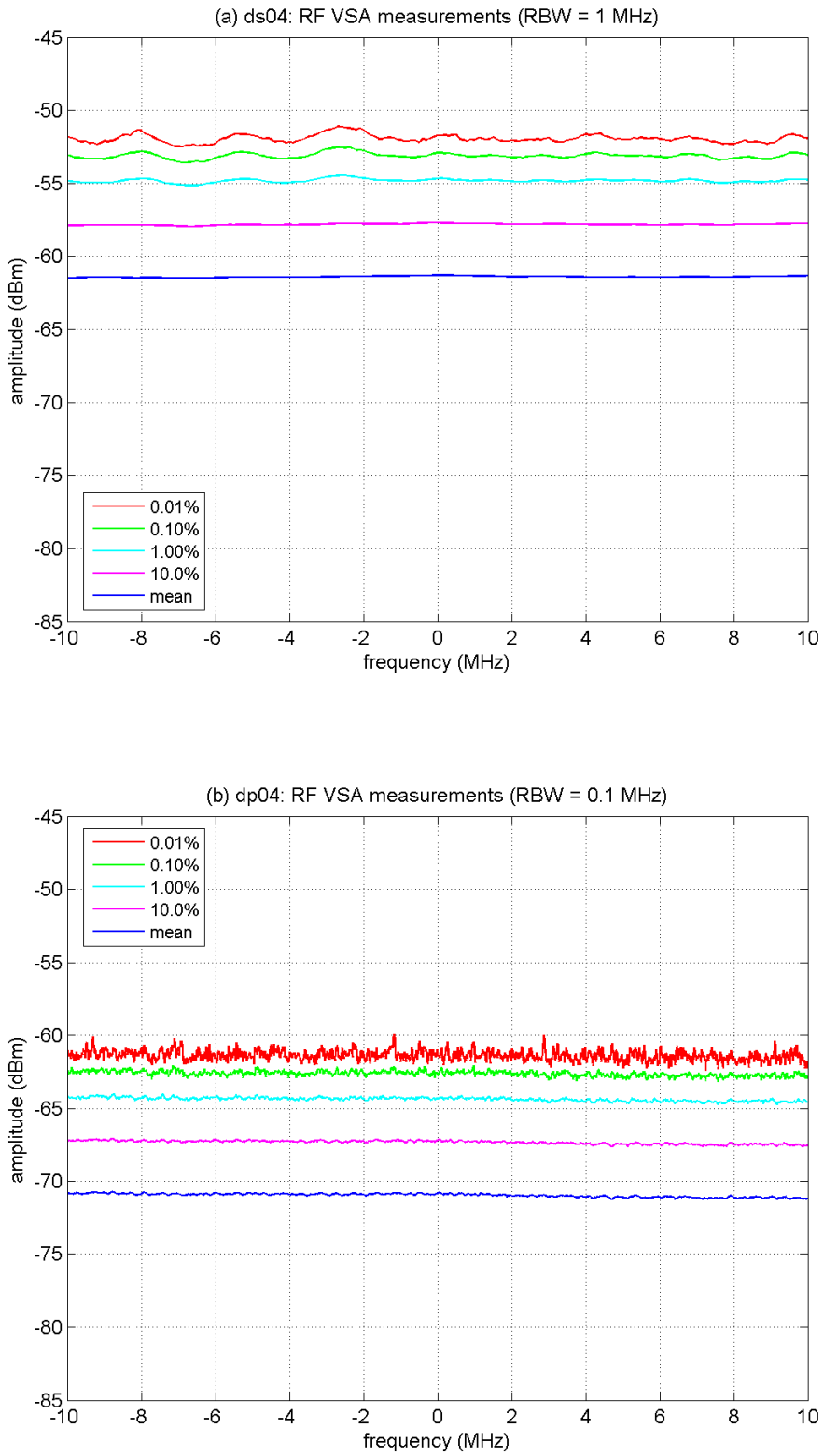

Figure B-70. RF spectral analyses of DS-04 (L = 12, DS code).

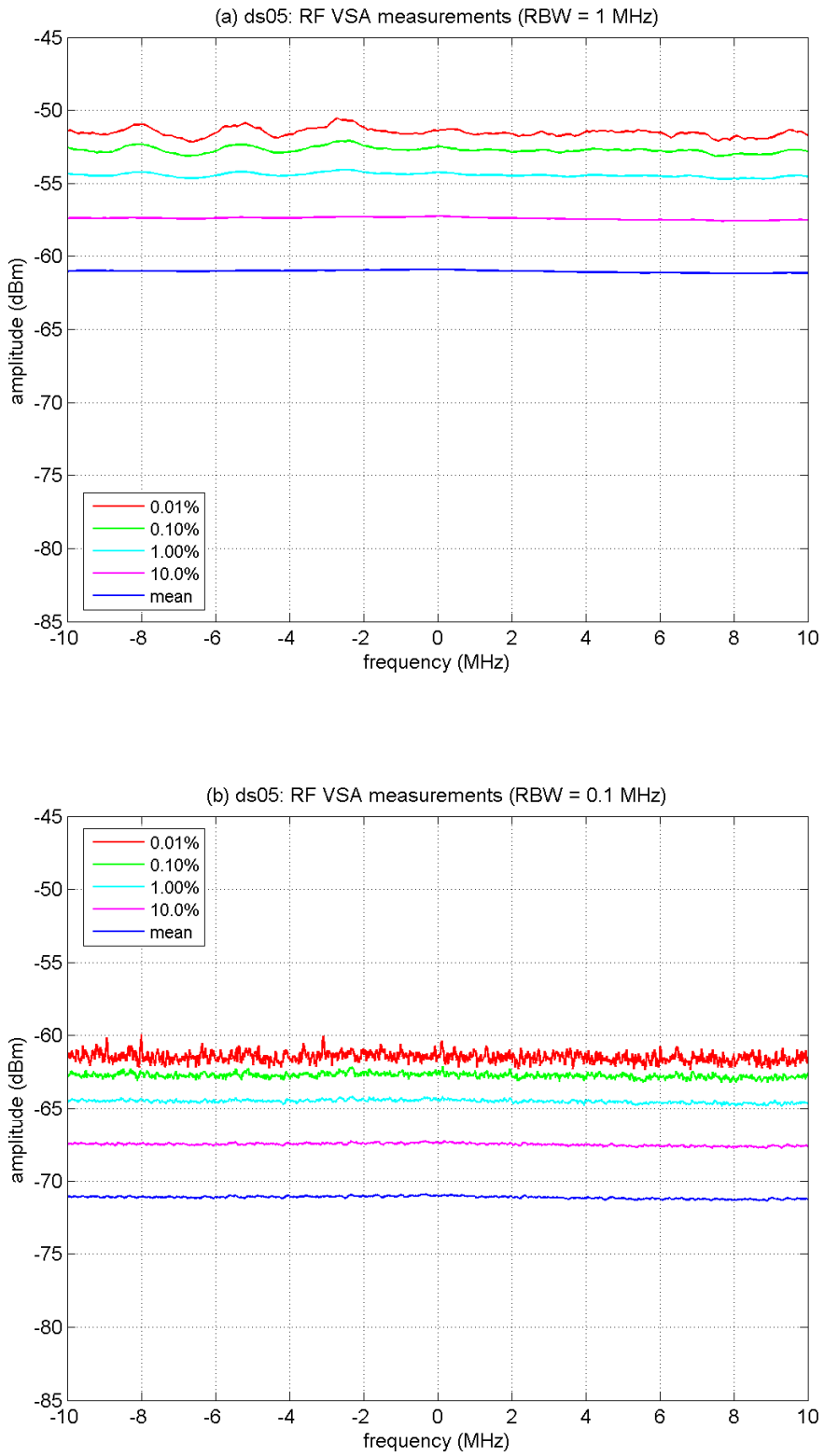

Figure B-71. RF spectral analyses of DS-05 (L = 12, sparse code).

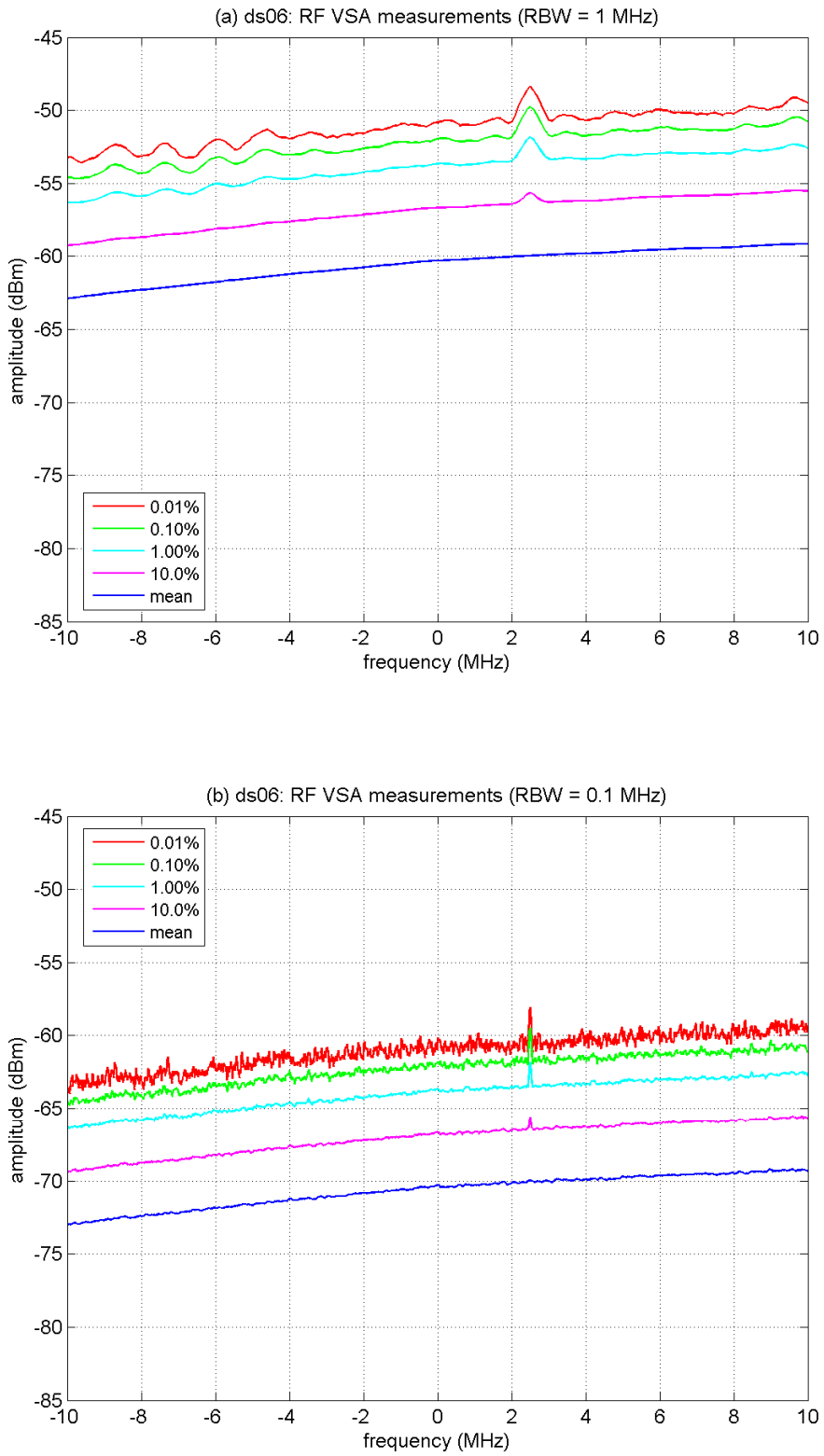

Figure B-72. RF spectral analyses of DS-06 (L = 24, DS code).

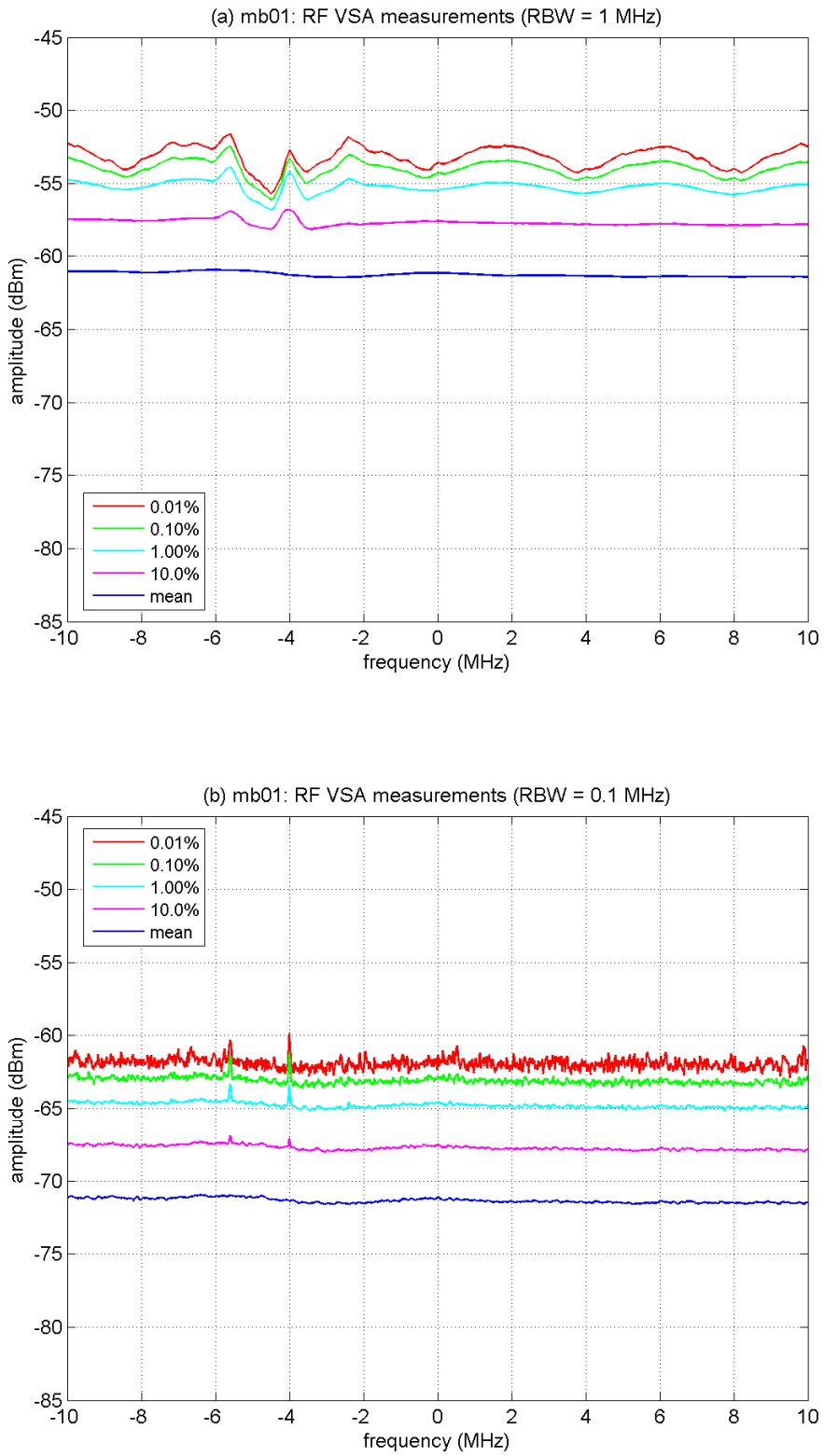

Figure B-73. RF spectral analyses of MB-01 ($b = 1$).

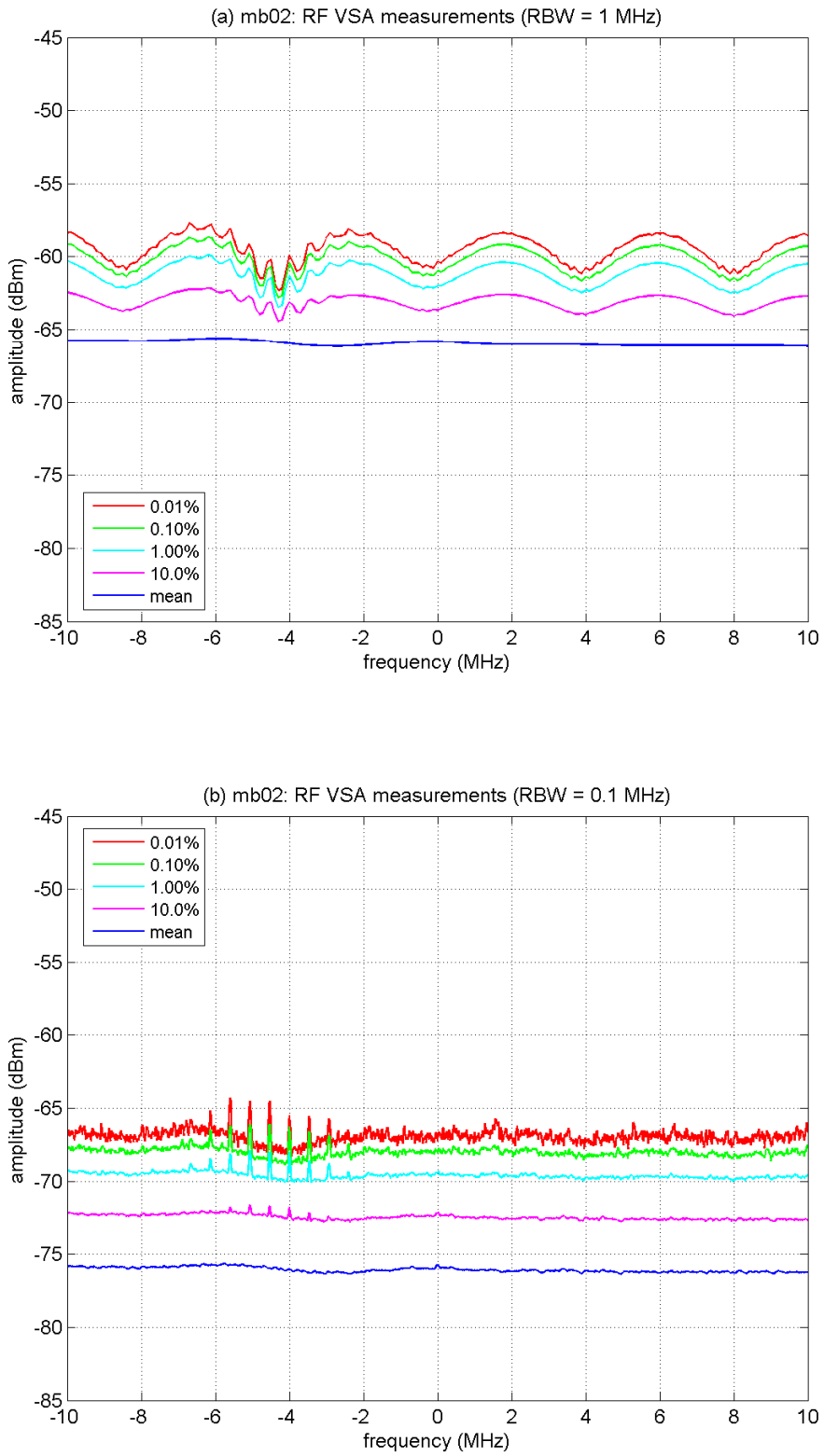

Figure B-74. RF spectral analyses of MB-02 ($b = 3$, $d = 1$).

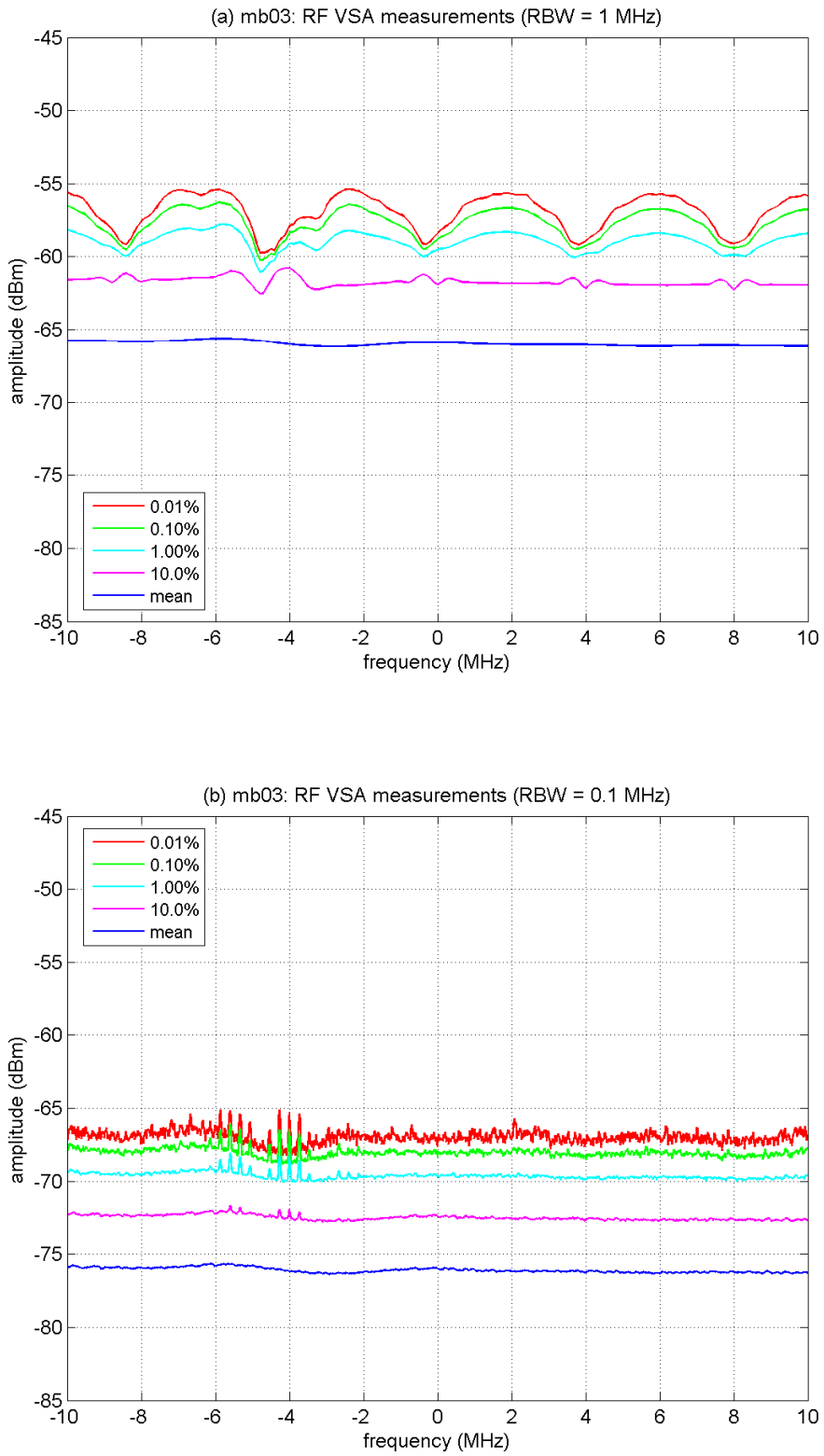

Figure B-75. RF spectral analyses of MB-03 ($b = 3$, $d = 2$).

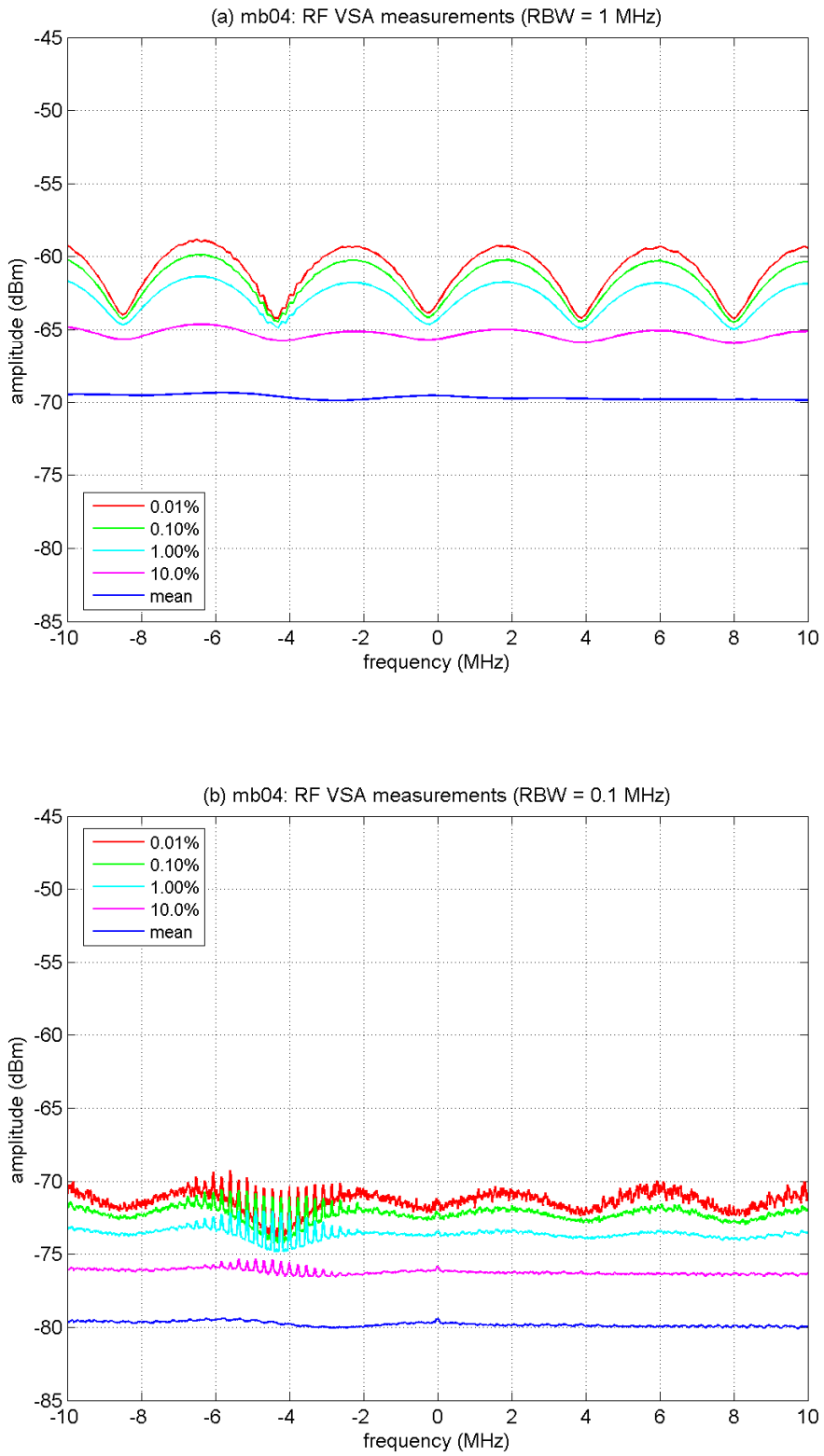

Figure B-76. RF spectral analyses of MB-04 ($b = 7$, $d = 1$).

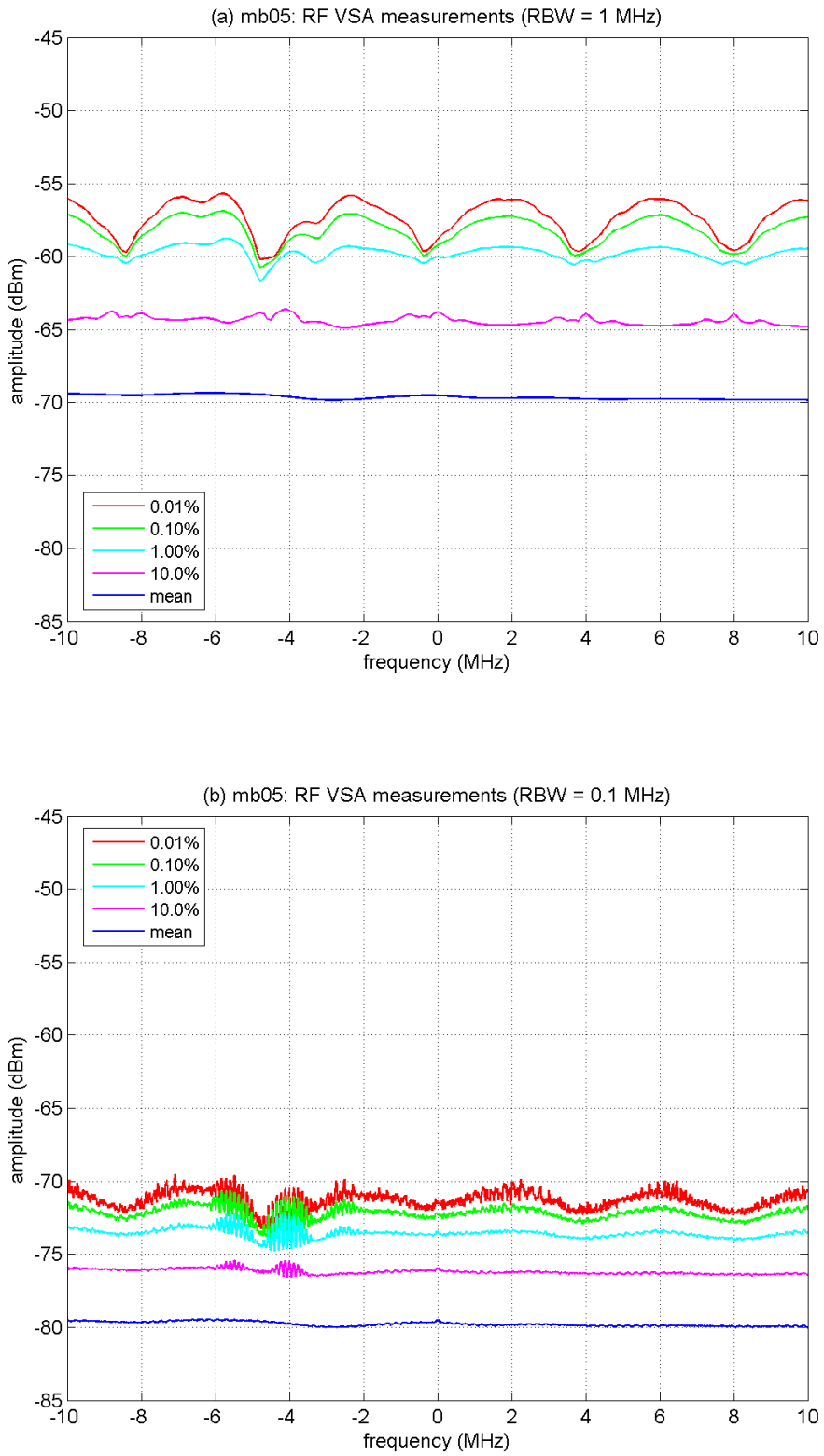

Figure B-77. RF spectral analyses of MB-05 ($b = 7$, $d = 2$).

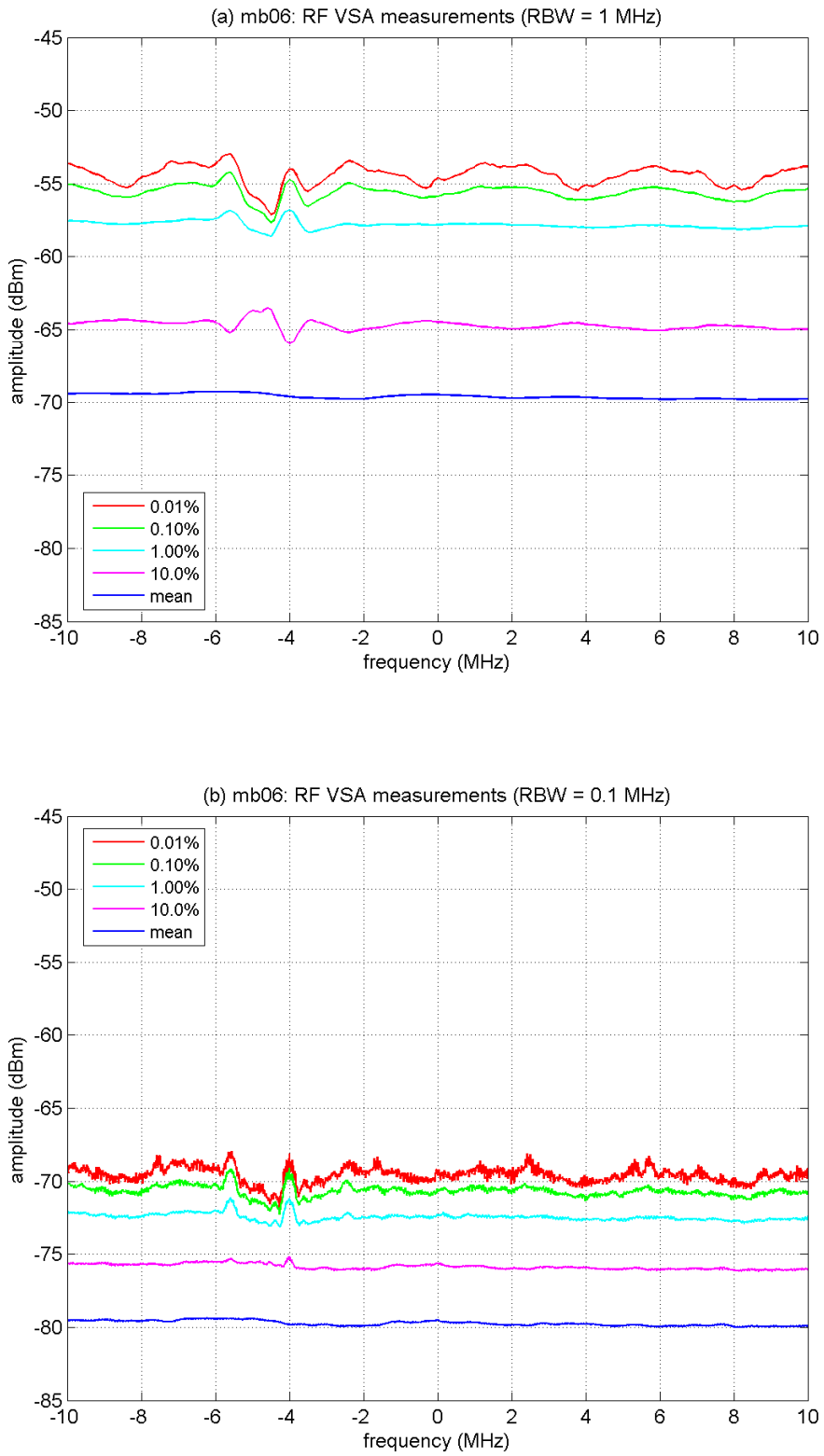

Figure B-78. RF spectral analyses of MB-06 ($b = 7$, $d = 6$).

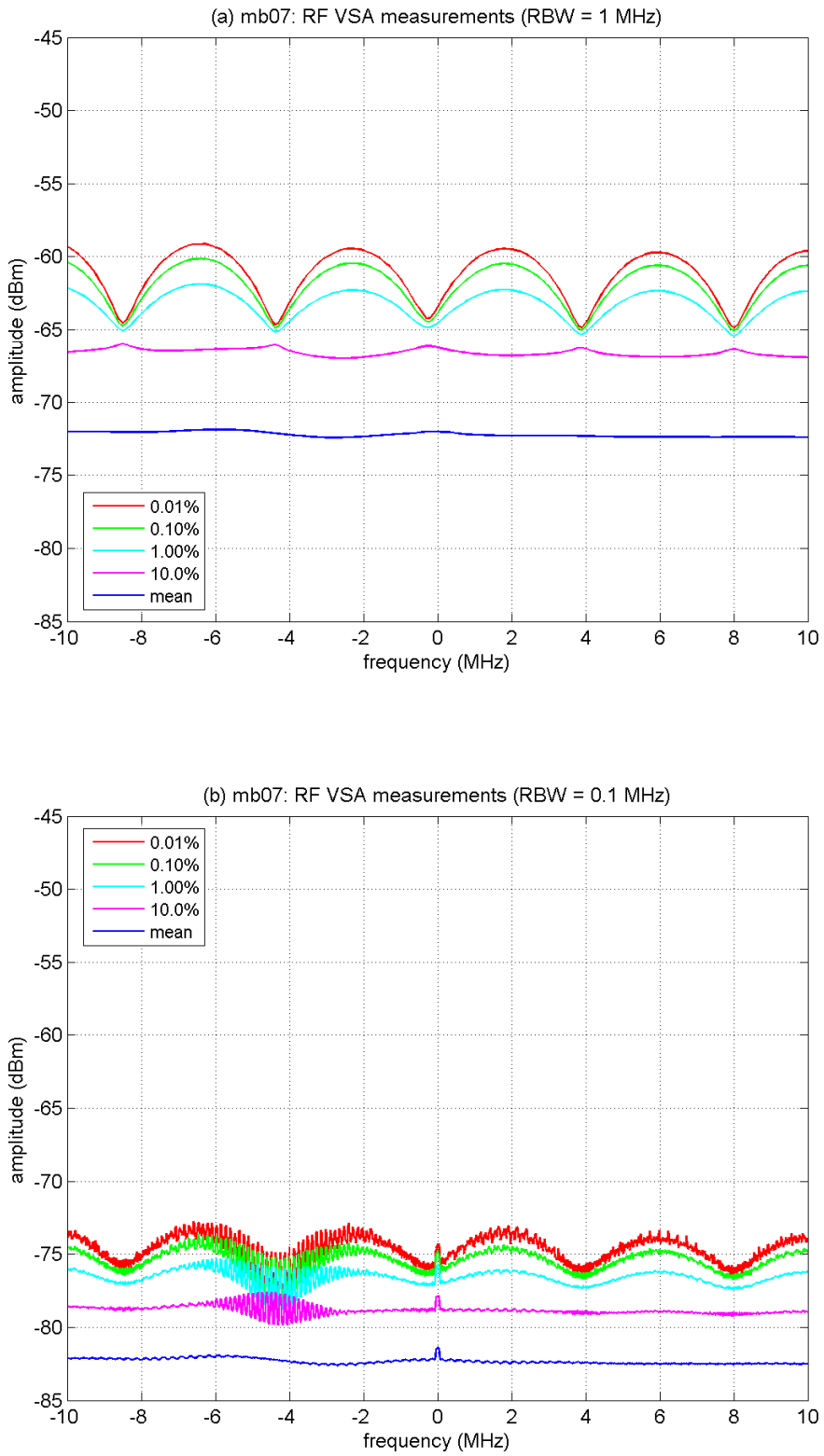

Figure B-79. RF spectral analyses of MB-07 (b = 13, d = 1).

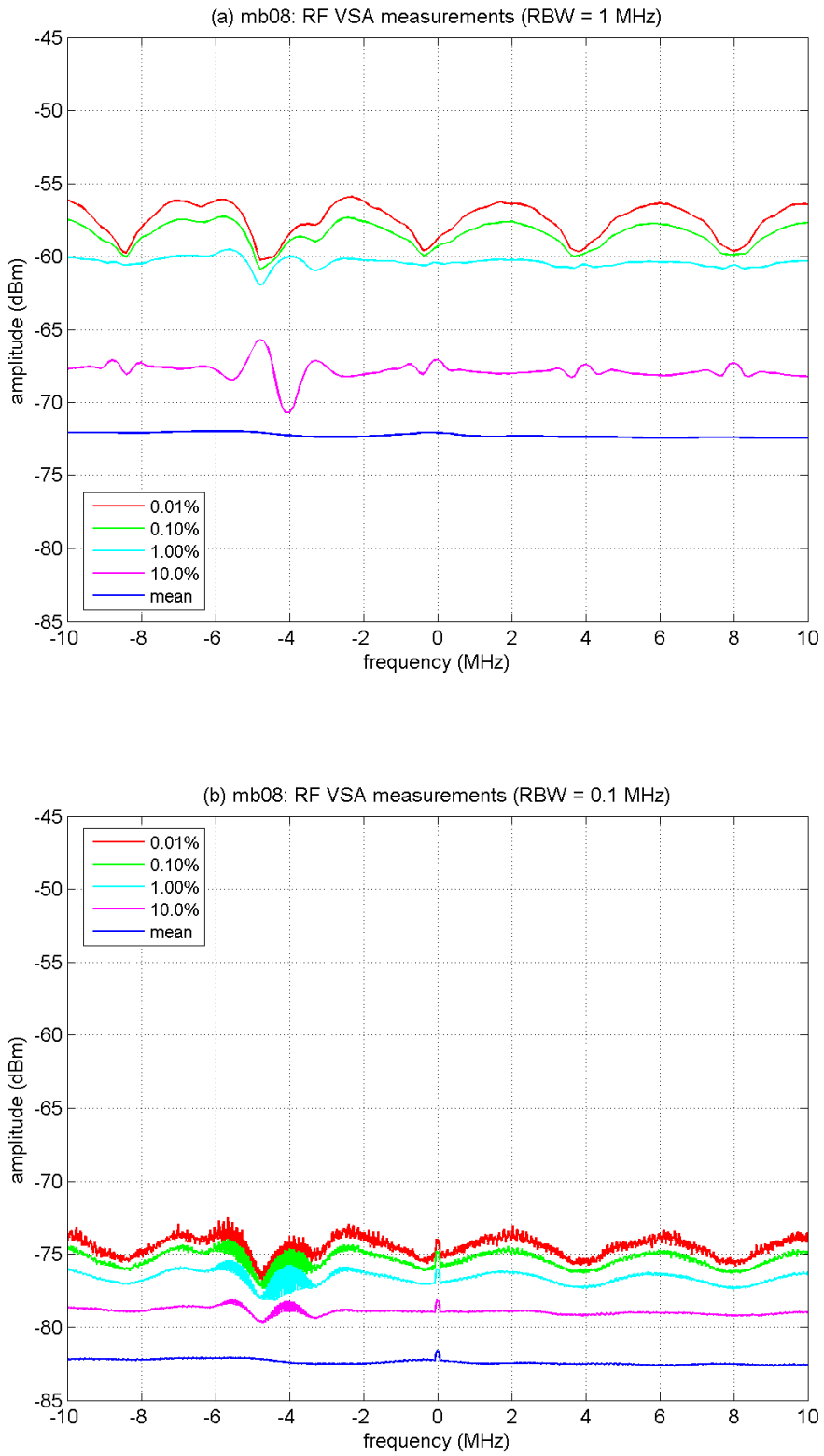

Figure B-80. RF spectral analyses of MB-08 (b = 13, d = 2).

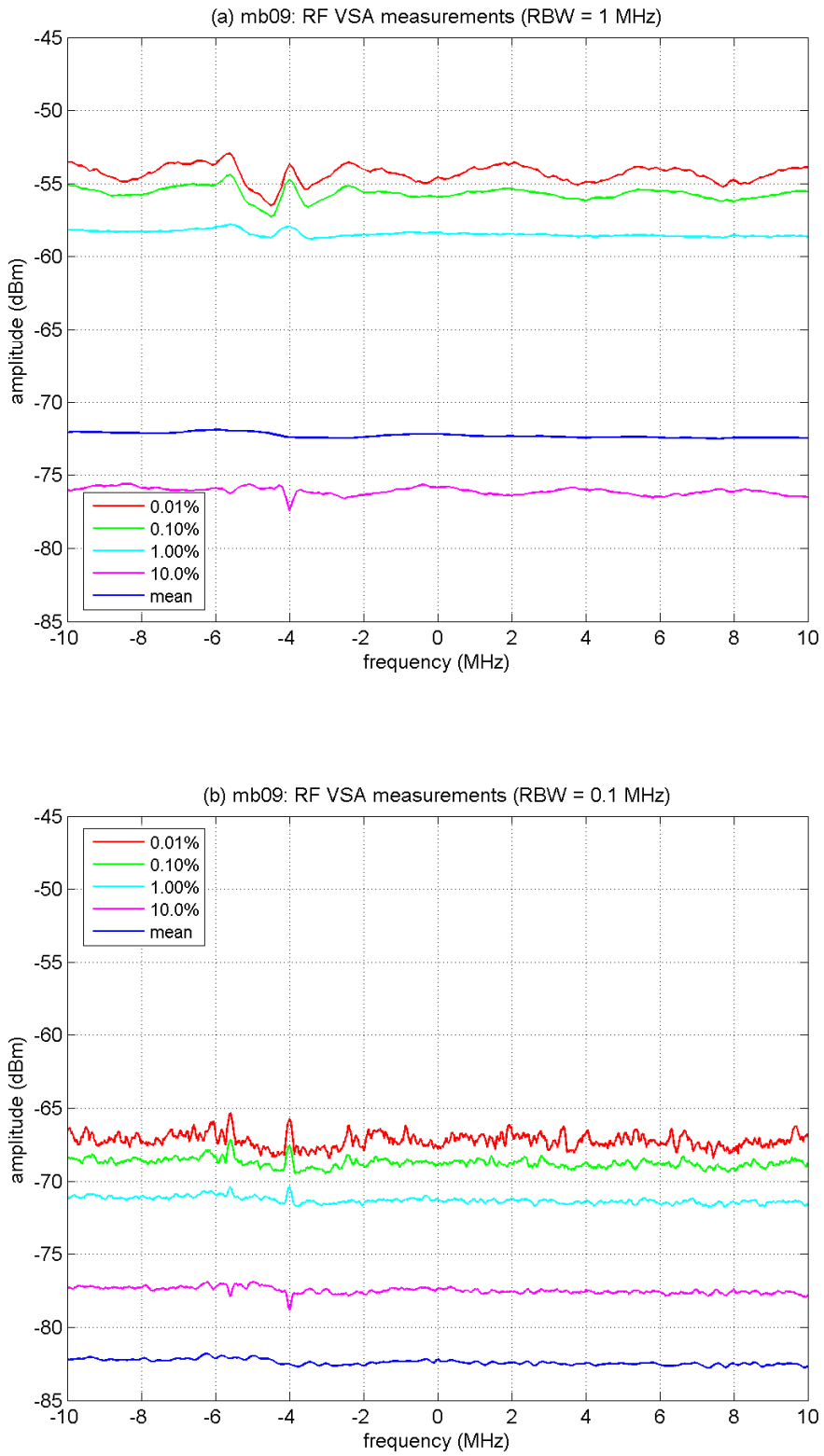

Figure B-81. RF spectral analyses of MB-09 (b = 13, d = 12).

FORM **NTIA-29**
(4-80)

U.S. DEPARTMENT OF COMMERCE
NAT'L. TELECOMMUNICATIONS AND INFORMATION ADMINISTRATION

BIBLIOGRAPHIC DATA SHEET

1. PUBLICATION NO.	2. Government Accession No.	3. Recipient's Accession No.
TR-06-437		

4. TITLE AND SUBTITLE	5. Publication Date
Interference Potential of Ultrawideband Signals --- Part 3: Measurements of Ultrawideband Interference to C-Band Satellite Digital Television Receivers	February 2006
	6. Performing Organization Code 511-6592000-300
7. AUTHOR(S) Michael Cotton, Robert Achatz, Jeffery Wepman, and Roger Dalke	9. Project/Task/Work Unit No.
8. PERFORMING ORGANIZATION NAME AND ADDRESS NTIA/ITS U.S. Department of Commerce 325 Broadway Boulder, CO 80305	10. Contract/Grant No.
11. Sponsoring Organization Name and Address	12. Type of Report and Period Covered

14. SUPPLEMENTARY NOTES

15. ABSTRACT (A 200-word or less factual summary of most significant information. If document includes a significant bibliography or literature survey, mention it here.)

This report provides results from tests that measured digital television (DTV) susceptibility to ultrawideband (UWB) interference. A test system was developed to inject interference with known characteristics into a victim receiver and quantitatively measure susceptibility. In this experiment, a C-band satellite DTV victim receiver was injected with Dithered-Pulse (DP), Direct-Sequence (DS), and Multi-Band OFDM (MB) UWB interference. Results showed that the UWB signals could be categorized into three signal sets of common DTV susceptibility behavior. Interestingly, the categorized signals, band-limited by the DTV receiver filter, also had common characteristics. Set 1 consists of signals whose DTV susceptibility and band-limited signal characteristics resemble Gaussian noise. Set 2 consists of signals more deleterious than Gaussian noise interference. Notably, these signals had a wide range of band-limited signal characteristics and susceptibilities. Set 3 consists of a signal that is relatively benign. Results also showed that measurable band-limited characteristics, e.g., burst duration (*BD*), burst interval (*BI*), fractional on-time (ζ_{DTV}), and peak-to-average ratio (*P/A*), of the interfering signal are useful for predicting susceptibility. Finally, it was determined that continuous and gated noise signals can be used to emulate the interference effects of DS and MB signals for the DTV victim receiver and operational scenarios tested in this study. This might not be true, however, for testing the susceptibility of other victim receivers operating in narrower bandwidths as indicated by amplitude probability distributions as a function of frequency for MB signals band-limited to relatively narrow bandwidths.

16. Key Words (Alphabetical order, separated by semicolons)
Digital television; interference; satellite communications; ultrawideband

17. AVAILABILITY STATEMENT	18. Security Class. (This report)	20. Number of pages
UNLIMITED.	19. Security Class. (This page)	21. Price:

NTIA FORMAL PUBLICATION SERIES

NTIA MONOGRAPH (MG)

A scholarly, professionally oriented publication dealing with state-of-the-art research or an authoritative treatment of a broad area. Expected to have long-lasting value.

NTIA SPECIAL PUBLICATION (SP)

Conference proceedings, bibliographies, selected speeches, course and instructional materials, directories, and major studies mandated by Congress.

NTIA REPORT (TR)

Important contributions to existing knowledge of less breadth than a monograph, such as results of completed projects and major activities. Subsets of this series include:

NTIA RESTRICTED REPORT (RR)

Contributions that are limited in distribution because of national security classification or Departmental constraints.

NTIA CONTRACTOR REPORT (CR)

Information generated under an NTIA contract or grant, written by the contractor, and considered an important contribution to existing knowledge.

JOINT NTIA/OTHER-AGENCY REPORT (JR)

This report receives both local NTIA and other agency review. Both agencies' logos and report series numbering appear on the cover.

NTIA SOFTWARE & DATA PRODUCTS (SD)

Software such as programs, test data, and sound/video files. This series can be used to transfer technology to U.S. industry.

NTIA HANDBOOK (HB)

Information pertaining to technical procedures, reference and data guides, and formal user's manuals that are expected to be pertinent for a long time.

NTIA TECHNICAL MEMORANDUM (TM)

Technical information typically of less breadth than an NTIA Report. The series includes data, preliminary project results, and information for a specific, limited audience.

For information about NTIA publications, contact the NTIA/ITS Technical Publications Office at 325 Broadway, Boulder, CO, 80305 Tel. (303) 497-3572 or e-mail info@its.bldrdoc.gov.

This report is for sale by the National Technical Information Service, 5285 Port Royal Road, Springfield, VA 22161,Tel. (800) 553-6847.